FROM PINNING TO LOCALIZATION IN GRAPHENE – ON THE STATISTICAL PROPERTIES OF RANDOMLY PINNED FLEXURAL PHONONS

A Dissertation

by

WEI ZHAO

Submitted to the Office of Graduate and Professional Studies of
Texas A&M University
in partial fulfillment of the requirements for the degree of

DOCTOR OF PHILOSOPHY

Chair of Committee,	Alexander Finkel'stein
Committee Members,	Valery Pokrovsky
	Donald Naugle
	Peter Kuchment
Head of Department,	Peter McIntyre

December 2017

Major Subject: Physics

ABSTRACT

We identify graphene layer on a disordered substrate as a system where Anderson localization of phonons can be observed. Generally, observation of localization for scattering waves is not simple, because the Rayleigh scattering is inversely proportional to a high power of wavelength. The situation is radically different for the out of plane vibrations, so-called flexural phonons, scattered by pinning centers induced by a substrate. In this case, the scattering time for vanishing wave vector tends to a finite limit. One may, therefore, expect that physics of the flexural phonons exhibits features characteristic for electron localization in two dimensions, albeit without complications caused by the electron-electron interactions. We confirm this idea by calculating statistical properties of the Anderson localization of flexural phonons for a model of elastic sheet in the presence of the pinning centers. Finally, we discuss possible manifestations of the flexural phonons, including the localized ones, and contribution to the electron dephasing rate.

DEDICATION

To my mother, my father, and my grandmother.

ACKNOWLEDGMENTS

First and foremost, I would express my special thanks to Prof. Alexander Finkel'stein, my graduate advisor, who really taught me how to think and act like a theoretical physicist, for his continuous support over the years, for all the encouragement on me and the patience and enlightenment that allowed me to grow as a theoretical physics researcher. Sasha gave me the opportunity to travel to places like the Weizmann Institute of Science in Israel and Karlsruhe Institute of Technology in Germany where I spent extended time doing research and study. The trips really opened my eyes and gave me a lot of precious chances to interact with the top condensed matter physicists and students. I still could remember the time I spent with Sasha for hours, either in front of the blackboard or by his desk, studying the interesting problems in condensed matter physics.

I will also extend my thanks to Prof. Pokrovsky, who has taught me several important topics in condensed matter physics, including the Quantum Mechanics and condensed matter field theory. The lessons prepared me well for my Ph.D. research and dissertation work, and throughout the interaction with Dr. Pokrovsky, I also learned tremendously about how to be a lifetime learner and researcher. Many thanks should also be given to my other committee members, Prof. Naugle and Prof. Kuchment who gave me precious opinions for this dissertation work.

Also, I would like to thank the Texas A&M University High Performance Research Computing to allow me to use the supercomputing nodes on the Ada and Terra cluster there. Portions of this research, especially the intensive computation task were conducted with the advanced computing resources provided by Texas A&M High Performance Research Computing.

There is another organization that I should give some credit: J.P. Morgan, with whom

I did two internships in the field of quantitative finance. I learned a lot of the numerical skills and also learned how to operate with supercomputers there, which really became the key to my dissertation work.

Ph.D. study is the longest and hardest commitment I have ever promised in my lifetime. Without the support of my family, mentors, and friends, it will never be possible. Prof. Chin and Prof. Hu have been my mentors and teachers throughout the year, I would like to thank them for all the precious advice that they have given to me. Dr. Konstantin Tikhonov is also a very important figure in my Ph.D. life, who joined Sasha's group roughly the same time as me. We are not only collaborators but also close friends. Dr. Tikhonov really taught me how to think theoretical physics problems like a professional physicist. I would like to thank all my friends in the Physics & Astronomy Department and also around the world for your company, especially Feng Li, Xiwen Zhang, Zhaokai Meng, Xiaoyun Ma, Shuoshuo Wang, Chen Sun and Mingjie Lu, etc,... The name lists are really endless, please forgive me if I omitted some of my most important friends.

Last but not least, I would thank my family in China for the continuous support, especially my mother and grandmother. It is their lasting encouragement, especially in the later stage that gave me the power to finish the last steps of my Ph.D. work. Of course, I have to give Dr. Ting Li, my fiancee, a big hug, for her continuous support throughout my graduate study.

CONTRIBUTORS AND FUNDING SOURCES

Contributors

This work was supported by a dissertation committee consisting of Professor Finkel'stein [advisor], Professors Pokrovsky and Naugle of the Department of Physics & Astronomy and Professor Kuchment of the Department of Mathematics.

All other work conducted for the dissertation was completed by the student independently.

Funding Sources

Graduate study was supported by the U.S. Department of Energy, Office of Basic Energy Sciences, Division of Materials Sciences and Engineering under Award DE - SC0014154.

NOMENCLATURE

AKL	Altshuler, Kravtsov, and Lerner
ALS	anomalously localized state
B-S	Bethe-Salpeter
DMPK	Dorokhov-Mello-Pereira-Kumar (equations)
DOS	density of states
FDM	finite difference method
F-E	Fal'ko-Efetov
F-M	Fyodorov-Mirlin
FP	flexrual phonon
GOE	Gaussian orthogonal ensemble
GUE	Gaussian unitary ensemble
IPR	inverse participation ratio
K-L	Kravstov-Lerner
LDOS	local density of states
LN	logarithmically-normal
MBL	many body localization
NLSM	nonlinear sigma model
PDE	partial differential equation
PRBM	power-law random banded matrix
P-T	Porter-Thomas
RBM	random banded matrix
RG	renormalization group
RMT	random matrix theory
RPFP	randomly pinned flexrual phonon
SUSY	supersymmetry
TAMU	Texas A&M University
TLCF	two level correlation function
WD	Wigner-Dyson (level statistics)
WL	weak localization
1D, 2D, 3D	one-dimensional, two-dimensional, three-dimensional

TABLE OF CONTENTS

Page

LIST OF FIGURES

FIGURE Page

LIST OF TABLES

TABLE Page

1. INTRODUCTION AND LITERATURE REVIEW

1.1 Transport Properties and Flexural Phonons in Graphene

The transport properties of graphene have attracted much attention [1] since the first discovery of this fascinating material [2]. It is promising for various applications due to its high charge mobility and unique heat conductivity. Theoretically, it was realized long ago, [3, 4, 5] that these transport properties of free-standing (suspended) graphene are strongly influenced by flexural (out-of-plane) vibrational modes which deform the graphene sheet. From the experimental point of view, the effect of flexural phonons (FPs) was clearly observed in heat transport [6, 7]. However, it is a more challenging task to identify the effect of flexural phonons in electronic transport [8, 9]. This is because the contribution of electron-phonon interactions to momentum relaxation remains small even at high temperatures, with the main source of the relaxation being elastic impurities [10]. The dephasing rate τ_ϕ^{-1}, on the other hand, is a more suitable quantity for studying FPs, since static impurities do not cause dephasing. Usually, electron-electron (el-el) interactions, [11, 12, 13, 14, 15, 16] are considered the primary mechanism for dephasing. Because of the quadratic spectrum of FPs, $\omega_k = \alpha k^2$ [17], they are much more populated as compared with in-plane phonons. In addition, the coupling to two FPs considerably increases the phase space available for inelastic processes as compared to the interaction with a single phonon. Thus, in a previous paper [18], we considered the influence due to the interaction of electrons with FPs to the dephasing rate. Though as expected, FPs indeed contribute to the dephasing rate substantially (to the same order of magnitude of what is given by el-el interactions), it still remains unclear why experimental data indicate even higher rate. This is the basic motivation of my PhD research which is presented in this dissertation.

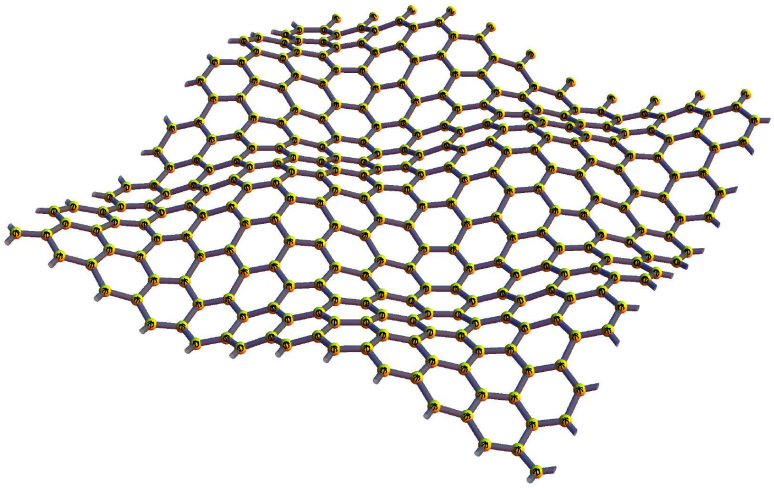

Figure 1.1: Illustration of graphene sample with out-of-plane vibrations.

1.2 From Pinning to Localization

Flexural phonons (FP) have the largest density of states in graphene owing to the softness of these modes. In particular, at low temperatures they store most of the heat. Therefore, it is of principal importance to understand their physics in order to understand thermal properties of graphene. In the dissertation work, we have in mind a graphene sheet on a non-ideal substrate like SiO_2. Here is a quotation from a (randomly chosen) paper by Dean et al., [19]: "Graphene devices on standard SiO_2 substrates are highly disordered, exhibiting characteristics far inferior to the expected intrinsic properties of graphene." A histogram of the height distribution (surface roughness) measured by AFM for SiO_2 presented in this article indicates a Gaussian like distribution with the half-width about 0.4 nm. On the other hand, the distance between graphene and the SiO_2 surface is only about 3Å [20]. Next, the AFM images show that the correlation length of the profile of the corrugated graphene exceeds 10nm. One has also to take into consideration that the interaction of the graphene with a substrate is due to the van der Waals forces. In

the Lennard-Jones potential which is used to describe the van der Waals force, the attractive long-range term decays with distance very rapidly as r^{-6}. We, therefore, come to a model of randomly *pinned-suspended* graphene in which the graphene sheet is pinned at the vicinity of the maximal heights of the substrate where the interaction with the substrate is the strongest, and there are extended areas that float (almost) freely in between. To understand the properties of the pinned-suspended graphene, we have studied the scattering of flexural phonons at the centers of pinning. An essential ingredient of physics of the scattering of flexural phonons is that for a mode with a wave vector k, the scattering cross-section on a rigid obstacle of size a is $\sigma(k) = 4/k$ in the limit of $ka \to 0$ [21, 22]. Taking into consideration that the spectrum of the flexural phonons is quadratic, i.e., velocity is linear in k, one could reach the conclusion that the scattering time in the low-energy limit is constant. This indicates that the mean free path l is constant at small k. According to the Ioffe-Regel criterion for Anderson localization, the physics described above suggests that, $kl \ll 1$, which leads to the localized phase, for k sufficiently small. All the physics described here is in stark contrast to the usual physics of propagation of phonons in random media, where the phonon scattering is usually controlled by the Rayleigh-like scattering. In the latter case, $\tau \to \infty$ when $k \to 0$.

Anderson localization is a key milestone for condensed matter physics. Since Anderson [23] started the topic, there are numerous reviews [24, 25, 26, 27] devoted to the topic. In fact, Anderson localization in phonon systems is not a new idea, for acoustic waves it was extensively studied in 80s [28, 29, 30, 31, 32], where localization was predicted to happen at high energies due to Rayleigh physics. Numerical studies of phonon localization in disordered systems were soon performed [33], whose result supported the theory. The potential well analogy method was also employed to study the phonon localization in disordered systems [34]. The theory was further validated by examining the low temperature thermal conductivity for a variety of glasses [35], where it suggests that

localization of the vibration modes appears. An interesting example for comparison is the localization of the third sound in a $_4$He-film by a disordered substrate[36]. It has been observed that propagating (i.e., delocalized) third sound modes with high frequency are not present on two-dimensional disordered substrate, in direct contrast to what was observed on the ordered substrate. Also, phonon localization has been studied in free standing films [37, 38]. There have been some claims about experimental observation of phonon localization in boron nitride nanotubes [39], but no clear consensus is reached on the issue yet [40]. Phonon localization is difficult to detect compared to the electron localization. The reason is simply in the bosonic character of phonons. However, the focus of study is on the in-plane phonons instead of out-of-plane ones, and the phenomenon of localization will depend critically on inelastic phonon processes, which are the main differences with the scope of this work. In recent years, numerical studies [41] for in-plane phonons for d = 1,2,3 also confirms the theoretical results. More recently, researchers start to apply the idea to the thermal phonons [40] and predicted a thermal conductivity maximum.[42] The idea of phonon localization was further extrapolated to the field of optics [43], where the concept of localization was useful for the creation photonic crystals [44].

In contrast to usual phonons, for flexural phonons, one may expect localization of the low-energy phonons for $\omega(k) < 1/\tau$. Moreover, since it is a two-dimensional system, one may expect that there is a gradual crossover from a strong localization to a regime of weak localization with an exponentially long localization length ξ. In the latter case, one has to compare the localization length with the size of a sample L.

1.3 Statistical Properties for Disordered System

Since the work of Wigner [45], statistical properties of the energy levels and wave functions of complex quantum systems has become a mainstream research direction in condensed matter physics. Wigner treated nuclear spectra based on a statistical point of

view. In order to describe excitation spectra of complex nuclei, he introduced the concept of random matrix theory (RMT), which was further developed by Dyson and Mehta in the early 1960's [46, 47, 48, 49]. A universal form of the spectral correlation functions was predicted, which is dictated entirely by the symmetry class of the system.

In fact, random matrix theory was first brought to mathematical statistics by Wishart [50] in 1928. Later it was realized that the RMT is not restricted to quantum systems, but has a much broader range of applicability, including social science [51] and quantitative finance [52, 53]. In particular, Bohigas, Giannoni, and Schmit [54] made a conjecture that the RMT describes adequately statistical properties of spectra of quantum systems whose classical analogs are chaotic, which is strongly supported by accumulated numerical evidence.

RMT also applies to disordered systems, where a quantum particle (electron, phonon or photon, etc.) moves in a random potential created by some kind of disorder. Gor'kov and Eliashberg [55] conjectured that statistical properties of the energy levels in such a disordered granule can be described by the random matrix theory, which was later proved by Efetov [56]. Efetov developed a very powerful tool for study of the disordered systems — the supersymmetry (SUSY) method (see the review [56] and the book [57]). The main idea is to map the problem under consideration onto a certain deterministic field-theoretical model (supermatrix σ-model), which generates the disorder-averaged correlation functions of the original problem. As was shown, one can use the zero-mode approximation of the σ-model supermatrix field to reproduce precisely Dyson's RMT results.

As has been already mentioned, σ-model formalism is not restricted to quantum systems, but is equally applicable to classical waves. Especially, it was applied in the optics to deal with a problem of intensity distribution of disordered media. By placing the source and detector in disordered media, the distribution of the detected intensity could be described in the leading approximation by the Rayleigh law [58]. Within the diagram-

matic technique, the result can also be reproduced [59]. To study the deviations from the Rayleigh distribution one has to go beyond RMT and consider the diffusive dynamics [60].

1.4 Randomly Pinned Flexural Phonon

It is reasonable to conjecture that σ-model approach will also work for our model of randomly pinned flexural phonons. Unlike in the cold atom or optical experiments, our system is intrinsically 2D, which is more close to the critical dimension of the σ-model, and in principle, could give a better chance for studying 2D localization physics. For disordered electrons, theory connects the behavior of various physical quantities in 2D with the value of the conductance, see the Ref. [61] for a review.

It turned out that the model of pinned sites is very convenient for studying the phenomenon of localization in two dimensions. We considered "samples" of the size up to 200×200 sites, with random realization of 5%, 10% and 20% of pinned sites. We first calculated numerically the same quantities for pinned flexural phonons, connected them with g_{ph}, and found a reasonable agreement with the theoretical predictions for the disordered electrons in the case of the orthogonal class of universality. We believe that the reason for the observed universal behavior is that the flexural phonons in the lattice with pinned sites are eventually described the same Non-Linear σ-Model (NLSM) as disordered electrons.

We then studied Inverse Participation Ratio (IPR) depending on the energy. From our simulations, it is absolutely obvious that low energy modes are localized: the IPR does not depend on the lattice length. For higher energies, the behavior changes, because localization length $\xi \gg L$. We were interested in studying the flexural phonons in this region. Questions that will be addressed: "Is there a transition at certain energy (the metal-insulator transition), or there is a crossover from strong to weak localization? If we compare with the electrons propagating in a disordered lattice, will the observed behavior, generally speaking, be the same or different?" These questions make sense because for

pinned phonons there is no analogue of the on-site disordered potential in the Anderson model [23]. Instead, there is the concentration of pinned sites. Furthermore, the flexural phonons are described by the square of the Laplacian (∇^4), rather than by the Laplacian in the case of electrons. Refs. [62, 63] also show that, a priori, one could not tell for sure which symmetry class will be responsible for the physics.

1.5 Outline of the Dissertation

This dissertation is thus organized as follows. In Chapter 1, we briefly introduce the related concepts and make a literature review. In Chapter 2 we derive the basic properties of flexural phonons and their scattering with pinning centers, and make qualitative analysis why Anderson localization is possible there. In Chapter 3, we layout the numerical scheme of our study and explain the strategy of the dissertation work. Starting from Chapter 4, we describe the various statistical properties of our model and compare the numerical results with the existing theory. In particular, we study the energy level statistics in Chapter 4, followed by the wave function statistics in Chapter 5. In Chapter 6, we show the results for the asymptotic tails of the wave function distribution, followed by the statistical properties of IPR in Chapter 7. Also, we demonstrate there clearly the multifractal property of the system and use it as a means to extract phonon conductance g_{ph}. In Chapter 8, we come back to the problem of dephasing and explain the contribution of pinned FPs to the dephasing rate. Finally, in Chapter 9 we summarize the dissertation work and assess the impact of research.

2. FLEXURAL PHONON IN GRAPHENE

2.1 Flexural Phonons

We define the displacement vector in Monge gauge $\mathbf{u} = (u_x, u_y, h)$ and the full non-linear strain tensor as: $u_{ij} = \frac{1}{2}(\partial_i u_j + \partial_j u_i + \partial_i h \partial_j h)$. The free energy of the graphene membrane in the harmonic approximation can be expressed as

$$\mathcal{H}_{ph} = \frac{1}{2}\int d^2x \left(\lambda u_{ii}^2 + 2\mu u_{ij}^2\right) + \frac{\kappa}{2}\int d^2x \left(\nabla^2 h\right)^2,$$

where the first term describes the elastic energy and, the second term, the bending energy [64]. The Flexural Phonon mode refers to the out-of-plane displacement h here, and it is well described by the Hamiltonian:

$$\mathcal{H}_{FP} = \frac{\kappa}{2}\int d^2x \left(\nabla^2 h\right)^2. \tag{2.1}$$

Here $\kappa \sim 1eV$ is the bending energy of graphene. One can write the out-of-plane displacement as $h(\mathbf{r}, t) = -i\sum_{\mathbf{k}} \phi_{\mathbf{k}}(t)\, e^{i\mathbf{k}\cdot\mathbf{r}}$, where $\phi_{\mathbf{k}}$ is the phonon operator. Thus, the bare retarded phonon green's function can be written as

$$D_0^{R(A)} = \frac{1}{2\rho\omega_q}\left(\frac{1}{\omega - \omega_q \pm i\delta} - \frac{1}{\omega + \omega_q \pm i\delta}\right). \tag{2.2}$$

Here ρ is the density of the graphene and $\omega_q = \alpha q^2$ is the flexural phonon dispersion [17].

2.2 Scattering of Flexural Phonons in Graphene

2.2.1 Interaction of FPs with the Pinning Centers

As has been discussed in the introduction, we are interested in the scattering of flexural phonons from the attached area of substrate. Let us comment upon the graphene layer deposited on the top of the corrugated substrate. Naively, the membrane-like layer either follows the substrate or hovers over the surface at some distance. Measurements of the Ref. [65] with the use of cantilevers indicate, however, towards a possibility of the detaching a graphene sheet from a substrate to relieve its strain by slipping. (This is manifest by straightening of the cantilever.) In the case of the SiO_2 substrate, both experiment and theory agree that for the typical magnitude for corrugations, the graphene layer is partially detached from the substrate. Moreover, the theoretical considerations [66, 67] justify the use of a contact force that is finite when graphene is conforming to the substrate and zero otherwise. Factors that may be particular for the SiO_2 substrate are charge-donating impurities below the graphene layer [68, 69, 70], and water molecules which may lie between graphene and the substrate [71, 72]. The basic experimental facts which lead to the conclusion that graphene layer deposited on SiO_2 is partly freely suspended are as follows [73]. The long-range corrugation of the substrate with the correlation length of about 25nm is also visible on the graphene sheet, but with a smaller amplitude than on the substrate. Mesoscopic corrugations with a smaller length of about 15nm not induced by the substrate were also identified. These short range corrugations are similar in height and wavelength to the ones observed on suspended graphene [74, 75].

We thus conclude that the scattering is similar to the scattering from a rigid obstacle. We will model the effect of pinning centers as a kind of phonon-impurity scattering, with the potential in a similar form to the electron-impurity scattering. Thus, the phonon green's function acquires an imaginary part due to self-consistent Born approximation, which we

denote as $\Sigma^R(\omega, q) \equiv -i/2\tau$, where $\tau(\omega, q)^{-1} = n_i v(k) \sigma_{fl}$ is the FP's scattering rate with pinning center. According to Ref. [21, 22] (see details in Section 3.1), the scattering cross section of the interaction is

$$\sigma_{fl}(\mathbf{k}) = 4/k. \tag{2.3}$$

Thus, our relaxation rate above can be written as

$$\tau^{-1} = 4 n_i \alpha, \tag{2.4}$$

where n_i is the concentration of the impurity (pinning centers) and $v(k) = 2\alpha k$ is the group velocity of the FPs.

One can try to write a Bethe-Salpeter (B-S) equation for this kind of impurity scattering in a similar manner as for the electron-impurity problem [76]. Thus, we denote the diffuson as P_d, and the B-S equation can be expressed as

$$\begin{aligned} P_d(\Omega, q) &= 8\alpha\rho^2\omega^2\tau^{-1} \\ &+ \frac{8\alpha\rho^2\omega^2\tau^{-1}}{V} \sum_k D^R(\omega + \Omega/2, k + q/2) D^A(\omega - \Omega/2, k - q/2) P_d(\Omega, q). \end{aligned}$$

Let us denote here $U^2 \equiv 8\alpha\rho^2\omega^2\tau^{-1}$. To perform analytical calculation we will restrict ourselves in the regime of $\omega \gg \tau^{-1} \sim \Omega$ and $q \ll k$ (which is equivalent to $\omega_q \ll \omega$). Thus, one can follow similar procedure as in the Ref. [77] and get

$$\frac{1}{V} \sum_k D^R(\omega_1, k + q/2) D^A(\omega_2, k - q/2) = \frac{\nu_p}{4\rho^2} \frac{2\pi}{\omega^2} \frac{1}{S},$$

where

$$S \equiv \sqrt{(vq)^2 + (\tau^{-1} + i\Omega)^2}. \tag{2.5}$$

Here we have introduced the flexural phonon density of states (DOS) $\nu_p = \frac{1}{4\pi\alpha}$. So, the equation for the diffusion pole (diffuson) is

$$P_d(\Omega, q) = U^2 + \frac{1}{S\tau} P_d(\Omega, q).$$

Solving for P_d, we get $P_d(\Omega, q) = \frac{U^2}{1-(S\tau)^{-1}}$. In the dirty limit where $\tau^{-1} \gg \Omega, Dq^2$, one can restore the familiar form of the diffusion pole:

$$P_d(\Omega, q) = \frac{U^2\tau^{-1}}{Dq^2 + i\Omega}. \tag{2.6}$$

Here $D = D(\omega, \Omega) = \frac{1}{2}v^2\tau = 2\alpha\omega\tau$ is the diffusion constant for FPs. Similarly, in the regime of $k \gg q$, the vertex correction can also be written as:

$$\Lambda_{\Omega,\omega,q}\mathbf{k}^2 = \mathbf{k}^2 + \frac{\omega}{\alpha} \times \Lambda_{\Omega,\omega,q}(S\tau)^{-1},$$

where $\Lambda_{\Omega,\omega,q}$ is the vertex correction factor. The above equation leads to $\Lambda_{\Omega,\omega,q} = \frac{1}{1-(S\tau)^{-1}}$. Again in the dirty limit, one can recover a more familiar form for the vertex correction

$$\Lambda_{\Omega,\omega,q} = \frac{\tau^{-1}}{Dq^2 + i\Omega}. \tag{2.7}$$

2.2.2 About the Anharmonic and Rippling Effects

Here we examine the situation when there is some finite rippling of the membrane. Rippling and anharmonic effects mixes in-plane and out-of-plane flexural phonons and it is known to be a major source of phonon scattering. Rippling takes place whenever there is some finite interaction with the substrate. It is well known that due to this mixing the phonon spectrum is renormalized [78, 79, 17, 80]. Therefore one may concern that a pure quadratic FP picture of phonon propagation is incomplete. However, this is not necessarily

true in our case, and the reasons are two fold as explained below.

(i). According to the analysis of Ref. [81], the momenta at which the anharmonicity becomes relevant for FPs are about 5 times smaller than the thermal momentum. Therefore, at any temperature only a small fraction of the phase space is occupied by the FPs for which effects of anharmonicity are relevant.

(ii). In the work of Ref. [82], the modeling of the surface gave ripples of the size 7nm at $T = 300$K (see also Refs. [83, 80]). This means that at temperatures about 1K, the size of the ripples will be very large, about 100nm, and correspondingly they will be too smooth to influence motion of the FPs which we are interested in. On the other hand, small-size built in ripples, which themselves originate as a result of pinning the graphene sheet, are not different for the FPs from the regions attached to the substrate. They will not allow the low-energy FPs to enter the area they occupy. As a result, such ripples will participate in the localization of the FPs along with attached regions. Thus, small size ripples do not interfere much in propagation of the long wavelength FPs which we are interested in, but may favor localization of the FPs. The large-size ripples are too smooth to influence the FPs. Furthermore, some of the ripples can be considered as a condensate of the localized FPs.

Therefore, we can safely treat our flexural phonons to be decoupled from other modes. Finally, let us comment upon the origin of the barrier which at low temperatures does not let the low-energy FP enter a region of attachment. The reason is simple: FPs oscillate against the surface of the substrate. In the areas of attachments where the distance of the sheet from the substrate is smallest and the interaction with the substrate strongest, they become similar to the optical phonons. The enhancement of the phonon's energy acts as a barrier which does not let the low energy phonons to enter the area of attachment. (The rigid obstacle acts in a similar way.) Of course, for high enough temperatures, the FPs may have enough energy to overcome the barrier. Moreover, we believe that the observed

rapid vanishing of the thermal conductivity below 80K [7] may indicate that FPs of the corresponding energy become ineffective as means of thermal contact with the substrate.

2.3 Toward Anderson Localization of the Flexural Phonons

2.3.1 Important Energy Scales

We have noticed from the above calculation that all the ω integral sit at the lower limit, which is τ^{-1}. This is a manual cut-off, below which the Born approximation is not valid for the retarded green's function. Thus, our field theoretical approach could not be invoked at this regime. However, the result of the calculations indicate that the regime of $\omega < \tau^{-1}$ is of critical importance. Thus, similar as the electron-impurity problem, we propose that investigating the localization regime for FPs will be necessary. Before we introduce any quantitative and qualitative argument, it is a convenient place here to introduce several important energy scales that will be used throughout the rest of the dissertation. We list them here in the increasing order of values (and we use $\hbar = 1$ throughout the dissertation):

1. Mean level spacing Δ, which is obviously defined via its name: the simple unweighted average of the level spacing. This is the smallest energy scale we will deal with, below which full quantum theory is needed.

2. Thouless energy $E_c \equiv D/L^2$. This energy is the inverse of the characteristic time $\tau_D = L^2/D$ for a particle to diffuse through the sample, where D is the diffusion coefficient. For energies $\Delta \leq \omega \leq E_c$, this regime is called ergodic regime, see Section 4.2 for details.

3. The scattering time of FPs due to the pinning centerτ^{-1}, which is defined above in details. For energies $E_c \leq \omega \leq \tau^{-1}$, the regime is called the diffusive regime, see Section 4.3 for details. If the energy is larger than τ^{-1}, one goes to the so called ballistic regime, which is beyond our discussion here.

Similar to the electronic system, one can also introduce the dimensionless conductance for phonon systems:

$$g_{ph} \equiv \frac{1}{2} k_F l = \frac{1}{2} E\tau = 2\pi E_c/\Delta. \tag{2.8}$$

To figure out the criteria for the localization of FPs to happen, we compare the Thouless energy with the mean level spacing:

$$\frac{g_{ph}}{2\pi} = \frac{E_c}{\Delta} = \frac{D/L^2}{1/\nu_{ph} L^2} = \frac{2\alpha\omega\tau}{4\pi\alpha} \sim \frac{\omega\tau}{2\pi} \tag{2.9}$$

So, for $\omega\tau \ll 1$, the flexural phonon should be in the localization regime. Also, from here on, we will not write the subscript ph, and just call g_{ph} as g.

2.3.2 Anderson Localization for FPs in Graphene

We argue that the graphene layer placed on the top of the corrugated SiO_2 substrate may indeed provide a unique opportunity to observe Anderson localization for the flexural phonons (the FPs). To get an idea, let us recall the known facts about a long-wave acoustic wave scattering on a cylinder. The output depends drastically on the boundary conditions for the velocity potential Φ on the surface of the cylinder.[84] If the velocity component normal to the surface of the cylinder vanishes, i.e., $\partial_r \Phi|_{r=a} = 0$, the scattering cross-section σ_R is proportional to $a(ka)^3$, where a is the radius of the cylinder and k is the wave vector. This is the conventional Rayleigh scattering result [85] for two dimensional $(2d)$ geometry. However, when pressure is constant, the boundary condition reads $\Phi(a) = 0$, and this influences forcefully the scattering. Unlike the Rayleigh scattering, the zero angular harmonic is involved, and as a result, the cross section diverges at small k as $\propto (k \ln^2 \frac{1}{ka})^{-1}$. (The same takes place for an electro-magnetic wave scattering on a metallic cylinder.)

In graphene, the substrate cannot scatter effectively the usual acoustic waves, longi-

tudinal and transverse, because graphene itself is one of the most rigid substances. The other things are the out of plane phonons. From the analysis of intrinsic and extrinsic corrugation of monolayer graphene deposited on the SiO_2 substrate, it has been concluded that in this system, the layer is suspended between hills of the substrate [20, 86, 73, 69]. We have checked that scattering of the FPs from areas attached to the substrate is similar to the scattering from a rigid obstacle [21]. The zero harmonic is also involved, and the scattering cross-section diverges as $\sigma_{fl} = 4/k$. As a result, the elastic scattering rate $1/\tau$ for low-energy FPs exceeds their energy. One may, therefore, expect localization for low-energy FP modes. This is in strike contrast with localization of acoustic modes which is known to happen only at high enough frequency [87, 28, 88, 29, 30, 89, 41].

3. NUMERICAL SCHEME

3.1 Randomly Pinned FP Model

In this work we study the statistical properties of the out of plane excitation in a model of a randomly pinned-suspended flexible sheet, see figure 3.1. Whether pinning centers are located in the vicinity of the maximal heights of the substrate where the interaction with the layer is the strongest, or there are charges on the substrate which interact strongly with their images, will be not important for our purposes. For simplicity, it will be assumed that centers of pinning are located randomly. First of all, we are interested in the scattering rate $\tau^{-1} = v\sigma_{fl}n_i$, where n_i is concentration of pinning centers. As we have already discussed, the scattering cross-section on a rigid obstacle is $4/k$. Taking into consideration that the spectrum of the flexural phonons $\omega(k) = \alpha k^2$ is quadratic, i.e., velocity is linear in k, one obtains a scattering time τ that is finite in the low-energy limit. Thus, in contrast to acoustic phonons, for flexural phonons, one may expect localization of the low-energy modes with $\omega(k) < \tau^{-1}$.

Notice that the point here is not in flexural phonons as such, but it is their softness that allows to realize the scattering by effectively rigid obstacles which leads to a non-vanishing scattering rate in the limit of small energy $\omega(k)$. Let us touch upon this point in more detail. Usually by a rigid obstacle one understands an inclusion with Young's modulus much higher than that in the surrounding area. For graphene, which itself is very rigid, this is not an issue. However, the pinning potential introduces a barrier with a finite height for the flexural modes:

$$\kappa\nabla^4 h(\boldsymbol{r},t) + \rho\frac{\partial^2 h(\boldsymbol{r},t)}{\partial t^2} = -\rho\omega_0^2(\boldsymbol{r})h(\boldsymbol{r},t), \tag{3.1}$$

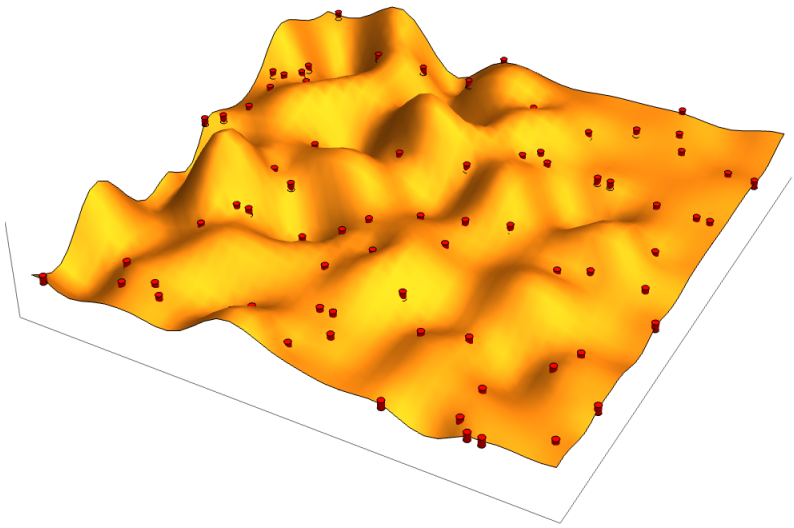

Figure 3.1: An elastic flexible 2D sheet on a substrate. Pinning centers are indicated as red cylinders.

Here $h(\boldsymbol{r}, t)$ is displacement in the out of plane direction; the term describing the barrier is on the right-hand side of the above equation. As a result, a flexural phonon with an energy smaller than ω_0 cannot enter the area of pinning. We have checked that such an inclusion is equivalent to a rigid obstacle. According to Ref. [21, 22], the scattering cross-section of the FP by a rigid obstacle of the radius a equals $\sigma_{fl} = \frac{4}{k} f(ka)$ for not small ka, where k is the characteristic momentum of the phonon and $f(z)$ is given by the following expression:

$$f(z) = \mathrm{Re} \sum_{n=0}^{\infty} \varepsilon_n \frac{J_n(z)K_n'(z) - J_n'(z)K_n(z)}{H_n^{(1)}(z)K_n'(z) - H_n^{(1)\prime}(z)K_n(z)}, \tag{3.2}$$

where $\varepsilon_0 = 1,\ \varepsilon_{n>0} = 2$ and $J_n; K_n; H_n$ are Bessel function of the first kind, modified Bessel function and Hankel function respectively. The function $f(z)$ with asymptotes $f(0) = 1$ and $f(z \gg 1) \approx z$ is shown in the Fig. 3.2. Interestingly enough, for $ka \gg 1$, $f(ka) \approx ka$. The limiting cross-section is $\approx 4a$, i.e., twice larger than the width of the obstacle [84]. (This is, of course, valid only when the energy of the phonon is much less

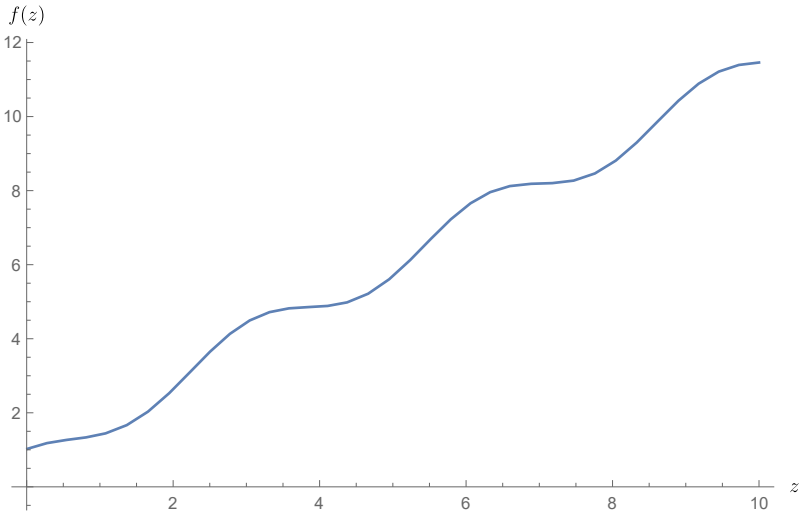

Figure 3.2: Function $f(z)$ determining the scattering cross-section, $\sigma_{fl} = \frac{4}{k} f(ka)$.

than the pinning potential, i.e., $\omega(k) \ll \omega_0$.)

3.2 Matrix Construction

To understand the general properties of flexural phonons in the presence of random scatters, we study a model of random pinning centers. Relying on the existing experimental data [90], we assume that the pinning potential ω_0 is about few meV. Hence, at the pinning centers the graphene sheet can be considered as completely attached. More studies on membrane pinning due to disordered substrate can be found in Ref. [91]. Here we will differentiate our research with the one in Ref. [92]. In that paper, the graphene was also considered to be attached to the substrate randomly, but the author only considered the stretching effect and completely ignore the bending waves, i.e., FPs. We solve for eigenmodes of discretized LHS of Eq. (3.1) with condition $h = 0$ at randomly chosen pinned sites, that is

$$\kappa \nabla^4 h\left(x, y\right) - \rho \omega^2 h\left(x, y\right) = 0. \tag{3.3}$$

We solve for our FP eigenmodes on a 2D square lattice using the finite difference method for partial differential equation (PDE) (3.3). As is well know, the finite difference method (FDM) [93] is just to discretize the domain of the PDE and then set a large sparse matrix to be solved by computer. Using the 12 point stencil formula in Ref. [94], we can represent the PDE in our problem as

$$\begin{aligned} -\frac{\rho a^4\omega^2}{\kappa}h(x,y) + 20h(x,y) + \\ h(x-2,y) + h(x+2,y) + h(x,y-2) + h(x,y+2) + \\ 2h(x-1,y-1) + 2h(x+1,y+1) + 2h(x-1,y+1) + 2h(x+1,y-1) + \\ [-8h(x-1,y) - 8h(x+1,y) - 8h(x,y-1) - 8h(x,y+1)] = 0, \end{aligned} \tag{3.4}$$

where a is the distance for which the continuous media description is valid (detail estimation is given below), and ω is the energy of the flexural phonon. Using a pictorial representation, one can write the laplacian square as:

$$\nabla^4 h = \frac{1}{a^4}\begin{Bmatrix} & & 1 & & \\ & 2 & -8 & 2 & \\ 1 & -8 & 20 & -8 & 1 \\ & 2 & -8 & 2 & \\ & & 1 & & \end{Bmatrix} h. \tag{3.5}$$

In order to match what could be represented in computer programs, we will use a row

major notation to set up a matrix for FDM:

$$\begin{aligned} -\frac{\rho a^4\omega^2}{\kappa}h(j) + 20h(j) + \\ h(j-2) + h(j+2) + h(j-2n) + h(j+2n) + \\ 2h(j-1-n) + 2h(j+1+n) + 2h(j-1+n) + 2h(j+1-n) + \\ [-8h(j-1) - 8h(j+1) - 8h(j-n) - 8h(j+n)] = 0, \end{aligned} \tag{3.6}$$

In what follows, we write energy in the lattice unit, that is $E = \omega/\omega_a$, where

$$\omega_a = a^{-2}\sqrt{\kappa/\rho} = \alpha a^{-2}$$

is close to the Debye frequency for the FPs.

3.2.1 Random Pinning

The random pinning is realized very conveniently in this model through setting

$$h(j) \mid_{pinned} = 0. \tag{3.7}$$

The pinned sites are chosen independently with uniform probability distribution $\mathcal{P}(j) = 1/N$, where N is the number of sites in the calculation. As is well known, Anderson localization is confirmed for the Laplacian operator for the random onsite potentials. It is less known about the localization properties of the ∇^4 operators, with the boundary equation shown above.

Note that one pinned site represents an attached area of the size $\approx a$. According to discussed experiments in Section 2.3.2, we estimate the size of an attached area to be $a \simeq 7nm$. The typical distance between the pinning centers a_i is around $20nm$; we will assume that $n_i = a_i^{-2}$. The representative fraction of the pinned sites is $(a/a_i)^2 \simeq (7/20)^2 \approx$

12.5%. Correspondingly, we studied "samples" with $5\% - 20\%$ of the pinned sites to determine the statistical properties of the eigenmodes and eigenvalues. In what follows, we measure the energy eigenvalues E in units of α/a^2 which approximately equals 0.08K for the parameters mentioned above. We found out that typical energy scale for strong localization for concentration of pinned sites in the range $5\% - 20\%$ is a fraction of 1K. Eigenmodes at three representative energies are shown in the figure 3.6 for a 200×200 sample.

3.3 Boundary Conditions

We still need to fix the boundary conditions for the PDE, which is done in the following two ways.

3.3.1 Dirichlet Boundary Conditions

To implement the Dirichlet boundary condition, one can set the boundary points of a square lattice as $h(:,0) = h(0,:) = h(:,N) = h(N,:) = 0$. Here ":" represent an arbitrary integer number $n \in [0, N]$. For all other points on the lattice, we keep their relationship as is in Eq. (3.6). Thus, one can obtain a set of linear equations, which combines to the form of

$$A\boldsymbol{h} = \mathbf{0},$$

where $\boldsymbol{h}$ is the column vector satisfying $\boldsymbol{h}_j = h(j)$. A is the matrix representation of the discretized differential operator governing Eq. (3.3), and below is an example of the resulting sparse matrix A for a 6×6 square lattice.

3.3.2 Periodic Boundary Conditions

We fix the boundary condition by setting end points of a square lattice as $h(:,0) = h(:,N)$ and $h(0,:) = h(N,:)$, which leads to the following equation:

```
 1  20  -8   1   0  -8   2   0   0   1   0   0   0   0   0   0   0
 2  -8  20  -8   1   2  -8   2   0   0   1   0   0   0   0   0   0
 3   1  -8  20  -8   0   2  -8   2   0   0   1   0   0   0   0   0
 4   0   1  -8  20   0   0   2  -8   0   0   0   1   0   0   0   0
 5  -8   2   0   0  20  -8   1   0  -8   2   0   0   1   0   0   0
 6   2  -8   2   0  -8  20  -8   1   2  -8   2   0   0   1   0   0
 7   0   2  -8   2   1  -8  20  -8   0   2  -8   2   0   0   1   0
 8   0   0   2  -8   0   1  -8  20   0   0   2  -8   0   0   0   1
 9   1   0   0   0  -8   2   0   0  20  -8   1   0  -8   2   0   0
10   0   1   0   0   2  -8   2   0  -8  20  -8   1   2  -8   2   0
11   0   0   1   0   0   2  -8   2   1  -8  20  -8   0   2  -8   2
12   0   0   0   1   0   0   2  -8   0   1  -8  20   0   0   2  -8
13   0   0   0   0   1   0   0   0  -8   2   0   0  20  -8   1   0
14   0   0   0   0   0   1   0   0   2  -8   2   0  -8  20  -8   1
15   0   0   0   0   0   0   1   0   0   2  -8   2   1  -8  20  -8
16   0   0   0   0   0   0   0   1   0   0   2  -8   0   1  -8  20
17
```

Figure 3.3: A sample sparse matrix representing a 6×6 square lattice with Dirichlet boundary conditions. For any reasonable sized problem, the kind of sparse matrix is typically solved numerically.

$$
\begin{aligned}
&-a^4\omega^2 h(j) + 20h(j) + \\
&h(j-2|n) + h(j+2|n) + h(j-2n|N^2) + h(j+2n|N^2) + \\
&2h(j-1-n|n,n^2) + 2h(j+1+n|n,N) + \\
&2h(j-1+n|n,N) + 2h(j+1-n|n,N) + \\
&\left[-8h(j-1|n) - 8h(j+1|n) - 8h(j-n|N^2) - 8h(j+n|N^2)\right] = 0. \qquad (3.8)
\end{aligned}
$$

Here the symbol $h(i|n)$ represents taking the mod n on i. One can obtain a similar sparse matrix A as in Fig. 3.3. Due to the sensitivity of the correlation functions to the boundary condition (see Ref. [27] and references there in), we will be using the periodic boundary conditions throughout the dissertation.

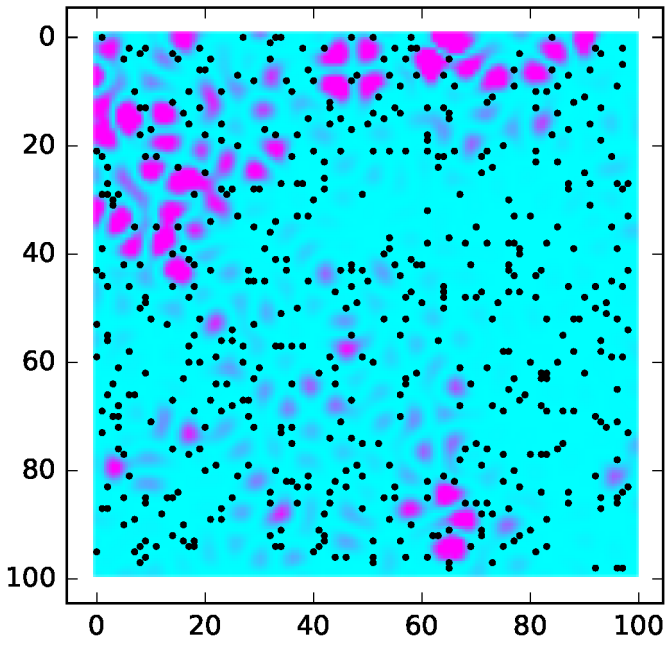

Figure 3.4: The intensity of the phonon wavefunctions h^2 for 5% of the pinned sites at $E = 0.5$. Pinned sites are indicated as black dots.

3.4 Numerical Solving the Sparse Matrix

We will solve this matrix equation (3.8) numerically with a Python program (attached in the appendix). For the consideration of speed, reliability, and implementation convenience [95], we choose to use the modern implicitly restarted Arnoldi method for diagonalizing matrices. With the help of TAMU High Performance Computing facility, we were able to solve "samples" of the sizes from 30×30 up to 200×200 sites, with random realizations of 5%, 10% and 20% of the pinned sites and up to 20000 sample averaging. We show here a 2D sample configuration of the pinned disorder (in black), for a 100×100 lattice along with the density plot for wavefunctions. The Figure 3.4 shows a localized behavior of the wavefunctions at very low energy, while the Figure 3.5's energy is higher and it shows a much more extended behavior for the wavefunctions. From our simulations, it

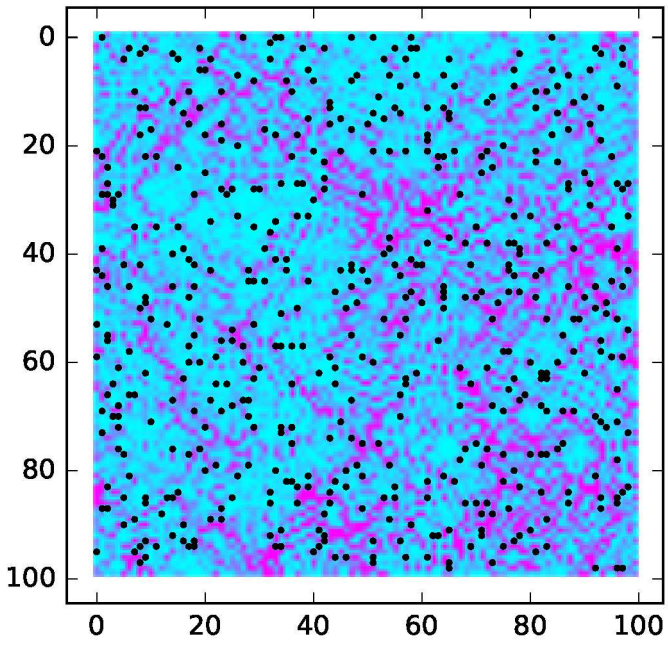

Figure 3.5: The intensity of the phonon wavefunctions for 5% of the pinned sites at $E \approx 3.1$.

is clear that low-energy modes are localized: the wavefunction is isolated and the inverse participation ration (IPR) scales with the sample size to a finite value, see figure 7.2 for details. For higher energies, the behavior of the wave functions changes, see Fig. 3.6, because the localization length ξ starts to exceed the sample size. Here is a sample 3D plot for the wave functions of a 200×200 lattice for three different energies, and the height is an indication of wavefunction intensity.

3.5 Density of States (DOS)

According to the numerical recipe of Eq. (3.6), and by translating it to equivalent tight binding language in momentum space (denoted by $\boldsymbol{k}$), the equation (3.6) actually describe the following Hamiltonian on a square lattice

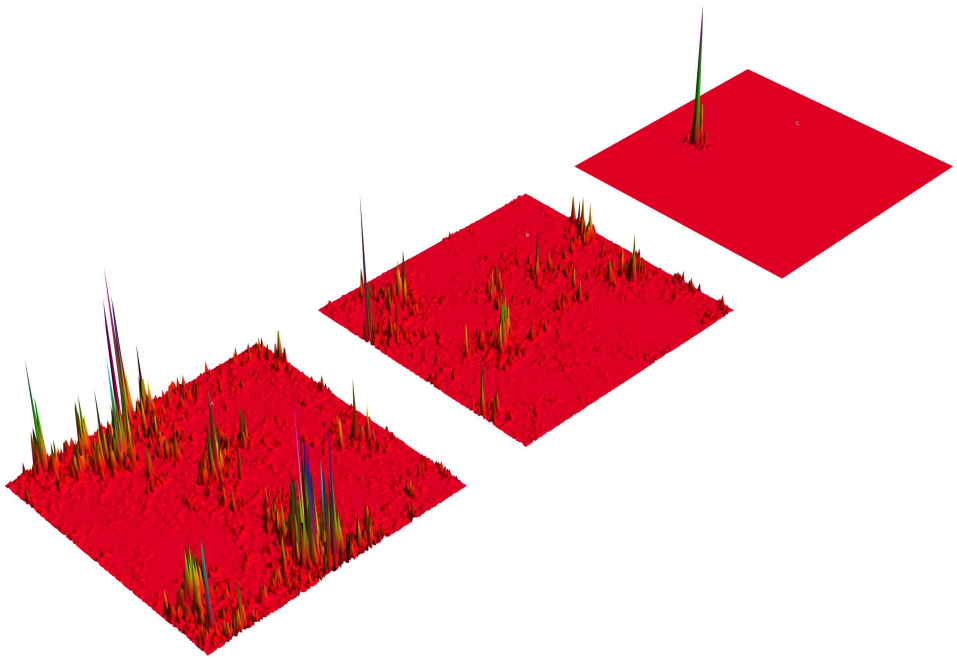

Figure 3.6: Phonon wavefunctions for three different energies. In the upper panel a strongly localized state with an energy $E < 1/\tau$ is shown. In two lower panels the density profiles of two "metallic" states with $E > 1/\tau$ are presented. A multifractal character of the eigenstates with the length of localization $\xi \gg L$ is clearly seen.

$$\frac{\rho a^2}{\kappa} H^2(\boldsymbol{k}) = 20 - 16\cos(k_x a) - 16\cos(k_y a) + 2\cos(2k_y a) + 2\cos(2k_x a)$$
$$+ 4\cos(k_x a - k_y a) + 4\cos(k_x a + k_y a),$$

whose expansion at low energies $\boldsymbol{k} \to \mathbf{0}$ is (Setting $a = \rho = \kappa = 1$, which defines the lattice unit.):

$$H_0^2(\boldsymbol{k}) = (k_x^2 + k_y^2)^2.$$

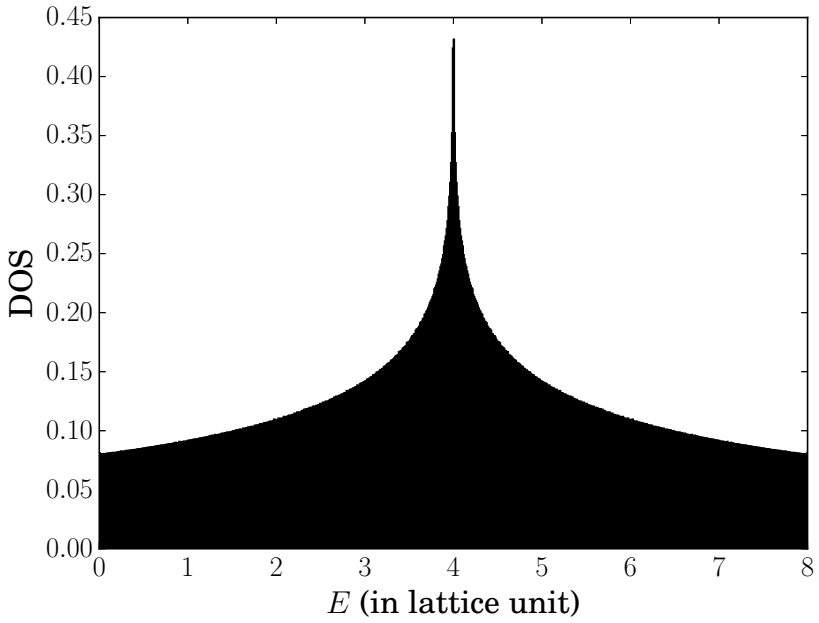

Figure 3.7: The theoretical density of states of clean flexural phonon. It exhibits a Van Hove singularity in the middle of the energy spectrum.

The analytic DOS ν is defined as

$$\nu(E) = V^{-1} \sum_{n} \delta(E - \epsilon_n),$$

whose result is shown in Figure 3.7. One can see that the Van Hove singularity occurs at $k_x = k_y = \pi$, and the corresponding energy is $H^2(\pi, \pi) = 16$. Thus, the Van Hove singularity occurs at $E = 4$ (in lattice unit). As one can see from the figure, the Van Hove singularity occurs in the middle of the energy spectrum. Moreover, the DOS distribution function was studied in Ref. [96].

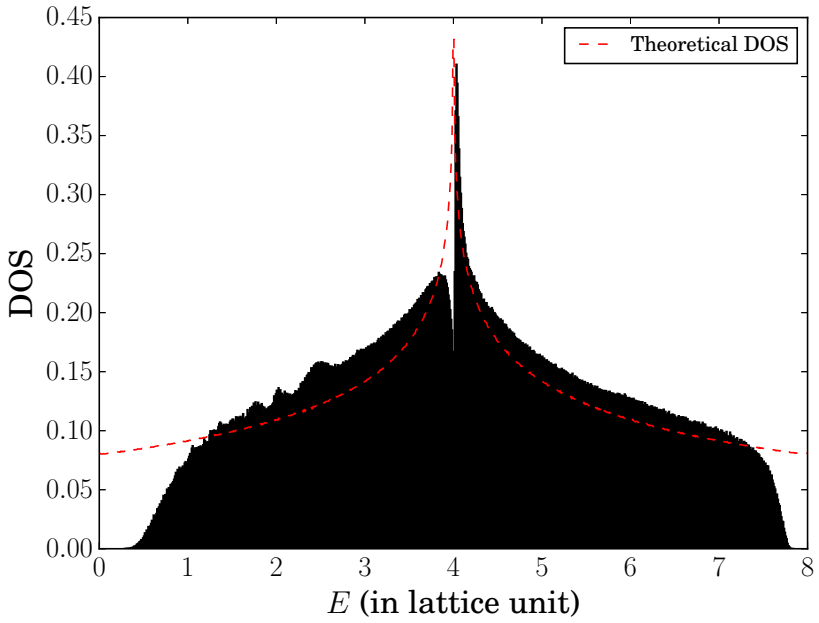

Figure 3.8: Normalized DOS for randomly pinned FPs after disorder averaging. Obtained from a sample of 140×140 lattice with 20% disorder concentration, after 100 disorder averaging.

3.5.1 Numerical Results of DOS

In Figure 3.8, we show the numerical result for the DOS of our randomly pinned FP system. Similar behavior could also be found in the 2D Anderson model with random hopping [97]. The singularity in the band center is not as much quickly suppressed with increasing disorder strength compared to the situation in the Anderson model. However, the behavior for the band edges are similar, with slightly more asymmetric edges in our case. A relation between DOS and localization range in 1D system could be found in Ref. [98].

3.6 Road Map and Strategy

Following questions will be addressed now for disordered flexural phonons: Is there a transition to delocalized states at a certain energy (i.e., the "metal-insulator" transition with the mobility edge), or there is a crossover from strong to weak localization? If to compare with the electrons propagating in a disordered lattice (Anderson model), will the observed behavior statistically the same or different? To figure this out, we will numerically study the dependence of the various statistical properties of the above model on the sample size L for various phonon energies. Using the conclusions of existing theory for electronic systems as an anchor point, such as the scaling analysis, diagramatics, and supersymmetry nonlinear σ-models [99], we will compare the output of numerical simulations with those conclusions. The idea is that the universal feature of the system would not change under details such as symmetry groups and localization properties. We are using well-established theory for electron systems to check how our phononic model behaves under the presence of pinning centers.

We are particularly interested in studying the flexural phonons in the region when localization length $\xi \gg L$. For comparison, note that although the 2D Anderson model does not constitute a truly critical system, thanks to exponentially large localization length at $g \gg 1$, the criticality takes place in a very broad range of the system sizes, $L \ll \xi$. Therefore, 2D samples with large g share many common properties with systems at the critical point of the metal-insulator transition. As we shall see, similar physics holds also for our system of FPs.

4. ENERGY LEVEL STATISTICS

4.1 Important Quantities in Energy Level Statistics

Several quantities are able to measure the fluctuations of energy levels ϵ_n. In order to characterize the distribution of eigen-energies, we first layout all the definition of relevant quantities that we will encounter in the following calculation:

1. The distribution function of the nearest neighbor level spacing $P(s)$.

2. The probability distribution function of $P(n, s)$: The probability of two levels separated by n other levels is equal to s.

3. The two-level correlation function of the Density of States (DOS), which is defined as:

$$R(\omega) = \frac{\langle \nu(E - \omega/2)\nu(E + \omega/2)\rangle}{\langle \nu \rangle^2} - 1, \tag{4.1}$$

where $\nu(E) = V^{-1}\sum_n \delta(E - \epsilon_n)$ is the density of states. Here ϵ_n is the eigen-eneriges of our Hamiltonian. The average $\langle ... \rangle$ is taken either over a given spectrum by considering different energy intervals or over different realizations of disorder (ergodic hypothesis [54, 100]). In the numerical simulation, we take the latter definition. $\langle \nu \rangle$ is the average density of states, it is related to Δ, the mean level-spacing as $\langle \nu \rangle = \frac{1}{\Delta V}$. An important relation between $R(s \equiv \omega/\Delta)$ and $P(n, s)$ is:

$$R(s) = \delta(s) + \sum_n P(n, s) - 1.$$

4. The number variance $\Sigma^2(\omega)$:

$$\Sigma^2(\langle n(E)\rangle, \omega) = \langle \delta n^2(E)\rangle = \langle n^2(E)\rangle - \langle n(E)\rangle^2. \tag{4.2}$$

It measures the fluctuation of the number of levels $n(E)$ in a strip of width ω. In $2d$ it becomes especially interesting to study the level number variance, $\Sigma^2(\omega, \Omega)$, which is a two-level correlation function characterizing the fluctuations of the number of levels n in a strip of width Ω around the energy ω. The reason why it is of particular interest is that, in contrast to $d = 1$ and 3, in two dimensions this quantity is directly related to the weak localization (WL) corrections [101].

5. The form factor $K(t)$, which is the Fourier transform of $R(\omega)$:

$$K(t) = \frac{1}{2\pi} \int_{-\infty}^{\infty} R(\omega) e^{-i\omega t} d\omega.$$

This form factor is closely related to the integrated return probability $Z(t)$ that appears in the dephasing problem by the following relation [102]:

$$K(t) = \frac{\Delta^2}{4\pi^2} t Z(t). \tag{4.3}$$

In fact, this relationship is quite similar to what appeared in the dephasing problem [18].

6. Level compressibility: The level compressibility χ is closely related to the level number variance, and has value between 0 (for random matrix ensemble) and 1 (for Poission statistics) [103]. Although here we do not perform numerical analysis in this quantity, in principle, one can do a finite size scaling simulation around the Anderson transition point, similar to situations in the electronic system [104, 105].

7. Level Curvature: Introduced in Ref. [106], and further connected with topological universality of level dynamics [107], the quantity describes the sensitivity of the energy levels to the boundary conditions, which is also beyond the scope of my

work.

4.2 Energy Level Statistic and Random Matrix Theory (RMT)

It was in the 1960s that researchers proved Random Matrix Theory (RMT) [49] could be used to describe the ergodic systems (e.g., electrons in metallic granules). In the RMT, the energy level statistics is universal and depend only on the symmetry of the Hamiltonian [49, 108]. If it is invariant under time reversal symmetry, the fluctuations are described by the Gaussian Orthogonal Ensemble (GOE) of random matrices ($\beta = 1$). When time reversal symmetry is broken, the spectrum becomes more rigid (Gaussian Unitary Ensemble, GUE, $\beta = 2$). And there is a third class called Gaussian Sympletic Ensemble (GSE, $\beta = 4$). Since our model is now restricted to real symmetric systems, we will mainly focus on the GOE ensemble for now.

4.2.1 Level Spacing Distribution

In the RMT, the distribution function is well described by the Wigner–surmise: $P(s) \propto s^{\beta} \exp(-c_{\beta} s^2)$, for GOE:

$$P_o(s) = \frac{\pi}{2} s \exp(-\frac{\pi}{4} s^2),$$

On the other hand, in the localized regime, the correlations between levels are weaker and in the limit of an infinite system the statistics of energy levels becomes Poisson: $P(s) = \exp(-s)$. In Fig. 4.1, the distribution function of the level spacing $P(s)$ is shown for localized states, which has almost Poissonian statistics, while for metallic states, it is of the Wigner-Dyson form (GOE class, due to the real symmetric nature of our model Hamiltonian). This is rather standard.

Figure 4.1 here shows both a GOE universality class behavior at high energies and a Poisson behavior at low energy, indicating a delocalized/localized phase at high/low energies respectively. Here we represent energy in terms of Δ, the mean level spacing.

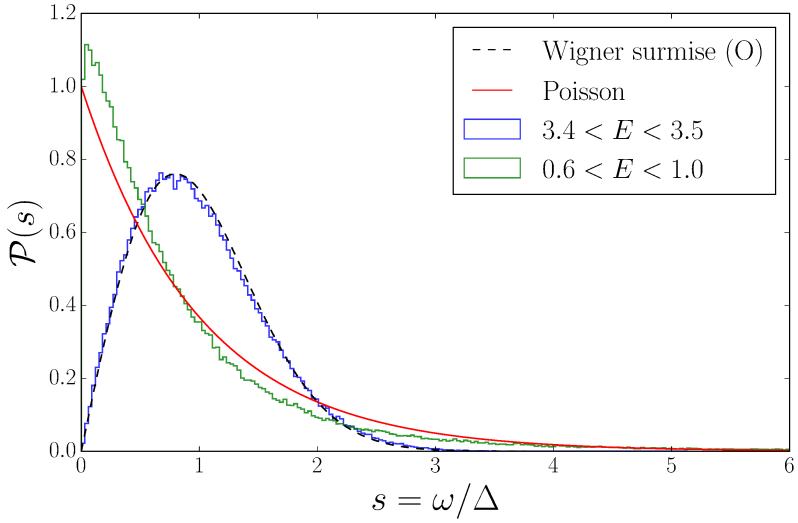

Figure 4.1: Crossover from Poisson (red dashed line) to Wigner-Dyson (GOE, black dashed line) level statistics at different energies for 20% of pinned sites. Lattice size $L = 140$, with $E \sim 3.5$, and $\Delta \simeq 0.0032$ (all in lattice unit).

Comparing the level spacing distribution for the localized states and in the metallic region, one may see the Poisson distribution for the localized states at low energies, and the Wigner-Dyson distribution for the orthogonal class for the states in the metallic region at higher energies. We then make more careful slices of energies, and investigate the distribution function of the level spacing at those energies, see Fig. 4.2. One finds really intricate behavior: The system is migrating from Poisson to GOE distribution gradually with increasing energy. Moreover, the distributions seem to cross at the same point, which is one of the characteristic feature for the a third universal distributions P_T that was studied in Ref. [109]. Similar behavior could also be found in the numerical study of the Anderson transition in disordered metals by tuning the parameter W of the band width of on-site potential. [110, 111, 112]

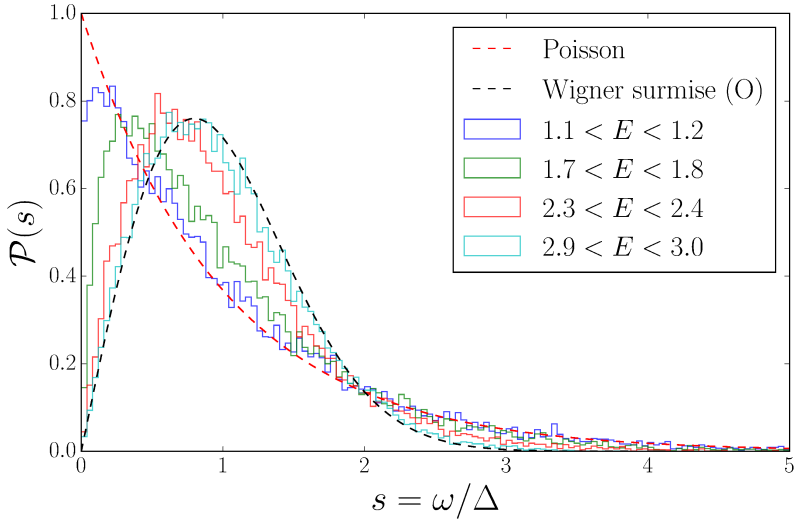

Figure 4.2: Nearest-neighbor level spacing distribution $P(s)$ for 20% pinned disorder on $L = 140$ lattice. Each histogram represents an energy slice, and the dashed lines are the theoretical distributions.

4.2.2 Two-Level Correlation Function (TLCF)

For GOE, the two level correlation function of Wigner-Dyson distribution can be written as [61]

$$R^{O}_{\mathrm{WD}}(s) = 1 - \frac{\sin^2(\pi s)}{(\pi s)^2} - \left[\frac{\pi}{2}\mathrm{sign}(s) - \mathrm{Si}(\pi s)\right]\left[\frac{\cos \pi s}{\pi s} - \frac{\sin \pi s}{(\pi s)^2}\right].$$

Thus, one could obtain its asymptotic behavior with s small. For $\omega \ll \Delta$,

$$R_{WD}\,(s) \simeq \frac{\pi^2}{6} s.$$

For large ω, $R_{WD} \to 1$. Detailed theoretical and numerical studies of TLCF can be found in Ref. [113]. In Figure , we have plotted the behavior of TLCF for our pinned FP system. The numerical results are well matched with the asymptotics listed above. In particular,

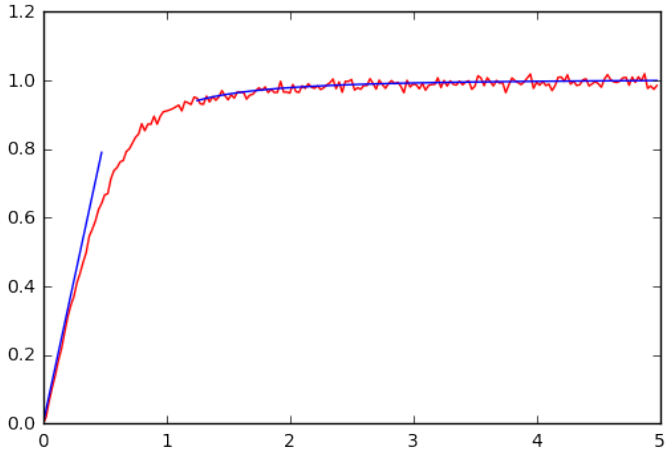

Figure 4.3: $R(s)$ for 40×40 lattice with 10% pinned sites average over 20,000 times. Horizontal axis represents $s = \omega/\Delta$, while vertical axes represents $R\,(s)$. Red line: numerical results. Blue lines: Theoretical predictions. The numerical curve is calculated via the formula $R(s) = \delta(s) + \sum_n P(n, s) - 1$.

one can see that the beginning of the $R\,(s)$ curve is linear with the slope matches the prediction of WD statistics in an excellent way.

4.2.3 Level Number Variance

For small enough $E \ll \Delta$, one gets the Poisson behavior, meaning that variance is equal to mean:

$$\Sigma^2\,(E) \simeq \langle n \rangle = E/\Delta.$$

In the RMT, $\Sigma^2(E)$ increases logarithmically with E. For $E \gg \Delta$, it varies as [108]

$$\Sigma^2(E) = \frac{2}{\beta\pi^2} \ln(2\pi\langle n\rangle) + c_\beta + O(\langle n\rangle), \tag{4.4}$$

where $c_\beta = 1 + \gamma - \frac{\pi^2}{8}$ and$\langle n\rangle = E/\Delta$. Here $\gamma = 0.577$ is the Euler constant and Δ being the average inter-level spacing. It was shown that in 2D quantum chaotic billiard systems [114], the level number variance exhibits the typical GOE RMT behavior Eq. (4.4) in the

diffusive regime. The number variance can obviously be written in terms of this two-point correlation function:

$$\Sigma^2(E) = \int_0^{\langle n\rangle}\int_0^{\langle n\rangle} R(s-s')dsds' \tag{4.5}$$

$$= 2\int_0^{\langle n\rangle}(\langle n\rangle - s)R(s)ds. \tag{4.6}$$

Or equivalently,

$$R(\omega) = \frac{\Delta^2}{2}\frac{\partial^2\Sigma^2(\omega)}{\partial\omega^2}.$$

And finally, an important relation between $K\left(t\right)$ and $\Sigma^2(E)$ is found to be [108]:

$$\Sigma^2(E) = \frac{8}{\Delta^2}\int_0^\infty dt\frac{K\left(t\right)}{t^2}\sin^2\left(\frac{Et}{2}\right). \tag{4.7}$$

For time scales larger than $\tau_D = \hbar/E_c$, the diffusion is homogeneous so that $Z(t)$ is independent of the starting point and thus depends only on the zero mode contribution, which gives a constant. This gives a linear behavior for $K(t) = 2/\beta$. It is easy to understand how β enters here: in the absence of the magnetic field (GOE), the return probability is doubled due to the presence of the Cooperon zero mode. And this leads to

$$K\left(t\right) = \frac{\Delta^2}{2\pi^2\beta}t,$$

which gives the expression for level number variance [108]:

$$\Sigma^2(E) = \frac{1}{\beta\pi^2}\ln\left(1+\frac{E^2}{\Delta^2}\right).$$

The level number variance is studied not only in the diffusive regime presented above, but in the ballistic regime as well [115, 116, 117], which is considered to be a future research

object for our random pinned FP model. Numerical studies of the level number variance could be found in Refs. [118, 119, 111, 120, 121, 122]. More recently level number variance was also observed and measured in the atomic matter wave [123].

4.3 Energy Level Statistics beyond RMT

At low energy scales, or the ergodic regime, the energy level correlation functions are well described by the RMT [49]. From the 1980s, the research focus has been shifted to the study of system-specific energy level deviations from RMT behavior. In the seminal paper of Altshuler and Shklovskii [124], the authors used diffuson-cooperon diagrammatic perturbation theory and showed that the behavior of the level correlation deviates from the RMT one in the high energy (frequency) regime due to the diffusive motion. This is the diffusive regime, i.e. $l \ll L$, where l is the mean free path and L the typical size of the system. If the energy scales become larger than the Thouless energy E_c, deviations from RMT occur. The method is perturbative and therefore, is restricted to $E \gg \Delta$. Moreover, it could not reproduce the oscillatory contribution to the level correlation function.[99]

In Ref. [125], nonlinear σ-model (NLSM) treatment of the level correlation function was introduced. The method developed there was later used for calculation of deviations from the RMT of various statistical characteristics of a disordered system. Here we will concentrate on the perturbation method and will not go into the details of the σ-model treatment (Introduction to the NLSM will be given in the Chapter 5). Instead of giving full details, here we just bring up the point that in the case of the level correlation function, the zero-mode approximation to the σ-model reproduces the RMT results above. It is the inclusion of the non-zero spatial modes that gives the analytical form of the deviation from universal RMT behavior. For level statistics, the calculation of [125] is valid for not too large energies ($E < E_c$) was complemented by Andreev and Altshuler [126] whose saddle-point treatment was, in contrast, applicable for larger energies. For a complete

review, see Ref. [99].

4.3.1 Qualitative Argument for the Deviation

In the 2D diffusive regime, the dimensionless (measured in units of e^2/h) conductance $g = 2\pi E_c/\Delta = 2\pi\nu D L^{d-2} \gg 1$. Consider in a metal the time evolution of a wave packet in the small time limit (or equivalently at large energies). In this limit, a diffusing electron cannot explore the entire volume of the system. In other words, for time t smaller than τ_D, spatial correlations do not extend over the entire sample, but only on a scale $\sim \sqrt{Dt}$. This corresponds to energies E larger than the Thouless energy, $E \gg E_c$. Spatial correlations extend up to scale $L_E = \sqrt{D/E} \ll L$. At this energy scale, the system of dimension d can be vied as being composed of $(L/L_E)^d$ independent subsystem. Therefore, variance $\Sigma^2(E) \sim (L/L_E)^d \sim (E/E_c)^{d/2}$. This heuristic argument indicates that spectral correlations in disordered conductors result from the diffusive motion of electrons [124, 127]. As we can see from the numerical simulation below, the variance $\Sigma^2(E)$ only follow RMT's logarithmic behavior to the energy scale of E_c, beyond which more careful consideration is needed.

4.3.2 Quantitative Derivation

Here we start with the DOS expression in terms of retarded (advanced) Green's function $G_{R(A)}$:

$$\nu(E) = \frac{i}{2\pi V} \int d^d\boldsymbol{r}[G_R(\boldsymbol{r},\boldsymbol{r},E) - G_A(\boldsymbol{r},\boldsymbol{r},E)],$$

The correlation function (4.1) can thus be expressed via $R\left(\boldsymbol{r},\boldsymbol{r}',\omega\right)$:

$$R\left(\omega\right) = \frac{\Delta^2}{2\pi^2} \int d\boldsymbol{r} d\boldsymbol{r}' \Re R\left(\boldsymbol{r},\boldsymbol{r}',\omega\right).$$

The function $R(\boldsymbol{r},\boldsymbol{r}',\omega)$ is long range, consists of a sum of two terms: Diffuson and Cooperon contributions. One can obtain [108]

$$R(\boldsymbol{r},\boldsymbol{r}',\omega)=P_d(\boldsymbol{r},\boldsymbol{r}',\omega)\,P_d(\boldsymbol{r}',\boldsymbol{r},\omega)+P_c(\boldsymbol{r},\boldsymbol{r}',\omega)\,P_c(\boldsymbol{r}',\boldsymbol{r},\omega),$$

where $P_{d,c}(\boldsymbol{r},\boldsymbol{r}',\omega)$ is the Diffuson (Cooperon) and satisfy the equation

$$(-i\omega-D\Delta_{r'})\,P_d(\boldsymbol{r},\boldsymbol{r}',\omega)=\delta(\boldsymbol{r}-\boldsymbol{r}').$$

Its solution takes the form of

$$P_d(\boldsymbol{r},\boldsymbol{r}',\omega)=\sum_n\frac{\psi_n^*(\boldsymbol{r})\,\psi_n(\boldsymbol{r}')}{-i\omega+E_n}$$

And thus leads to

$$R(\omega)=\frac{\Delta^2}{2\pi^2}\Re\sum_n\left[\frac{1}{\left(-i\omega+E_n^{(d)}\right)^2}+\frac{1}{\left(-i\omega+E_n^{(c)}\right)^2}\right] \tag{4.8}$$

Thus, one can use Eqs. (4.3) and (4.7) to obtain

$$\Sigma^2(E)=\frac{2}{\pi^2}\int_0^\infty dt\frac{Z(t)}{t}\sin^2\left(\frac{Et}{2}\right),$$

where $Z(t)=\int_V P(\boldsymbol{r},\boldsymbol{r},t)\,d\boldsymbol{r}$, and

$$P(\boldsymbol{r},\boldsymbol{r},t)=P_d(\boldsymbol{r},\boldsymbol{r},t)+P_c(\boldsymbol{r},\boldsymbol{r},t),$$

is the total return probability from Diffuson and Cooperon. In practice, one may substitute the summation of Eq. (4.8) by integration and could celebrate the success of such formula

Figure 4.4: Diagrammatic representation for the level correlation function.

for calculating $\Sigma^2(E)$ in 1D and 3D. The result can be expressed as ($c_d \sim 1$, is some numerical constant)

$$R(\omega) = c_d \frac{d}{4} (d/2 - 1) \frac{\Delta^2}{\omega^2} \left(\frac{\omega}{E_c} \right)^{d/2}.$$

However, in 2D the situation is more subtle because the coefficient after such integration gives zero, and one needs to more careful calculation in this case.

4.4 Level Correlations Driven by Weak Localization in 2D System

In a seminal paper by Kravstov and Lerner [101] (K-L), where they identified that in 2D the level correlation $R(\omega)$ is totally governed by the weak localization (WL) effects [128] which corrects the diffusion constant. And for level number variance, WL effects could also result in some corrections. Here we give a brief derivation about this effect. The Eq.4.8, $R(\omega) = \frac{\Delta}{\pi^2} \sum_q \mathrm{Re} \frac{1}{(Dq^2 - i\omega)^2}$, for level correlation can be expressed diagrammatically as Figure 4.4. Furthermore, if one take into account the Hikami box contribution [129, 108] for Diffuson/Cooperon as in Figure 4.5, we can write diffusion constant as $D' = D + \delta D$ where

$$\delta D = -D \frac{\Delta}{\pi} \sum_Q \frac{1}{DQ^2 - i\omega}.$$

After some algebra, one can write the correlation function as

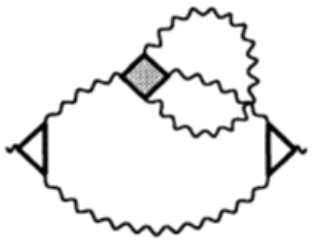

Figure 4.5: Hikami box contribution for the level correlation function.

$$R(\omega) = \frac{\Delta}{\pi^2}\Re\sum_q \frac{1}{\left[Dq^2\left(1-\frac{\Delta}{\pi}\sum_Q \frac{DQ^2}{(DQ^2)^2+\omega^2}\right) - i\omega\left(1+\frac{\Delta}{\pi}\sum_Q \frac{Dq^2}{(DQ^2)^2+\omega^2}\right)\right]^2}$$
$$\sim \frac{\Delta}{\pi^2}\Re\sum_q \frac{1}{\left[Dq^2 - i\omega\left(1+\frac{\Delta}{\pi}\sum_Q \frac{Dq^2}{(DQ^2)^2+\omega^2}\right)\right]^2}.$$

The last step is because the main contribution always come from the imaginary part correction of the diffusion constant [101]. It turns out that if one imposes the condition $Dq^2 \sim \omega \gg DQ^2$, which is equivalent to the situation $s \sim g$, one can essentially get a compact formula from the summation above, without the need to break the expression into two parts as in Ref. [101]. Here we are using the formula (4.6) to calculate the level number variance. The result after integrating in Q and s is:

$$\Sigma^2(\langle n\rangle) = \Sigma^2_{RMT}(\langle n\rangle) + \frac{1}{\pi^2}\sum_{\boldsymbol{m}\neq 0}\left[\log\left(1+\frac{\pi\langle n\rangle}{g_*^2\boldsymbol{m}^2}+\frac{\langle n\rangle^2}{g_*^2\boldsymbol{m}^4}\right) - \frac{\pi\langle n\rangle}{g_*^2\boldsymbol{m}^2}\right], \qquad (4.9)$$

where $g_* = 2\pi g + \frac{\pi^2}{4}$ and $\Sigma^2_{RMT}(\langle n\rangle)$ is the RMT result given by Eq.(4.4). Here $\boldsymbol{m} = (m_{x,}m_y)$, $m_x, m_y \in \mathbb{Z}$. One can do this summation numerically and it converges very fast.

4.5 Numerical Result

Here, we demonstrate the numerical simulation result for the flexural phonon level number variance as a function of the ratio ω/Δ in Figure 4.6, where Δ is the average level spacing. The numeric result starts with Poisson behavior for $\omega \ll \Delta$. Soon, the ergodic

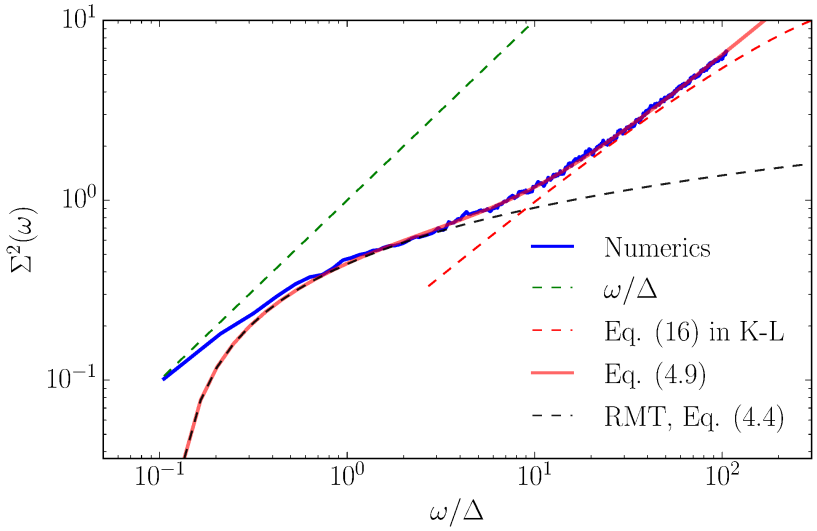

Figure 4.6: Level number variance from an 80×80 lattice with 20% disorder, averaged over 1000 realization. We use energy slice $E \in [3.5, 3.6]$. Estimated $\Delta \simeq 0.00095$ (in lattice unit), and $g_{ph} \simeq 1.63$.

behavior described by Random Matrix Theory (blue dashed line) kicks in. The ergodic regime holds up to ω that is about the Thouless energy. For larger ω there is a noticeable deviation: the variance starts to increase more rapidly than could be described by Eq. (16) in Ref. [101] (red dashed line). Nevertheless, as Fig. 4.6 shows, it is in full accord with the expression (4.9) obtained by us for $d = 2$, including a cross over regime (red line). (To the best of our knowledge, this is the first demonstration of the mesoscopic fluctuations of the number of levels in $d = 2$. For $3d$ Anderson model, the function $\Sigma^2(\omega)$ and the cross over regime was studied in Ref. [119], see Fig. 3 and surrounded text there.) To see the cross over regime more clearly, see Fig. 4.7 here. The deviation from the theory of Kravtsov and Lerner [101] could be seen more clearly in the 200×200 sample, as shown in Fig. 4.8. Since there are fewer numbers of disorder averaging (~50) due to limited computation resources, the numerical results showed more noise. However, the energy span of the plot is much larger, and still, one can clearly see the excellent match of numerical results with

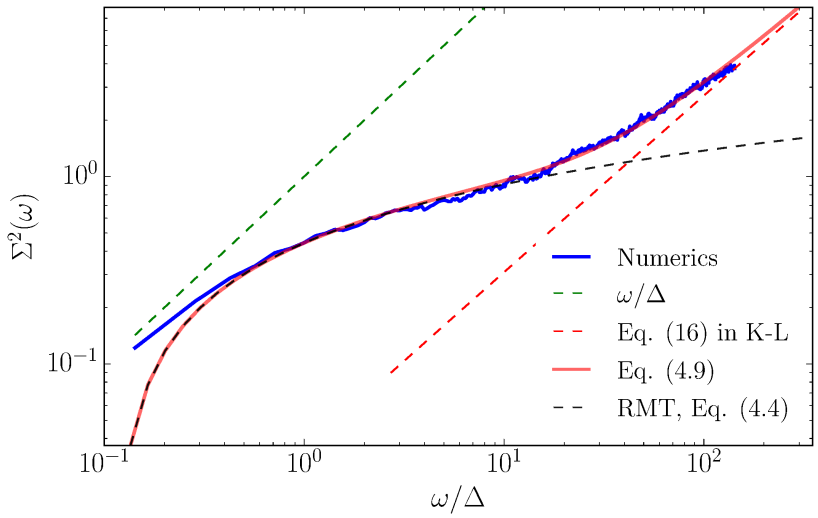

Figure 4.7: Level number variance for 90×90 lattice with 10% disorder, averaged over 1000 realizations. $E \in [3.5, 3.6]$, $\Delta \simeq 0.00070$ (in lattice unit), and $g_{ph} \simeq 5.53$.

our theory (4.9). Also, the abrupt downturn of the red dashed line in larger energy clearly demonstrate that the theory of Kravtsov and Lerner could not be applicable in this case.

Some comments are in place here. Here we have demonstrated that the properties of our 2D FP system are governed by weak-localization corrections. Weak localization in 2D is basically diffusion. In particular, the inverse participation ratio (which is related to the return probability of a random walk) in Figure 7.4 with an energy-dependent exponent means that we are in the diffusive regime. This is not surprising, since the condition of localization length $\xi \gg L$ enforces diffusive behavior.

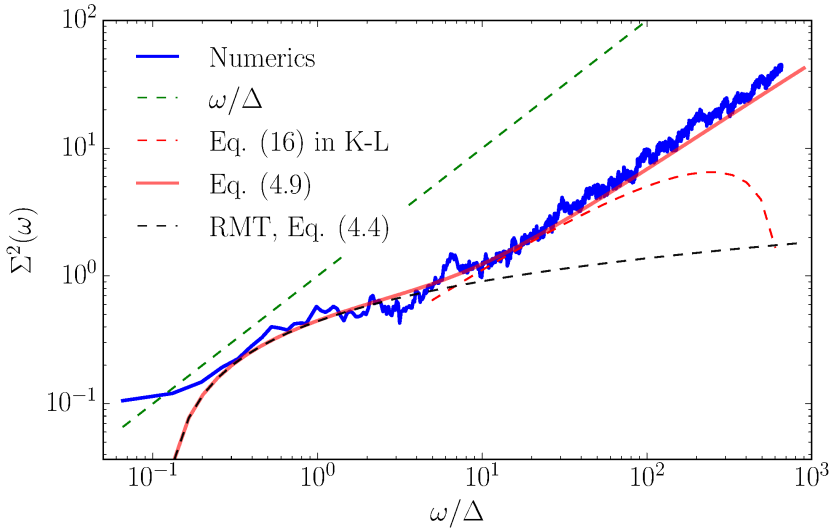

Figure 4.8: Level number variance for 200×200 lattice with 20% disorder, averaged over 50 realization. $E \in [3.5, 3.6]$, $\Delta \simeq 0.00015$ (in lattice unit), and $g_{ph} \simeq 1.38$.

5. STATISTICAL PROPERTIES OF THE WAVE FUNCTION

Like all coins that have two sides, after a detailed study of energy level statistics, we come to the other side of the coin – statistical properties of wave functions, which are also of great interest with a long history. This interest first started in nuclear physics. In the case of nuclear spectra, the statistics determine fluctuations of widths and heights of the resonance [130, 131]. In the case of disordered (or chaotic) electronic systems, eigenfunction fluctuations govern, in particular, the statistics of the tunnel conductance in the Coulomb blockade regime [132]. In optics, the eigenfunction amplitude can be directly measured in microwave cavity experiments [133, 134, 135, 136]. In this case one considers the intensity of a classical wave rather than of a quantum particle, all the results are equally applicable. In fact, this is more similar to the situation we have here than the electronic ones. Let us also turn from the energy level statistics to the statistical properties of the eigenvectors in the discussed pinned FP model. As indicated in the previous sections, the important property is the distribution of the amplitude of the eigenmodes, which is called the wave function intensity distribution $\mathcal{P}(y)$, where in our case, y is $\propto h^2$. Within the random matrix theory, the distribution of eigenvector amplitude is simply Gaussian, leading to the χ^2 distribution of the "intensities" $|\psi_i|^2$ (Porter-Thomas distribution) [130].

Supersymmetry (SUSY) method was invoked to the study for the theoretical properties of eigenfunction statistics in a disordered system. The corresponding formalism, which was developed in Refs. [137, 138], allows one to express various distribution functions characterizing the eigenfunction statistics through the correlation function of the SUSY nonlinear σ-field. Similar to the case of the level statistics, Porter-Thomas distribution of eigenfunction amplitude could be reproduced by just using the zero-mode approximation to the σ-model. However, one can go beyond this approximation. In fact,

for quasi-one-dimensional system, the σ-model can be solved exactly using the transfer-matrix method. Thus, one can get the exact analytical solutions with for the eigenfunction statistics for arbitrary length of the system, from weak to a strong localization regime [139, 138, 137, 140]. Since for $d = 2, 3$ no exact solution of the problem cannot be found, one has to use some approximate methods which will be introduced below. In Refs. [138, 141] by generalizing the scheme of [125] to eigenfunction statistics, the authors calculate the distribution of eigenfunction intensities and its deviation from the universal RMT form. The theory is further supported by numerical [142] and experimental [136] studies in various systems. Here we will apply the same methodology to the FP system and show excellent agreement with the existing theory [138, 141, 99].

5.1 Eigenfunction Statistics in the Ergodic Regime

The distribution function of the eigenfunction intensity $u = |\psi^2(\mathbf{r_0})|$ in a point $\mathbf{r_0}$ at energy E is defined as,

$$\mathcal{P}_E(y) = \frac{1}{\nu} \left\langle \sum_\alpha \delta(V|\psi_\alpha(\mathbf{r_0})|^2 - y)\delta(E - E_\alpha) \right\rangle . \tag{5.1}$$

Note that here y is dimensionless, ν is the DOS and $V = L^2$ is the area (volume) of the 2D system. For convenience in notation we will suppress the energy E and instead always write $\mathcal{P}(y)$ instead of $\mathcal{P}_E(y)$ for the understanding that (at least in theory) the intensity distribution behave uniformly in energy space. It was Porter and Thomas [130] who first studied the distribution of eigenfunction amplitudes within the RMT framework. It was recognized that in the ergodic regime, where $\Delta \ll E \ll E_c$, the distribution of eigenfunction amplitudes is simply Gaussian. Their results thus show the following χ^2 distribution of the intensities y:

$$\mathcal{P}^U(y) = e^{-y}, \tag{5.2}$$

$$\mathcal{P}^O(y) = \frac{e^{-y/2}}{\sqrt{2\pi y}}. \tag{5.3}$$

The upper script here labels the symmetry class of the system here. Eq.(5.3) is known as the Porter-Thomas distribution; it was originally introduced to describe fluctuations of widths and heights of resonances in nuclear spectra [131].

5.1.1 Numerical Calculation of the Wave Function Intensity

In the pinned disordered FP model we have described in the previous sections. We randomly pick a node $\mathbf{r_0}$ in our square mesh and record the wave function intensities of that point which is $h\left(\mathbf{r_0}\right)^2$ of the node. We calculate the intensity distribution according to Eq. (5.1). After proper normalization, we come up with the intensity distribution profile as in Fig. 5.1. As one can see, for y to up the order of unity, the intensity (the blue line) matches the behavior of that was predicted by Porter and Thomas Eq. (5.3), indicated by the green dashed line.

5.2 Wave Function Statistics in terms of the Supersymmetric σ-model

Properties of eigenfunctions in disordered and chaotic systems has been a growing interest in academic research since the eighties. On the experimental side, the tunneling conductance fluctuations of quantum dot was measured in 1990s [143], and the results were related to statistical properties of wave function amplitude [132]. Moreover, the microwave cavity technique allows one to observe experimentally spatial fluctuations of the wave amplitude in chaotic and disordered cavities [133, 134, 135].

Theoretical studies of the eigenfunction statistics in a d-dimensional disordered system are possible with the use of the SUSY field theoretical methods [137, 140, 144]. Here we

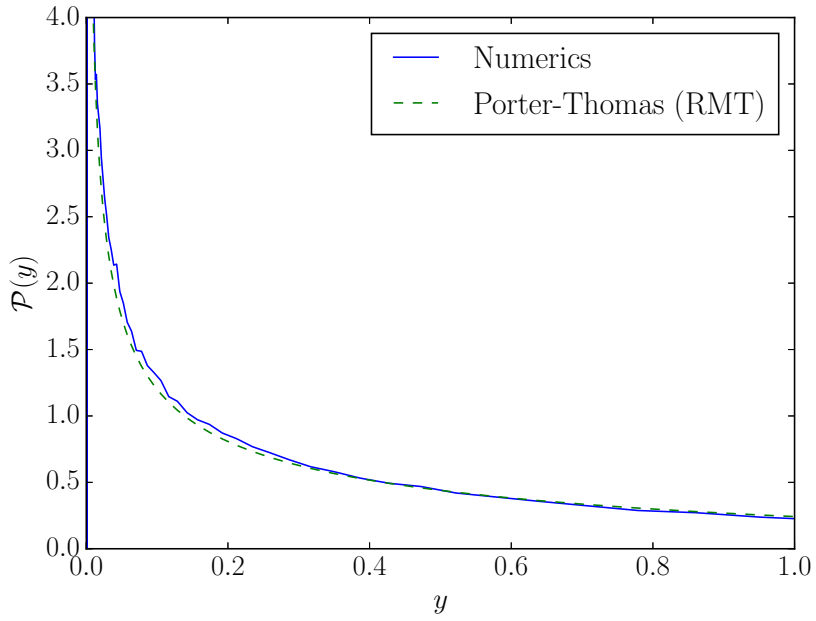

Figure 5.1: The wave function intensity distribution of 80×80 lattice with 10% pinned sites, after 2000 disorder averaging. The energy is sliced at $3.5 < E < 3.6$.

sketch a derivation given by Mirlin [61]. The distribution function of the eigenfunction intensity $u = |\psi^2(\mathbf{r_0})|$ in a point $\mathbf{r_0}$ is defined as

$$\mathcal{P}(u) = \frac{1}{\nu V} \left\langle \sum_{\alpha} \delta(|\psi_\alpha(\mathbf{r_0})|^2 - u)\delta(E - E_\alpha) \right\rangle . \tag{5.4}$$

One can always rewrite above $\mathcal{P}(u)$ in terms of $\mathcal{P}(y)$ in the form of Eq. (5.1). The key point is that the moments of $\mathcal{P}(u)$ can be written through the retarded and advanced Green's functions $G_{R(A)}$ in the following way

$$\langle |\psi(\mathbf{r_0})|^{2q} \rangle = \frac{i^{q-2}}{2\pi\nu V} \lim_{\eta \to 0} (2\eta)^{q-1} \langle G_R^{q-1}(\mathbf{r_0}, \mathbf{r_0}) G_A(\mathbf{r_0}, \mathbf{r_0}) \rangle. \tag{5.5}$$

The product of Green's functions can be expressed in terms of the integral over a super-

vector field $\Phi = (S_1, \chi_1, S_2, \chi_2)$,

$$G_R^{q-1}(\mathbf{r_0}, \mathbf{r_0}) G_A(\mathbf{r_0}, \mathbf{r_0}) = \frac{i^{2-q}}{(q-1)!} \int D\Phi D\Phi^\dagger (S_1(\mathbf{r_0}) S_1^*(\mathbf{r_0}))^{q-1} S_2(\mathbf{r_0}) S_2^*(\mathbf{r_0}) \times \exp\left\{ i \int d\mathbf{r} \Phi^\dagger(\mathbf{r}) \Lambda^{1/2} (E + i\eta\Lambda - \hat{H}) \Lambda^{1/2} \Phi(\mathbf{r}) \right\} \quad (5.6)$$

To proceed, we represent the right hand side of Eq. (5.6) in terms of σ-model correlation function. One then apply the supersymmetric field theoretical approach to express the above quantity as a path integral of the Q matrices [61]. As a result, one finds

$$\langle |\psi(\mathbf{r_0})|^{2q} \rangle = -\frac{q}{2V} \lim_{\eta \to 0} (2\pi\nu\eta)^{q-1} \int DQ Q_{11,bb}^{q-1}(\mathbf{r_0}) Q_{22,bb}(\mathbf{r_0}) e^{-S[Q]}, \quad (5.7)$$

where $S[Q]$ is the σ-model action,

$$S[Q] = -\frac{\beta}{2} \int d^d r \mathrm{Str} \left[\frac{\pi\nu D}{4} (\nabla Q)^2 - \pi\nu\eta\Lambda Q \right] \quad (5.8)$$

($\beta = 1$ for the considered case of orthogonal symmetry). Here $\Lambda = \mathrm{diag}\{1,1,\text{-}1,\text{-}1\}$ and $\eta \to 0+$. $Q = T^{-1}\Lambda T$ is the 4×4 supermatrix satisfy the condition of $Q^2 = 1$ (nonlinear), with T being some group transformation in the SUSY coset space. We remark here again that to reach σ-model action $S[Q]$ above, one uses electronic Green's function. However, as we stated in the section 3.6, and in addition, for the universal applicability of the σ-model, we are applying the well-established theory for statistical properties of electron wave function to our FP wave function. The applicability will be checked and confirmed by the numerical results shown below. Let us now define the function $Y(Q_0)$ as

$$Y(Q_0) = \int_{Q(\mathbf{r_0}) = Q_0} DQ(\mathbf{r}) \exp\{-S[Q]\}. \quad (5.9)$$

Here $\mathbf{r_0}$ is the spatial observation point. For invariance reasons, the function $Y(Q_0)$ turns

out to be dependent in the unitary symmetry case on two scalar variables $1 \leq \lambda_1 < \infty$ and $-1 \leq \lambda_2 \leq 1$ only, which are the eigenvalues of the "retarded-retarded" block of the matrix Q_0. Moreover, in the limit $\eta \to 0$ (at a fixed value of the system volume) only the dependence on λ_1 persists and we denote the asymptotic behavior of $Y(Q_0)$ as Y_a:

$$Y(Q_0) \equiv Y(\lambda_1, \lambda_2) \to Y_a(2\pi\nu\eta\lambda_1) \tag{5.10}$$

With this definition, Eq. (5.7) takes the form of an integral over the single matrix Q_0,

$$\langle|\psi(\mathbf{r_0})|^{2q}\rangle = -\frac{q}{2V}\lim_{\eta\to 0}(2\pi\nu\eta)^{q-1}\int DQ_0\, Q^{q-1}_{0;11,bb}Q_{0;22,bb}Y(Q_0) \tag{5.11}$$

Evaluating this integral, we find

$$\langle|\psi(\mathbf{r_0})|^{2q}\rangle = \frac{1}{V}q(q-1)\int du\, u^{q-2}Y_a(u). \tag{5.12}$$

Consequently, the distribution function of eigenfunction intensity is given by [137]

$$\mathcal{P}(u) = \frac{1}{V}\frac{d^2}{du^2}Y_a(u) \qquad (U)\,, \tag{5.13}$$

where V is the sample volume.

In the case of orthogonal symmetry, $Y(Q_0) \equiv Y(\lambda_1, \lambda_2, \lambda)$, where $1 \leq \lambda_1, \lambda_2 < \infty$ and $-1 \leq \lambda \leq 1$. In the limit $\eta \to 0$, the relevant region of values is $\lambda_1 \gg \lambda_2, \lambda$, where

$$Y(Q_0) \to Y_a(\pi\nu\eta\lambda_1) \tag{5.14}$$

The distribution of eigenfunction intensities is expressed in this case through the function

Y_a as follows [137]:

$$\begin{aligned} \mathcal{P}(u) &= \frac{1}{\pi V u^{1/2}} \int_{u/2}^{\infty} dz (2z-u)^{-1/2} \frac{d^2}{dz^2} Y_a(z) \\ &= \frac{2\sqrt{2}}{\pi V u^{1/2}} \frac{d^2}{du^2} \int_0^{\infty} \frac{dz}{z^{1/2}} Y_a(z+u/2). \qquad (O) \end{aligned} \tag{5.15}$$

In the diffusive sample, typical configurations of the Q–field are nearly constant in space, so that one can approximate the functional integral (5.9) by an integral over a single supermatrix Q. This procedure, which makes the problem effectively zero-dimensional and is known as zero-mode approximation, gives

$$Y_a(z) \approx e^{-Vz} \qquad (O,U)\,, \tag{5.16}$$

and consequently,

$$\mathcal{P}(u) \approx V e^{-uV} \qquad (U)\,, \tag{5.17}$$

$$\mathcal{P}(u) \approx \sqrt{\tfrac{V}{2\pi u}} e^{-uV/2} \qquad (O)\,, \tag{5.18}$$

which are just the RMT results for the Gaussian Unitary Ensemble (GUE) and Gaussian Orthogonal Ensemble (GOE) respectively, Eqs. (5.2), (5.3).

Therefore, using the zero mode approximation we have reproduced the RMT results for the distribution of the eigenfunction amplitude. To calculate deviations from RMT, one has to go beyond the zero-mode approximation and to evaluate the function $Y_a(z)$ determined by Eqs. (5.9), (5.10) for a d-dimensional diffusive system. In the case of a quasi-1D geometry, this can be done exactly via the transfer-matrix method. [99] For higher d, in particular the 2D case, the exact solution is not possible, and one should rely on approximate methods. Corrections to the "main body" of the distribution can be found by

treating the non-zero modes perturbatively (see Sec. 5.2.1.1 below), while the asymptotic "tail" can be found via a saddle-point method (see Chap. 6.1).

5.2.1 The Metallic (To Weak Localization) Regime

5.2.1.1 Distribution of the Eigenfunction Amplitude

For metallic granules, in the ergodic regime described by the RMT, the intensity distribution is given by the Porter-Thomas distribution denoted as $\mathcal{P}_{RMT}(y)$. Owing to the fluctuations in diffusive motion, there appear deviations from ergodic behavior. In the case of $d = 2$, deviations from the RMT distribution $\mathcal{P}(y)$ for not too large y can be calculated via the perturbation method. Applying this method to the moments (5.7), one gets [141]

$$\langle|\psi(r)|^{2q}\rangle = \frac{q!}{V^q}\left[1 + \frac{1}{2}\kappa q(q-1) + \ldots\right] \qquad (U) \tag{5.19}$$

$$\langle|\psi(r)|^{2q}\rangle = \frac{(2q-1)!!}{V^q}[1 + \kappa q(q-1) + \ldots] \qquad (O), \tag{5.20}$$

where, in the case of 2D geometry,

$$\kappa = \Pi(\mathbf{r}, \mathbf{r}) = \frac{1}{\pi g}\ln\frac{L}{l}, \tag{5.21}$$

with $g = 2\pi\nu D$. Correspondingly, the correction to the distribution function reads

$$\mathcal{P}(y) = e^{-y}\left[1 + \frac{\kappa}{2}(2 - 4y + y^2) + \ldots\right] \qquad (U) \tag{5.22}$$

$$\mathcal{P}(y) = \frac{e^{-y/2}}{\sqrt{2\pi y}}\left[1 + \frac{\kappa}{2}\left(\frac{3}{2} - 3y + \frac{y^2}{2}\right) + \ldots\right] \qquad (O). \tag{5.23}$$

In classical disorder and chaotic system, numerical studies of the wave function amplitudes have been performed in Ref. [145] for the 2D and in Ref. [146] for the 3D case. In the weak localization regime, the deviations from $\mathcal{P}_{RMT}(y)$ are found to be well described

by the above theoretical results. Statistical properties of the eigenfunction intensity have also been studied for microwaves in a disordered cavity [134, 136]. For a weak disorder, the experimentally found deviations are also in good agreement with Eq. (5.23) as well. Deviations of the eigenfunction distribution function $\mathcal{P}(y)$ from its RMT form in our randomly pinned FP model will be illustrated and studied in the section below.

The formulas (5.22), (5.23) are valid in the region of not too large amplitude, where the perturbative correction is smaller than the RMT contribution, i.e. at $y \ll \kappa^{-1/2}$. In the region of large amplitude, $y > \kappa^{-1/2}$ the distribution function was found by Fal'ko and Efetov [147, 148], who applied to Eqs. (5.13), (5.15) the saddle-point method suggested by Muzykantskii and Khmelnitskii [149]. Behavior of the large amplitudes asymptotics will be introduced in the Chapter 6.

5.2.1.2 Numerical Results

If we plot the intensity distribution function of the eigenfunction with a wider range than that of Fig. 5.1, as shown in Fig. 5.2, one sees that the numerical results (the blue line) deviates from the Porter-Thomas formula (green dashed line) at $y > 1$. However, there is an excellent match between the theory of Fydorov & Mirlin (Eq. 5.23, red line) and the numerical results. For 20% of the pinned sites, we can see similar behavior, with a more distinct deviation from RMT behavior, as shown in Figs. 5.3 and 5.4. Unlike 10% sample, at small y, the difference of our numerical results with Porter-Thomas formula is quite obvious, owing to the smaller conductivity, see the inset in Fig. 5.4. When calibrated with respect to $\mathcal{P}_{RMT}(y) \equiv \frac{e^{-y/2}}{\sqrt{2\pi y}}$ (Eq. 5.3), the function $\mathcal{P}(y)$ yields a curve with a very specific non-monotonous shape. As Fig. 5.5 shows, an excellent agreement with the theory developed in Ref. [141] is found. From Eq. (5.23),

$$\mathcal{P}(y)/\mathcal{P}_{RMT}(y) = 1 + \frac{\kappa}{2}\left(\frac{3}{2} - 3y + \frac{y^2}{2}\right), \tag{5.24}$$

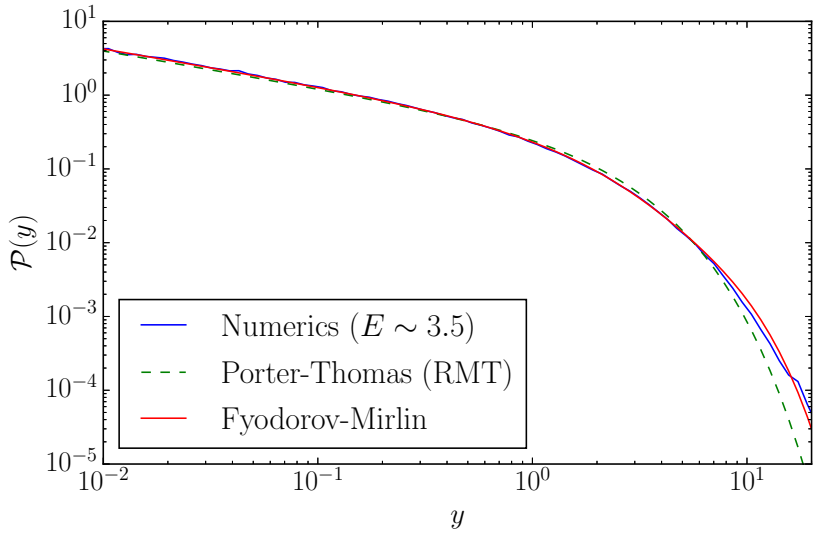

Figure 5.2: The log-log plot of the wave function intensity distribution. Data comes from 80×80 lattice with 10% pinned sites, after 2000 disorder averaging. The energy is $E \sim 3.5$; Estimated $g_{ph} = 1.63$ and $\kappa = 0.35$.

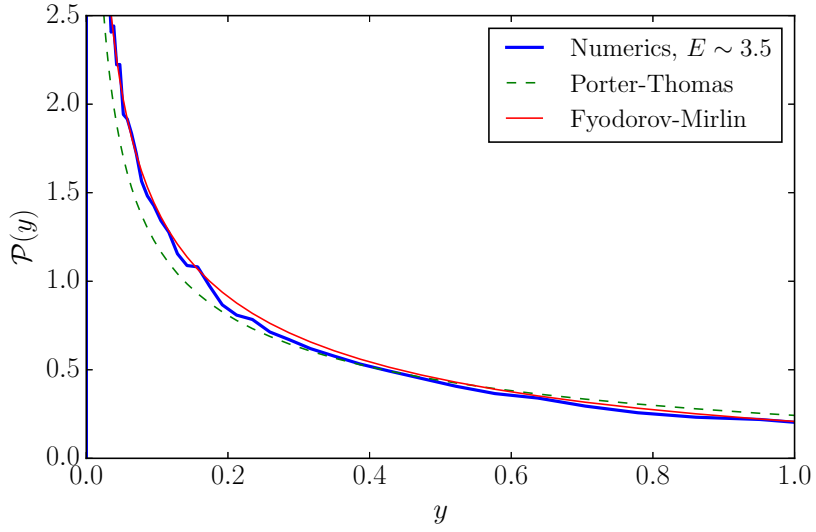

Figure 5.3: The wave function intensity distribution of 80×80 lattice with 20% pinned sites. Data obtained after 2000 disorder averaging. The energy is again $E \sim 3.5$; Estimated $g_{ph} = 5.63$ and $\kappa = 0.09$.

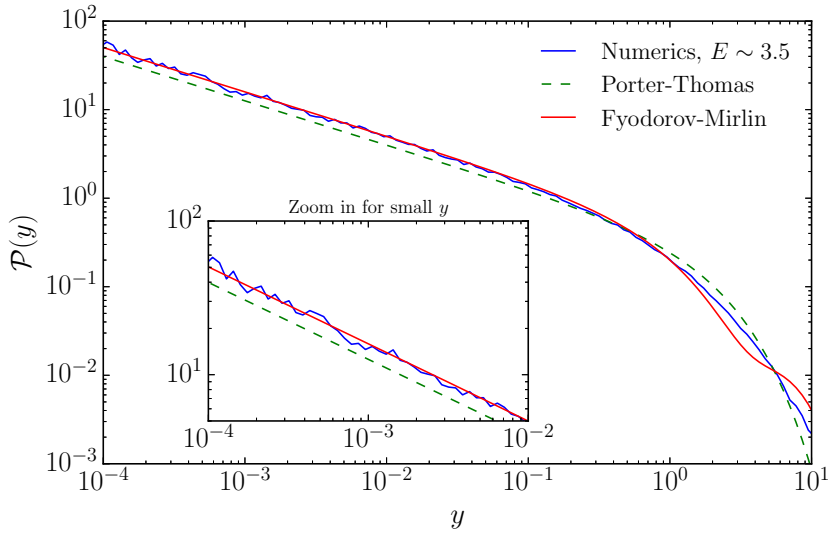

Figure 5.4: Log-log plot of the wave function intensity distribution for 20% of pinned sites. Sample specification is the same as Figure 5.3.

with $\kappa = \frac{1}{\pi g} log \frac{L}{l}$, one can obtain the conductivity g from fitting. Similar agreement between numerical study and theory could also be found in the 2D quantum kicked rotors [150], exact diagonalization studies of the Anderson model [151, 152] and random banded matrices [153].

Intensity distribution is controlled by the parameter κ, which is related to the two-particle correlation function at the coinciding points and describes the probability of return. The theoretical formulas compare intensity y with κ^{-1} (a large number for weak disorder). We demonstrate an excellent agreement with the theoretical formulas for intensity $y < \kappa^{-1}$. However, κ^{-1} decreases with growing L/l, and one has to deal with the part of the distribution corresponding to $y > \kappa^{-1}$. These intensities are controlled by rare events, rather than by regular fluctuations. These rare events can be universal (i.e., non-dependent on the character of disorder), or can be controlled by non-universal realizations of disorder centers (in our case centers of pining). Although for not too large intensities y

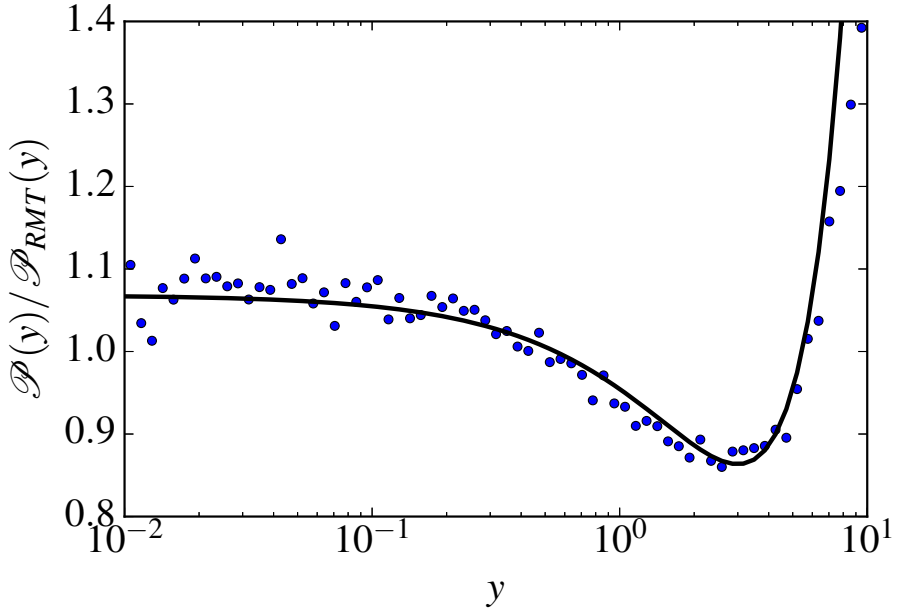

Figure 5.5: The intensity distribution calibrated with respect to the RMT result for 10% of the pinned sites at $E \sim 3.5$. Blue dots: the numerical result; Solid line: fit with Eq. (5.24) with estimated $g_{ph} = 5.63$ and $L/l = 5$.

we always observe the distributions described by the universal curve presented in Figure 5.5, it follows from the data that in our system the rare events are non-universal and they are controlled by certain realizations of the pinning centers. Therefore, for very large L/l, when the eigenfunctions in our 2D system approach localization, the plot is controlled by another non-universal asymptotic, see the next Chapter for detail discussions. One could further study whether there is pure diffusion effect or mixed with ballistic effect via detail analysis of κ [152], which is beyond our scope here.

5.2.2 The Localized Regime

In the localized regime, one can parameterize the wave function in an exponential decay form:

$$\psi(r) = c \exp(-r/\xi)$$

where ξ/L is the ratio of localization length to the system size and

$$c^2 = \frac{2L^2}{\pi\xi^2}\left[1-(1+L/\xi)\exp\left(-L/\xi\right)\right]^{-1}.$$

Thus, the wave function intensity distribution has the following form [145]

$$\mathcal{P}(y) = \frac{\pi\xi^2}{2L^2}\frac{\ln\left(c^2/y\right)}{y}. \tag{5.25}$$

An estimation of the the localization length is in place here. The localization length ξ is determined by the logarithmic corrections to the parameter g:

$$g(L) = g_0 - \frac{1}{\pi}\ln\frac{L}{l} \tag{5.26}$$

here l is the mean-free path of FPs at a given energy, and $g_0 = g(l)$. Correspondingly, ξ is the length scale when the correction become comparable with g_0, that is $\xi/l \simeq \exp\left(\pi g_0\right)$.

5.2.2.1 Numerical Results for Localized Regime

We first come across in the localized regime at energy $E \sim 0.6$, where most of the states are localized. In contrast with the higher energy states, the wave function intensity is described by Eq. (5.25). One can see in the log-log plot of Figure 5.6, the theory matches with the numerical results over a range of 9 orders of magnitude, which should be considered an excellent manifestation of the localized wave function assumption. The parameter estimated in the plot is $\xi/L = 0.022$. Similar plots also could be found in the numerical study of 2D tight-binding Anderson model in the Ref. [145].

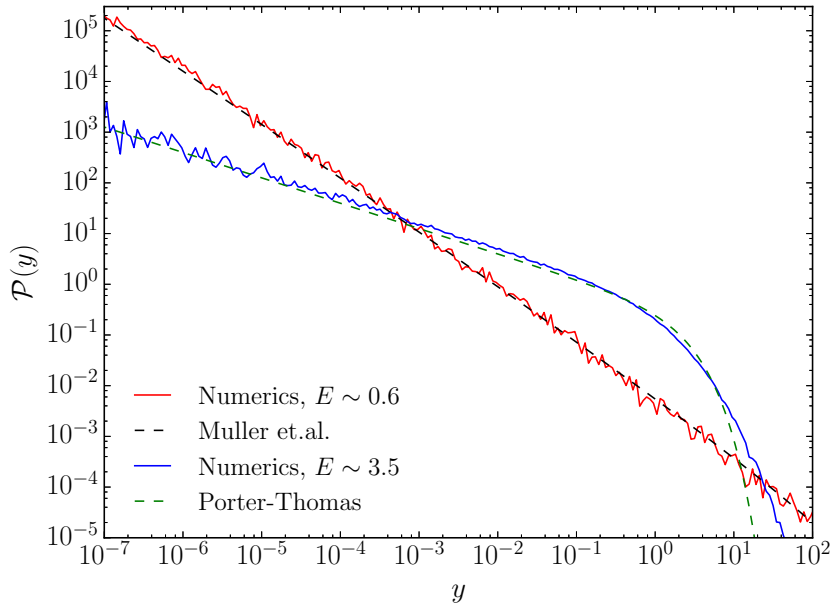

Figure 5.6: Wave function intensity distribution for localized regime. The sample has 20% of pinned sites, and 80×80 lattice with 2000 disorder averaging.

6. ASYMPTOTIC TAILS

This chapter is devoted to the asymptotic "tails" of the distribution functions of wave-function amplitude. The definition of the quantity was introduced in Eq. (5.1). Using renormalization group (RG) approach, it was conjectured by Altshuler, Kravtsov, and Lerner (AKL) [154, 155] that the rare realization of disorder will determine the tail behavior of the amplitude distribution function. The states thus formed would show some kind of localization while all "normal" states are ergodic; in the quasi-1D case they have an effective localization length much shorter than the "normal" one. Thus, those states were named "anomalously localized states" (ALS). Through searching a non-trivial saddle-point configuration of the supersymmetric σ-model, Muzykantskii and Khmelnitskii [149] established a novel way to study the asymptotic tails of the distribution functions. Further development and generalization of the method allowed one to calculate various distribution function's asymptotic behavior including relaxation times [149, 156], eigenfunction intensities [147, 148], local density of states [157], inverse participation ratio [158] and level curvatures [159], etc.

6.1 Anomalously Localized States and Distribution of Large Eigenfunction Amplitudes

Altshuler, Kravtsov and Lerner [155] found that the distribution functions of conductance, density of states, local density of states (LDOS), and relaxation times all have slowly decaying logarithmically–normal (LN) asymptotics at large values of the arguments. Using the renormalization group treatment of the σ–model, those results are valid in 2D and $2+\epsilon$–dimensional systems, with $\epsilon \ll 1$. At the same time, those quantities in 1D disordered chains were studied using the Berezinski and Abrikosov–Ryzhkin techniques [160]. In 1D, where all states are strongly localized, the corresponding distributions were also

found to be of the LN form. Based on this similarity, it was conjectured [154, 155] that there is a finite probability to find "almost localized" eigenstates even in a metallic sample, and that these states govern the slow asymptotic decay of the distribution functions. In Ref. [141] the exact results for the statistics of the wave function amplitude in the quasi-one-dimensional case were obtained and similar conclusion was drawn. The study showed that the identical asymptotic behavior exists both in the localized and metallic regimes.

Muzykantskii and Khmelnitskii [149] gives a new boost to the theoretical study along this direction. In order to calculate the long-time dispersion of the average conductance $G(t)$, they proposed to use the saddle-point method for the supersymmetric σ-model. The idea was to reproduce the AKL result by means of more direct calculation. However, in the intermediate range of time t, a power-law decay behavior of $G(t)$ in 2D was found. As was shown in Ref. [161], the far asymptotic behavior is indeed of log-normal form, in agreement with AKL. The conclusion is then reproduced by Ref. [156] within the ballistic σ-model approach. Moreover, the saddle-point method could be applied beyond the average conductance and also allowed us to study the asymptotics of various quantity's distribution functions. The form of the saddle-point solution describes directly the spatial shape of the corresponding anomalously localized state [149, 158].

6.2 Saddle Point Method

Fal'ko and Efetov [147, 148] applied the saddle-point method to the study the statistics of eigenfunction amplitudes. Here, one looks for the saddle-point of the functional integral (5.9) determining the function $Y_a(u)$ (which in turn determines the eigenfunction statistics, see Eqs. (5.13), (5.15)). One could follow the standard derivation of the saddle point equation in Ref. [148, 99], which is omitted here. The saddle-point thus derived is parameterized by the bosonic non-compact angle $\theta(\mathbf{r})$ only, and the corresponding saddle-point

equation has the form [147, 148]

$$\pi\nu D\nabla^2\theta - ue^{\theta} = 0. \tag{6.1}$$

The boundary condition now has the form

$$\theta(0) = 0, \tag{6.2}$$

and

$$\nabla_n Q|_{bdy} = 0$$

at the boundary. The action determining the distribution function $\mathcal{P}(u)$ is given by

$$-\ln \mathcal{P}(u) = S = \int d^d r \left[\frac{\pi\nu D}{2}(\nabla\theta)^2 + ue^{\theta}\right]. \tag{6.3}$$

The formula (6.3) acquires a very transparent meaning if we take into account the two factors contributing to the large amplitude $|\psi^2(0)| = u$. Firstly, this is the non-uniform smooth envelope $\propto e^{\theta(\mathbf{r})}$ yielding

$$|\psi^2(0)|_{\text{smooth}} = \frac{e^{\theta(0)}}{\int d^d r e^{\theta(\mathbf{r})}} = \frac{1}{\int d^d r e^{\theta(\mathbf{r})}},$$

the corresponding weight is represented by the first term in the action (6.3). Secondly, these are the local Gaussian fluctuations of the wavefunction amplitude, which should provide the remaining factor

$$J = \frac{u}{|\psi^2(0)|_{\text{smooth}}} = u\int d^d r e^{\theta(\mathbf{r})},$$

the corresponding probability $\mathcal{P}(J) = e^{-J}$ reproduces the second term in the action (6.3).

6.3 Saddle Point Solution in 2D geometry

6.3.1 Exact Solution

We will follow Refs. [147, 148] to derive the saddle point solution for weakly disordered 2D conductors. We consider a disk-shaped sample of a radius L with the observation point $\mathbf{r} = 0$ in the center of the disk, the saddle-point of Eqs. (6.1), (6.2) could be rewritten in the polar coordinates as

$$\left(r^{-1}\partial_r r\partial_r\right)\theta_u = -\frac{u}{\pi\nu D}\exp(-\theta_u)$$
$$\theta_u\left(r_0\right) = 0,$$

where $r_0 \sim l$ is the lower cut-off scale (roughly, the scale of the mean free path). It appears because of the restriction of the diffusion approximation put on the momenta q of σ-model field: $q < l^{-1}$. This equation can be solved exactly and it yields the solution of the following form [147]

$$\exp\left(-\theta_u\right) = \left[\frac{2\left(l/r\right)^{1-A}\left[\sqrt{(A\rho)^{-2}+1}+1\right]}{\left[\sqrt{(A\rho)^{-2}+1}+1\right]^2 - (A\rho)^{-2}\left(r/l\right)^{2A}}\right]^2,$$

where $\rho = \sqrt{\frac{2\pi\nu D}{ul^2}} = \frac{L}{l}\sqrt{\frac{g}{y}}$. Here A is found from the boundary condition at the edge L, and satisfy

$$\sqrt{A^2+\rho^2} + A = \frac{\left(L/l\right)^A}{\rho}\sqrt{\frac{1+A}{1-A}}. \tag{6.4}$$

Thus, the action (for GOE systems) can be expressed as

$$S = 2\pi^2\nu D\left\{\ln\left(\frac{\left(L/l\right)^{\left(1+A^2\right)}}{\rho^2(1-A^2)}\right) + 2\left(1-\sqrt{A^2+\rho^{-2}}\right)\right\},$$

and at the same time, the distribution of the wave function intensity can be expressed as

$$\mathcal{P} = e^{-S} = \exp\left[-2\pi^2\nu D\left\{\ln\left(\frac{(L/l)^{\left(1+A^2\right)}}{\rho^2(1-A^2)}\right) + 2\left(1-\sqrt{A^2+\rho^{-2}}\right)\right\}\right]. \quad (6.5)$$

6.3.2 Asymptotic Tail of the Intensity Distribution $\mathcal{P}(u)$

We are interested in the asymptotic region $\rho > \ln(L/l) \gg 1$, where the equation 6.4 has positive root and an ALS is formed. The condition is equivalent to

$$y < g\frac{(L/l)^2}{\ln^2(L/l)}.$$

Taking the square of Eq. (6.4), we assume $\rho^{-1} \ll 1$, then the roots of Eq. (6.4) can be approximated by

$$A = 1 - \mu.$$

Here we define $\mu \equiv 1 - A$, where $0 < \mu < 1$ depends on u. The resulting squared equation can be written as

$$(2A)^2 = 4(1-\mu)^2 = \frac{(L/l)^{2-2\mu}}{\rho^2}\frac{2-\mu}{\mu}. \quad (6.6)$$

Thus, the above equation could be rewritten to the following form

$$\frac{(L/l)^{2-2\mu}}{\rho^2} = \frac{4\mu(1-\mu)^2}{2-\mu}.$$

For $\mu \ll 1$, one can approximate

$$\frac{(L/l)^{2-2\mu}}{\rho^2(1-\frac{3}{2}\mu)} \sim 2\mu. \quad (6.7)$$

Note that the left-hand side is different from what was above Eq. (70) in Ref. [147]. We remark here that it crucial for the higher order asymptotics to be correct. Under the same condition, the exact solution is found to have the approximate form of

$$e^{\theta(r)} \approx \left(\frac{r}{l}\right)^{-2\mu} \qquad \text{for } l \leq r \ll L, \tag{6.8}$$

Then substituting the definition of ρ in the Eq. (6.7), the exponent μ can be approximated as by

$$\mu \simeq \frac{\ln\left(\frac{L^2 u}{2\pi\nu D}\ln\frac{L}{l}\right)}{2\ln(L/l)}. \tag{6.9}$$

Plugging the approximation Eq. (6.7) back into the expression for S in Eq. (6.3), one gets to the lowest order in μ

$$\begin{aligned} S &= 2\pi^2\nu D\left\{\ln\left(\frac{(L/l)^{2-2\mu+\mu^2}}{\rho^2(2\mu-\mu^2)}\right)+2\mu\right\} \\ &\sim 2\pi^2\nu D\left\{\ln\left(\frac{2\mu(1-\frac{3}{2}\mu)}{2\mu(1-\mu/2)}\right)+2\mu\right\} \\ &= 2\pi^2\nu D\left\{\ln(1-\mu)+2\mu\right\} \\ &\sim 2\pi^2\nu D\mu \end{aligned} \tag{6.10}$$

The corresponding asymptotic behavior of intensity distribution function $\mathcal{P}(u)$ is

$$\mathcal{P}(u) \sim \exp\left\{-\pi^2\nu D\frac{\ln^2\left(\frac{Vu}{2\pi^2\nu D}\ln\frac{L}{l}\right)}{\ln(L/l)}\right\}. \tag{6.11}$$

By definition $\kappa = \frac{1}{\pi g} log\frac{L}{l}$ and $g = 2\pi\nu D$, the above distribution can be rewritten in terms of the argument $y = Vu$ as

$$\mathcal{P}(y) \sim \exp\left(-\frac{1}{2\kappa}\ln^2\kappa y\right).$$

6.3.3 Summary of the Result for Wave Function Amplitude

We thus summarize the results for wave function amplitude in 2D GOE class here [99]:

$$\mathcal{P}(y) \simeq \begin{cases} \frac{e^{-y/2}}{\sqrt{2\pi y}} \left[1 + \frac{\kappa}{2}\left(\frac{3}{2} - 3y + \frac{y^2}{2}\right) + \dots\right], & y < \kappa^{-\frac{1}{2}} \\ \frac{e^{-y/2}}{\sqrt{2\pi y}} \exp\left(\frac{\kappa}{4}y^2 + \dots\right), & \kappa^{-\frac{1}{2}} \leq y < \kappa^{-1} \\ \propto \exp\left\{-\frac{1}{2\kappa}\ln^2(\kappa y)\right\}, & \kappa^{-1} \leq y \leq \kappa^{-1}\left(\frac{L}{l}\right)^2 / \log\frac{L}{l}. \end{cases} \tag{6.12}$$

Here the last restriction of y happens because the framework of the σ-model could not apply to sizes smaller than mean free path l. Note that there is an intermediate range where a correction in the exponent is large compared to unity, but small compared to the leading RMT term (Eq. 5.3) and a far asymptotic region (Eq. 6.11), where the decay of $\mathcal{P}(y)$ is much slower than in RMT.

6.4 Numerical Result

One may have already noticed that in the part of blue curve in figure 5.6 could not be explained by the Porter-Thomas theory curve (dashed green), especially in the larger y regime. Let us examine now closely the behavior of the tail behavior of the wave function intensity. Let us comment first that apart from the asymptotic distributions listed in Eq. (6.12), one can further use Eq. (6.5) along with Eq. (6.4) to solve numerically an exact solution for the intensity distribution. We now put all these pieces together in the figure 6.1. One can see that the asymptotics of Fyodorov-Mirlin works great for $y < \kappa^{-\frac{1}{2}}$, after which one enters a short intermediate asymptotic region. One the other hand, the exact solution of Fal'ko-Efetov [147, 148] fails to match the numerical results well, nor could the RMT (Porter-Thomas) theory. In addition, at $y \gtrsim \kappa^{-1}\left(\frac{L}{l}\right)^2 / \log\frac{L}{l}$, the root for the exact solution stops to exist. The intermediate region which is between $\kappa^{-\frac{1}{2}}$ and κ^{-1}, is too small a region for us to get enough data for decent analysis. Finally one can see that the far

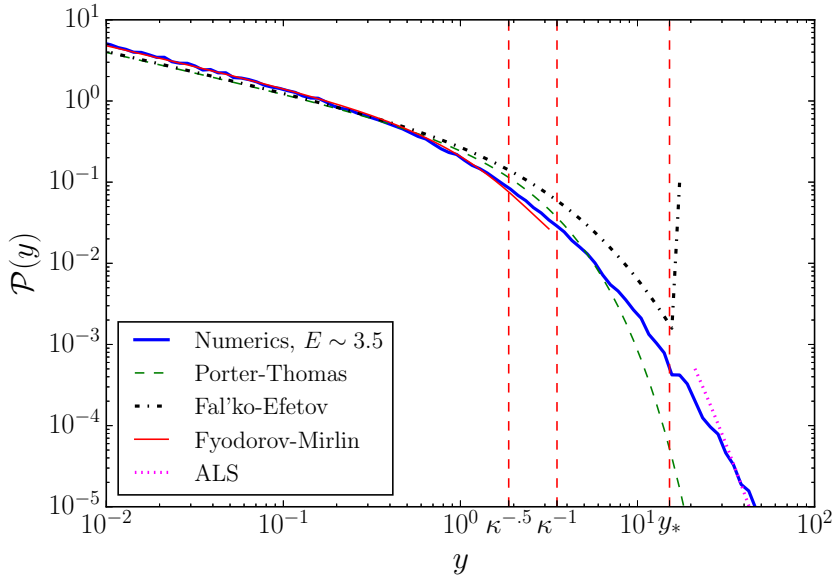

Figure 6.1: The log-log plot of the wave function intensity distribution for 20% of pinned sites, with 80×80 lattice and averaged over 2000 times. Estimated $\kappa \sim 0.35$. The exact solution labeled as Fal'ko-Efetov was obtained by solving numerically Eq. (6.4) using the estimated parameter as follows: $g \sim 1.6$ and $L/l \sim 4.3$. The cusp in the solution (black dashed line) is due to the fact that for y larger than $y_* \equiv g\frac{(L/l)^2}{\ln^2(L/l)} \sim 15$, there is no root available for Eq. (6.4).

asymptotics can match the very large y (tail) region reasonably well. However, due to the uncertainty of the pre-factor and limitation in the data quality of the tail region, we were not certain if the numerical result has indeed reached the asymptotic region. Moreover, there are also different opinions about how the rare events will affect the statistics of the disordered system [162, 163, 164]. We expect that our randomly pinned FP model will serve a good candidate to test different theories in addition to the usual Anderson models.

7. INVERSE PARTICIPATION RATIO AND MULTIFRACTALITY OF THE WAVE FUNCTION

In the electronic system, multifractality, in a rough term, could be understood as the eigenfunctions is neither extended, nor localized, but effectively located in a vanishingly small portion of the system volume. It could be used to characterize strong fluctuations of the wave function amplitude at the mobility edge. Wegner's renormalization group calculation[165] first discovered the phenomena, however, he did not propose the term "multifractality". Later the multifractality of the critical wave functions was discussed in [166] and confirmed by numerical simulations of the disordered tight-binding model in Refs. [167, 168, 169]. Here we ask the question: could the theory of wavefunction multifractality be applied to phonon systems? If so, is there any numerical evidences? One can thus continue to ask a deeper question about the behavior of fluctuations in the wave functions, which are usually determined by the diffusive dynamics in classical systems [141, 170, 171]. The inverse participation ratio (IPR) was first studied in the context of the Anderson model, and then was applied to study the localization length in quantum hall effect. [172] IPR was widely used to investigate the localization properties of systems including Dirac semimetals [173]. Thus, fluctuations of the inverse participation ratio in the FP system are also considered here.

7.1 Weak Multifractality of Eigenfunctions

As is well known, localization is a quantum critical phenomenon. The peculiarity of $2d$ is that the critical point is at $1/g_{\Box} = 0$, where $g_{\Box}$ is electrical conductance per square measured in units $e^2/(2\pi\hbar)$. At a finite $g_{\Box}$, statistical properties are determined by the localization length ξ, which is the analogue of a correlation length at a quantum phase transition. A sample of size $L < \xi(g_{\Box})$ is in the regime of criticality which may take place

in a very broad range of sample sizes, because for small $g_\square$ the localization length is exponentially large [128]. A consequence of strong fluctuations of the wave function amplitude in the critical region is the multifractality (that is, while an eigenstate may be extended, the occupied volume is noticeably smaller than the volume of the sample). Since $d = 2$ is the lower critical dimension for the Anderson localization problem, many common properties with systems at the critical point of the metal-insulator transition are shared with metallic 2D samples (with $g_\square \gg 1$) share . Although the localization length ξ in 2D is not infinite (as for truly critical systems), it is exponentially large, and the criticality takes place in the very broad range of the system size $L \ll \xi$.

7.1.1 Multifractality: Basic Definition

Multifractality is a way to demonstrate the criticality of eigenfunctions. First introduced by Mandelbrot [174], multifractal structures are characterized by an infinite set of critical exponents describing the scaling of the moments of a distribution in terms of some quantity such as size. Since the discovery of multifractality, the feature has been observed in various objects, such as the energy dissipation in turbulence [175, 176], strange attractors in chaotic dynamical systems [177, 178], and the growth probability distribution in diffusion-limited aggregation [179, 180]; see Ref. [181] for a review. It was also noticed fractal characters exist in the eigenstates of weakly disordered systems through investigating inverse participation ratios [182].

The fact that an eigenfunction at the mobility edge has the multifractal structure was noticed for the first time in [166], though the underlying renormalization group calculations were done by Wegner several years earlier [165].

7.2 Inverse Participation Ratio

The spatial distribution of wave functions is conveniently characterized by inverse participation ratios:

$$P_q = \int d^d r |\psi(r)|^{2q}.$$

After sample averaging $\langle P_q \rangle$ shows the following scaling behavior with the system size L:

$$\langle P_q \rangle = L^d \langle |\psi(r)|^{2q} \rangle \sim L^{-\tau_q}, \tag{7.1}$$

where τ_q is some exponent that can be expressed via $\tau_q = D_q(q-1)$. Obviously, in the insulating state $D_q = 0$, while in a normal metal $D_q = d$. At a critical point, D_q is fractional, which leads to anomalous scaling behavior in $\langle P_q \rangle$. This is a manifestation of the wave function multifractality. Next, one can introduce anomalous dimensions Δ_q via:

$$\tau_q \equiv d(q-1) + \Delta_q,$$

in order to describe the deviation of the scale dependencies at the critical point from the one in the metallic phase. In fact, Δ_q determines the spatial correlations of the wave function. In particular, Δ_2 governs the spatial correlations of the intensity $|\psi(r)|^2$,

$$L^{2d} \langle |\psi^2(r)\psi^2(r')| \rangle \sim (|r-r'|/L)^{\Delta_2}.$$

In the field-theoretical language (Section 5.2), Δ_q are the leading anomalous dimensions of the operators $\mathrm{Tr}(Q\Lambda)^q$ [165]. The strong multifractal fluctuations of wave functions at criticality are related to the fact that $\Delta_q < 0$ for $q > 1$, so that the corresponding operators increase under RG. In this formalism, the scaling of correlation functions results from an operator product expansion.

7.2.1 IPR and Multifractality in 2D

In 2D GOE systems, the IPRs scale as (Again, here we denote $g \equiv g_{ph}$)

$$\langle P_q \rangle \simeq (2q-1)!! L^{-2(q-1)} \left(\frac{L}{l}\right)^{\frac{1}{\pi g} q(q-1)}. \tag{7.2}$$

In fact, the above Eq. (7.2) can be derived using the field theoretical method. We note first that the formulas (5.19), (5.20) for the IPR's with $q \leq \kappa^{-1/2}$ can be rewritten in the 2D case (with Eq. (5.21) taken into account) as

$$\frac{\langle P_q \rangle}{P_q^{RMT}} \simeq \left(\frac{L}{l}\right)^{\frac{1}{\beta\pi g} q(q-1)}, \tag{7.3}$$

where P_q^{RMT} is the RMT value of P_q which equals to $q! L^{-2(q-1)}$ for GUE and $(2q-1)!! L^{-2(q-1)}$ for GOE. We see that (7.3) has precisely the form (7.1) with

$$D_q = 2 - \frac{q}{\beta\pi g}. \tag{7.4}$$

As was found in [147, 148], the eigenfunction amplitude distribution (6.12) leads to the same result (7.4) for all $q \ll 2\beta\pi g$. Here the deviation of D_q from the normal dimension 2 is determined by a small parameter $1/\pi g$, in analogous to weak localization, the phenomena is coined "weak multifractality". The result (7.4) was first obtained by Wegner [165] via RG calculations. One of the questions will be investigated in the future is the boundary multifractality brought up by authors in Ref. [183]. We will not discuss the problem here, but reserve it as a topic for future study.

Note that, because of the absence of the genuine critical point in 2D, g becomes size-dependent, i.e. Eq. (5.26). This implies that for each scale L one can use the standard formula given above, but with slowly varying $g(L)$ in the exponent. This is possible because

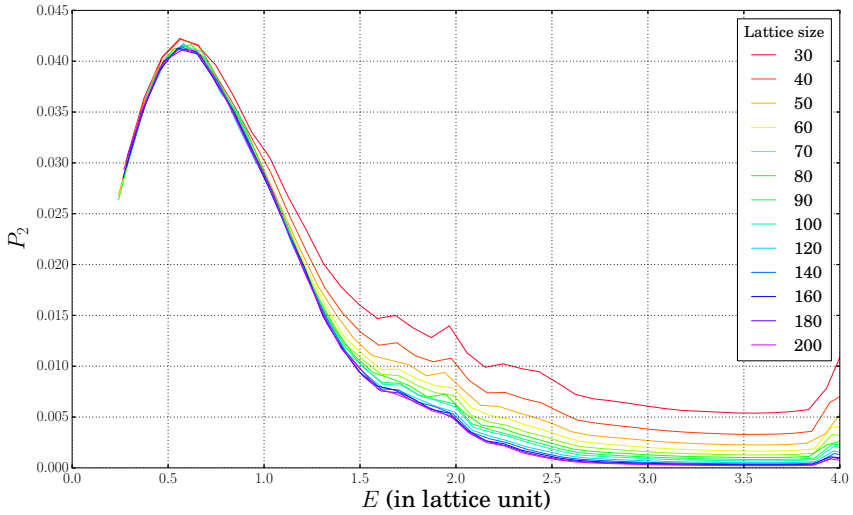

Figure 7.1: IPR for lattices of different sizes averaged over many realizations (at least 50) as a function of E (in lattice units).

corrections to g are not large in a finite size sample, and owing to the slow dependence of g on spatial scale L. With this procedure, we have obtained an excellent agreement between the theory of the logarithmic corrections to the conductivity and our numerical results as illustrated below.

7.2.2 Numerical Results

For disordered electrons in $2d$, the well-developed theory connects the behavior of various physical quantities with the value of the conductance.[99] We have calculated numerically the same quantities for flexural phonons, using the values of g_{ph} extracted from IPR, and found a very good agreement with the theoretical predictions existing for the disordered electrons in the case of the GOE. We present the findings in the remaining part of the chapter.

We see that for energies $E < 1$, IPR does not change with lattice size, indicating a localized phase. On the other hand, for energies $E > 1$, IPRs clearly change with

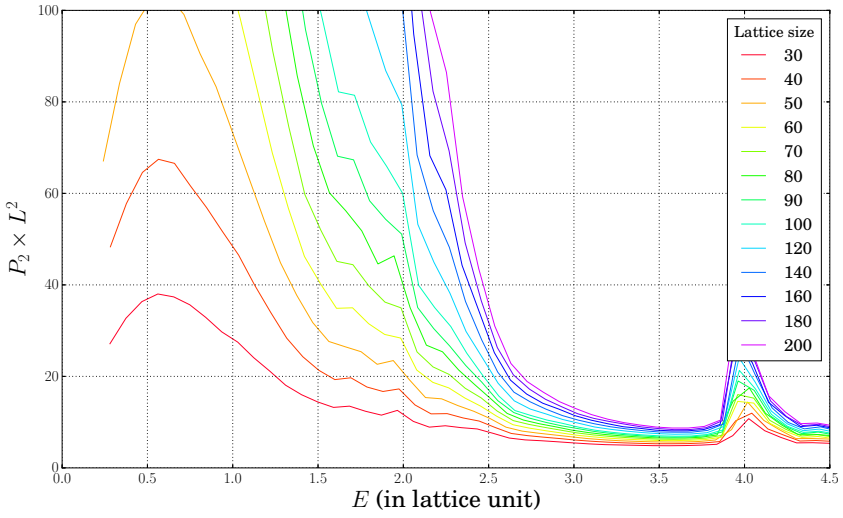

Figure 7.2: IPR scales with sample area L^2, L being the lattice size. Note that none of the lines cross at any energy. The cusp at $E \simeq 4.0$ is due to the Van Hove singularity.

increasing sizes. The middle bump represents the Van Hove singularity in momentum space. Thus, one thing we want to see is that if the IPR scales with the area of the sample, which is a signature of the metallic phase. For that matter, we will make further analysis. We are particularly interested in studying the flexural phonons in this region when $\xi \gg L$. As Figure 7.2 indicated, we see that there is no normal metallic phase for all energies in the sense that if one scales the IPR with the sample area, no line collapses on each other.

However, if one scales the IPR with a power less than 2 (but larger than 0), the lines will always cross at certain point. For example, in Figure 7.3 we have used the power 1.6, and the IPR lines cross at $E \sim 3.2$. The point of intersection ("critical point") allows to find the energy which corresponds to a given value of power-law exponent; By extracting from the IPR(L) the exponent of a power law for different energies, one may get the dependence of the dimensionless "conductance" $g(\varepsilon)$ on energy.

The phenomena above are closely related with the multifractality properties of the

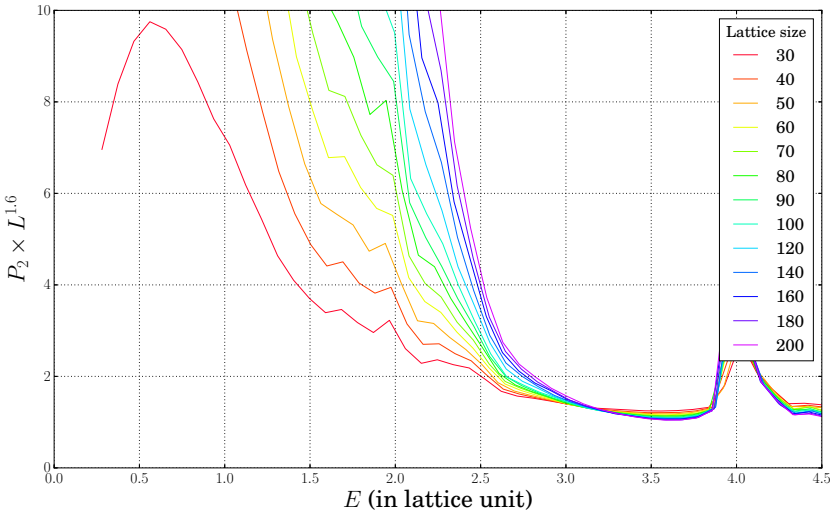

Figure 7.3: IPR scales with $L^{1.6}$ for different energies. Here all IPR lines for different sizes intersect at $E \sim 3.2$.

wave-functions in the diffusive regime. The scaling law $L^{1.6}$ rather than L^2, manifests the multifractality of the wave functions. Here we show a plot that illustrates the feature more explicitly. The fractal dimension mentioned above will be extracted directly through Eq. 7.1. From the size dependence of the IPR at a given energy, as is shown in the Fig. 7.4, we can extract an energy-dependent fractal dimension. Here we are in the diffusive regime. At a given concentration of the pinning centers the effective level of disorder is different for different energies, hence energy dependent effective diffusion coefficient. As a result, the IPR exponent now depends on the energy of the eigenstate. Like in the case of the disordered electronic system of a given symmetry class, the fractal dimension is determined by the conductance g_{ph}. For example, in the case of the Gaussian Orthogonal Ensemble (GOE), the size dependence of the IPR is described by the fractal dimension equal to $D_2(L) = 2 - 2/\pi g(L)$, where dependence of $g(L)$ on L is due to the weak-localization (WL) correction. [128] Thus, for each concentration of the pinned sites we can

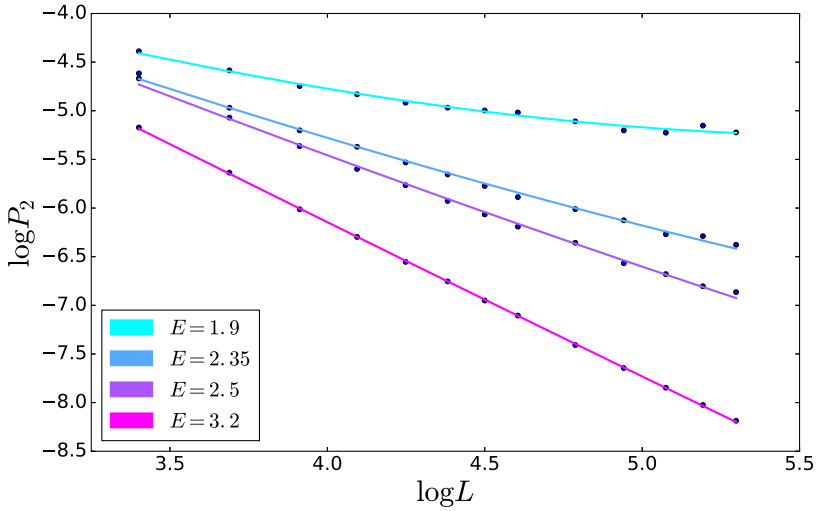

Figure 7.4: Scaling of the IPR with the system size for 20% of the pinned sites at several values of energy E. For example, the fitted slope for $E = 3.2$ is -1.59. The slope was used to find $g_{ph}(\varepsilon)$ presented in the blue line of figure 7.12. For the smallest energy ($E = 1.9$) the effect of the weak localization correction is clearly seen.

prescribe for different energies E the corresponding value of the phonon "conductance" $g(\%, E)$, using the expression for fractal dimension D_2 in Eq. (7.4).

Furthermore, since our "samples" are of limited size due to restrictions of numerics, in order to get a noticeable fractal dimension (in the example above, it is deviation of 1.6 from 2), we have used relatively large concentrations of the pinning centers (20%), in order for the parameter g_{ph} extracted from the IPR to be not too large. For a finite value of g_{ph}, it acquires logarithmic corrections $\sim \ln L/l$, which modify g_{ph} and hence the IPR exponents rendering them slowly dependent on the system size. The values of g_{ph}, including the corrections to g_{ph}, extracted from the IPR exponents are shown in Figure 7.4. The observed corrections are in excellent agreement with the theoretical corrections to the conductance previously evaluated for electrons. This was one of the checks of the connection between the parameter g_{ph} describing FPs and the conductance g of non-interacting electrons in

disordered conductors.

Although the localization length ξ in 2D is not infinite (as for truly critical systems at the Metal Insulator transition), it is exponentially large when $g \gg 1$, and the criticality takes place in a very broad range of the system sizes, $L \ll \xi$. Therefore, 2D samples with $g \gg 1$ share many common properties with systems at the critical point of the metal-insulator transition. Similar physics is valid for our system of FPs. In both cases it is crucial that due to absence of the genuine critical point, g is size-dependent. In our case, this dependence is logarithmic. This implies that for each scale L, one can use the standard formula with the scale-dependent $g(L)$ in the exponent, even when g is not too large. This is possible because (i) corrections to g are still not large, and (ii) due to the logarithmic dependence, they are "slow". With this procedure, we have obtained an excellent agreement between the theory of the logarithmic corrections to the conductivity and numerical results as it is shown in Figure 7.4.

7.3 Distribution and Fluctuation of IPR

Using the supersymmetry method, one can calculate also higher order correlation functions of the eigenfunction amplitude. In particular, the correlation function

$$\langle |\psi_k^4(\mathbf{r_1})||\psi_k^4(\mathbf{r_2})| \rangle_E$$

determines fluctuations of the inverse participation ratio P_2. We do not cover the details of calculation using the field theoretical method, which can be found in the Ref. [141]. For the relative variance of IPR, $\delta(P_2) \equiv \mathrm{var}(P_2)/\langle P_2 \rangle^2$ the result for GOE systems reads

$$\delta(P_2) = \frac{32 a_d}{g^2}, \tag{7.5}$$

with a numerical coefficient a_d depends on dimensionality and boundary conditions. For periodic BC in 2D, $a_2 = 0.00387$ [61]. The fluctuations (7.5) have the same relative magnitude ($\sim 1/g$) as the famous universal conductance fluctuations. Note also that extrapolating Eq. (7.5) to the Anderson transition point, where $g \sim 1$, one finds $\delta(P_2) \sim 1$, so that the magnitude of IPR fluctuations is of the order of its mean value (which is, in turn, much larger than in the metallic regime). At $1/g \ll P_2/\langle P_2\rangle - 1 \ll 1$, the distribution function is of the exponential form,

$$\mathcal{P}(P_2) \sim \exp\left\{-\frac{\pi}{4}\frac{\epsilon_1}{\Delta}\left(\frac{P_2}{\langle P_2\rangle} - 1\right)\right\}, \tag{7.6}$$

where ϵ_1 is the lowest non-zero eigenvalue of the diffusion operator. According to Ref. [184], $g = \frac{\epsilon_1}{2\Delta}$, thus it means that the IPR distribution could also provide some way to measure the phonon conductivity g. For our particular system,

$$\mathcal{P}(P_2) \sim \exp\left\{-\frac{\pi g}{2}\left(\frac{P_2}{\langle P_2\rangle} - 1\right)\right\}. \tag{7.7}$$

Note that for negative deviations $P_2/\langle P_2\rangle - 1$ with $|P_2/\langle P_2\rangle - 1| \gg 1/g$, the distribution function decays much faster, so that the distribution is strongly asymmetric [184].

7.3.1 Tail Distribution in 2D Geometry.

As stated in Ref. [61], to the leading order in $1/g$, the "body" of the distribution $\mathcal{P}(P_2)$ is described properly by the Liouville theory. This is also true for the asymptotic "tail" of $\mathcal{P}(P_2)$. Nevertheless, a more rigorous and relevant way to derive the asymptotic distributions of the IPR is to use the same saddle point method described in the above Chapter 6. Our consideration of asymptotics of the IPR distribution is based on Ref. [61]. Using the field theoretical description, the saddle point configuration can again be written as a function of the bosonic angle θ. And the equation resulting from the saddle point

method allow one to calculate the far asymptotics of $\mathcal{P}(P_2)$ at $P_2 \gg P_2^{RMT}$:

$$\mathcal{P}(P_2) \sim \frac{1}{P_2}\left(\frac{P_2}{\langle P_2\rangle}\right)^{-\beta\pi g/2} \quad \text{for} \quad 1 \ll P_2/P_2^{\mathrm{RMT}} \ll (L/l)^2 \ . \tag{7.8}$$

Thus, for the tail behavior of the IPR distribution, it has a transition from exponential decaying function to a power law one, with the exact same argument. This is a rather convenient way of checking the consistency of the data.

Conductance distribution is closely related to the distribution of IPR. We do not investigate in details of how the phonon conductance is distributed, however, it could become another gateway to the further study of our randomly pinned FP model. Theoretical [185, 186] and numerical [187, 188, 189, 190] methods of study the conductance distribution is listed here for reference.

7.3.2 Numerical Result

Let us first show the result where disorder concentration equals 10%. From the Fig. 7.5, one can see that the $\log$ IPR distributions have a scale-invariant shape[191], with an approximate normal distribution (there is a small skew to the right), while as expected, the centers of the distribution that represents the mean of IPR move toward lower values with increasing lattice size. The width of the individual bell shaped distribution is an indication of IPR variance. Next, we show a similar plot for lower concentration (5%) for a comparison. From Fig. 7.6, one can see that the distributions are more concentrated around the mean, which means they have less variances. This is consistent with Eq.. 7.5 where one can assume for the 5% concentration of disorder the fractal dimension D_2 is closer to normal dimension 2. In fact, the distribution of fractal dimension was directly studied numerically at the Anderson transition regime. [192] A $\log$ IPR distribution for 20% concentration of pinned disorder is also shown in figure 7.7 for completeness.

One sees similar behavior for IPR distributions in the numerical study of both 3D An-

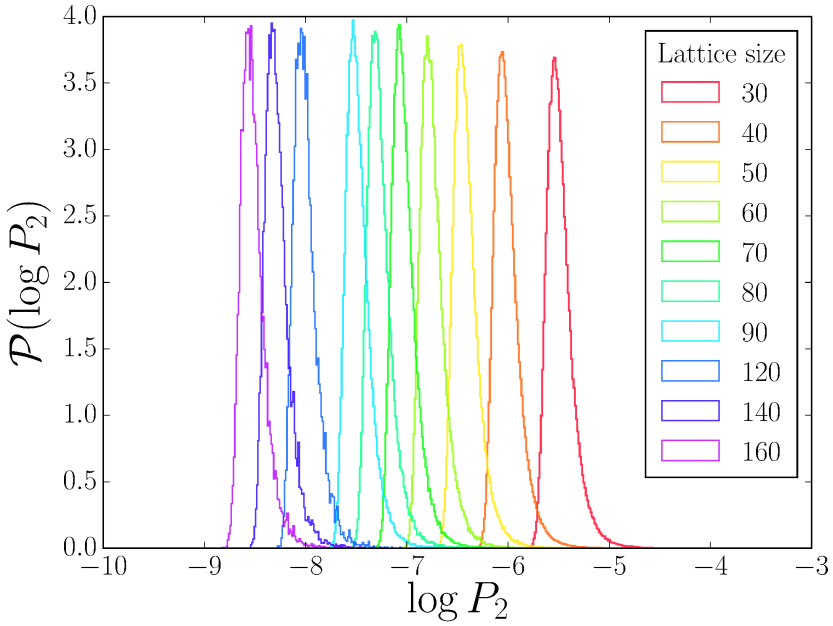

Figure 7.5: The probability distribution function of $\log$ IPR for 10% of pinning sites. Energy slice is taken around $E = 2.9$. For each lattice size, there are at least 50 disorder averaging performed.

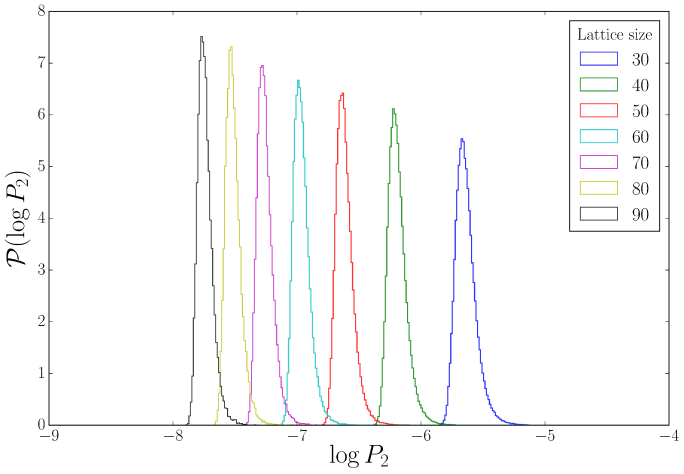

Figure 7.6: Distribution functions of $\log$ IPR for 5% of pinned sites. Energy is again $E \sim 2.9$. The variance of the bell-shaped curves are used to find $g_{ph}(\varepsilon)$ presented in the green line of figure 7.10.

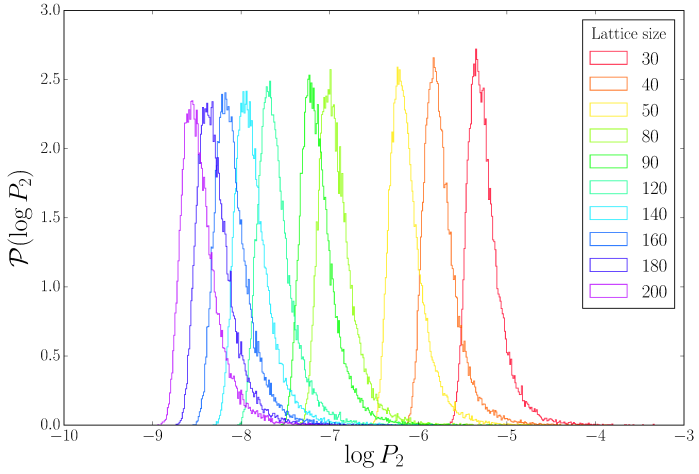

Figure 7.7: Distribution functions of $\log$ IPR for 20% of pinned sites. Energy is taken the same as in the previous plot ($E \sim 3.6$).

derson transition [193] and PRBM model [194, 195] for various system sizes. The questions of whether there is a finite size effect for the variance σ in the numerical calculation shown above is still to be investigated in future study.

Equally, we can obtain the statistical information of the IPR through its distribution. Figure 7.8 is a plot of the probability distribution of the rescaled IPR $\widetilde{P}_2 = \frac{P_2}{\langle P_2 \rangle} - 1$. One can see a similar plot of IPR distribution for the PRBM model at Fig.3 of the Ref. [191]. Here, we have shown two ways of rescaling, by the mean and median of the IPR respectively. The difference between the two ways of scaling is minimal. First, one can clearly see the exponential decay, then the curve starts to deviate the Eq. (7.6) at around $\widetilde{P}_2 \sim 0.5$, which is an indication of entering the power law decay region Eq. (7.8). Note that we plot the Fig. in a log-log plot, in order to show clearly the power law decay of the IPR distribution (Eq. 7.8) in the regime $\widetilde{P}_2 \geq 1$. The fitted $g = 3.5$, in excellent agreement with the previous fittings.

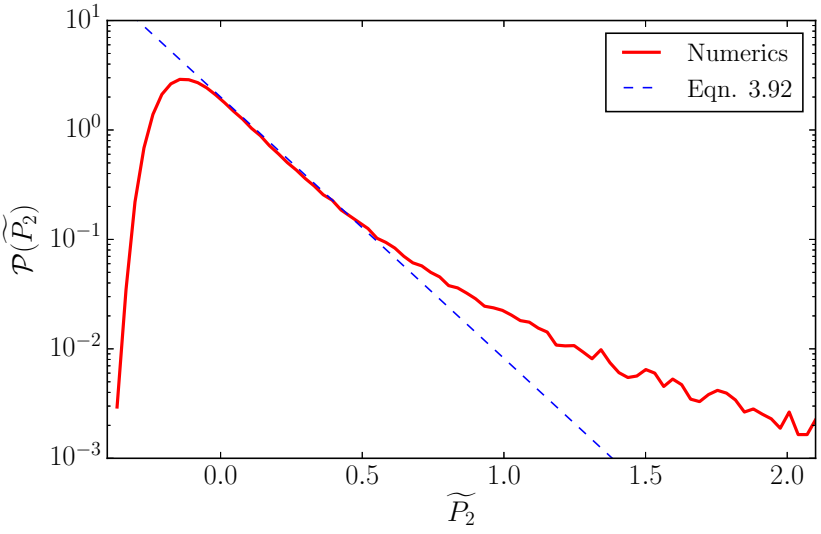

Figure 7.8: The semi-log plot of the IPR distribution. The sample has 40×40 lattice, with 20% of pinned sites and 20,000 disorder averaging. The energy is taken around $E \sim 3.6$. The estimated $g = 3.5$ according to Eq. (7.7).

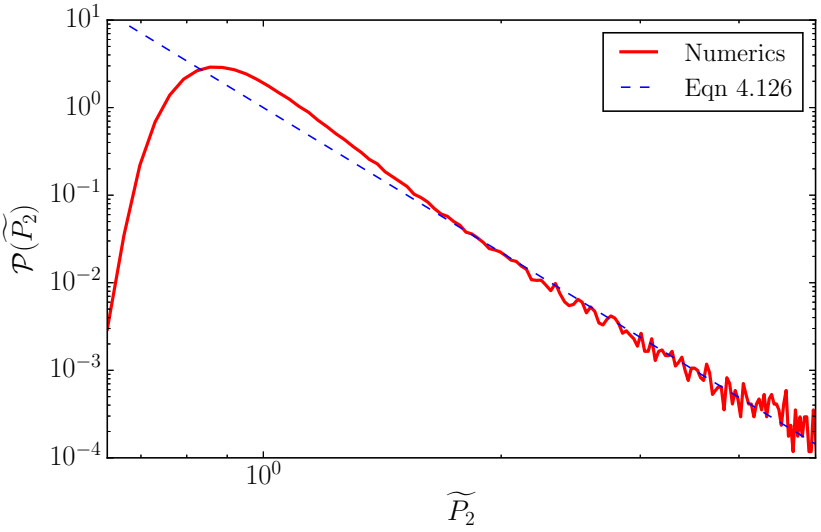

Figure 7.9: Log-log plot of the IPR distribution. The sample feature and parameter estimations coincide with the previous Figure 7.8.

7.4 Extract g_{ph} from IPR

A reasonable agreement for $g_{ph}(\varepsilon)$ found in two ways (reasonable because g is not large enough) can be seen in Fig. 7.10. g_1 was found by applying Eq. (7.1) to the fraction dimensions for different energies, where $E \in [1.0, 3.5]$ of the sample. Also, in Figures

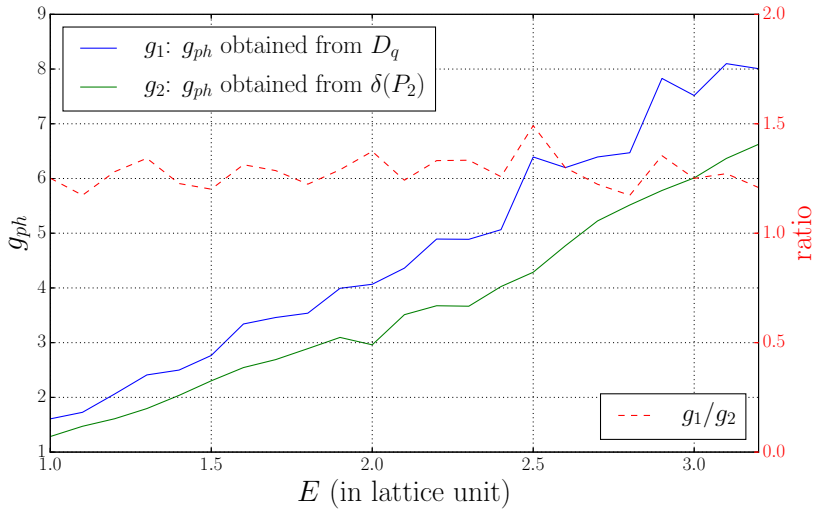

Figure 7.10: The dimensional "conductance" as a function of energy in the metallic region $\xi > L$. Data come from lattices with 5% of pinning sites. The conductance is found from scaling behavior of the IPR as described in Figure 7.3's caption, and also from the variance of the IPR at different energies.

7.11 and 7.12, we show the result of calculating g in two ways using 10% and 20% concentration respectively.

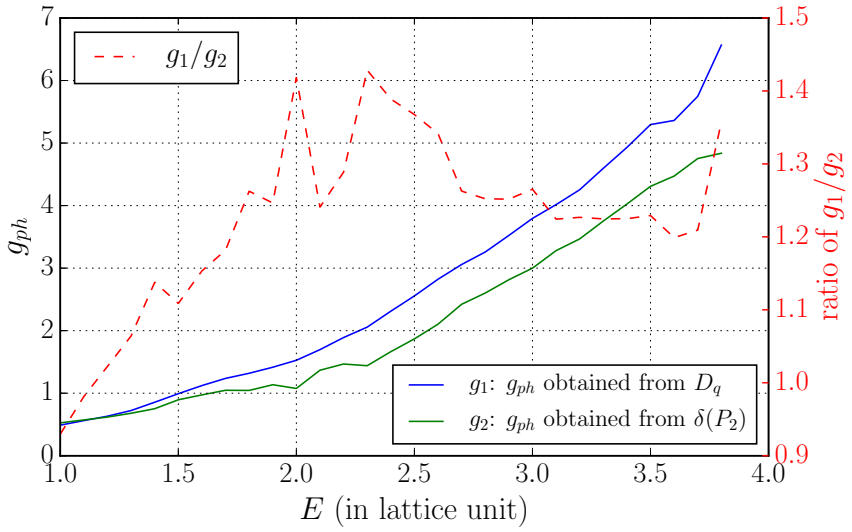

Figure 7.11: The dimensional "conductance" as a function of energy in the metallic region for lattices with 10% pinned sites.

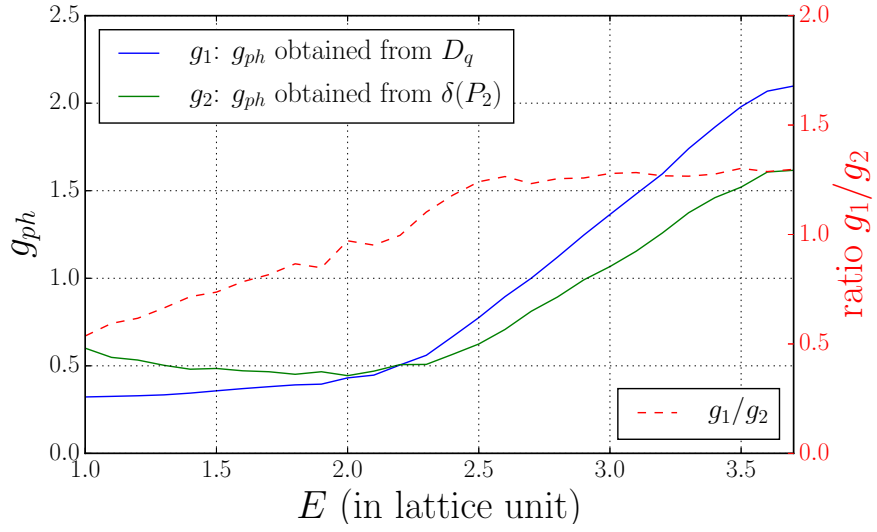

Figure 7.12: The dimensional "conductance" as a function of energy in the metallic region for lattices with 20% pinned sites.

8. IMPACT ON THE DEPHASING RATE IN GRAPHENE

In this chapter we come back to evaluate the effect on the dephasing rate due to the interaction of FP with pinning centers. In the quantum hall transition, multifractality of the wave function is closely related to the dephasing properties [196]. Here we concentrate more on theoretical approach and analysis, which to some extent will give the necessary support for the numerical result we have discussed in the earlier chapters.

8.1 The Dephasing Rate due to FPs

One can express the dephasing problem with the time decay functional as

$$F(t) = t \int (d\Omega)(dQ) \langle \phi\phi \rangle_{\Omega,Q} B(Q) C(\Omega, t),$$

where the functions

$$B(Q) = \frac{2}{v_F Q} \left(1 - \left(\frac{Q}{2k_F}\right)^2\right) \theta(2k_F - Q)$$
$$C(\Omega, t) = 1 - \sin(\Omega t) / (\Omega t),$$

and

$$\langle \phi\phi \rangle = \frac{1}{2} g(Q)^2 \Sigma^k(\Omega, Q).$$

The formulas follow the definitions and calculations in our previous publication [18]. Here $g(Q) = g\frac{Q}{Q+4g_e k_F}$ is the screened coupling constant of electron-FP interaction, and $g \sim 30eV$ is the unscreened coupling constant. For the self-energy operator, it can be expressed

as

$$\Sigma^k(\Omega,Q) = -(2\pi)^3 \int (d\mathbf{p})(d\mathbf{q})(d\epsilon_1)(d\epsilon_2)\left[\coth(\epsilon_1/2T)\coth(\epsilon_2/2T)+1\right] \times \Re\left[D^R(\epsilon_1,\mathbf{p})D^A(\epsilon_2,\mathbf{q})\right]\frac{(\mathbf{pq})^2}{4}\delta(\epsilon_1+\epsilon_2-\Omega)\delta(\mathbf{p}+\mathbf{q}-\mathbf{Q}).$$

We will proceed the calculation with $\epsilon_1 = \omega + \Omega/2$ and $\epsilon_2 = \omega - \Omega/2$, $p = k + Q/2$,$q = k - Q/2$. After plugging in the definition of FP Green's function is defined in Eq. (2.2), one arrives at the expression for the self-energy

$$\Sigma^k(\Omega,\mathbf{Q}) = \frac{\nu_p\tau^{-1}T^2}{2\rho^2\alpha^2}\int_{\tau^{-1}}^{\infty}\frac{(d\omega)}{\omega^2}\frac{1}{\tau^{-2}+(\Omega - v(\omega)\cdot\mathbf{Q})^2}.$$

In the rest of the chapter, we are concentrated with time $t \gg \tau$, where τ is the elastic scattering time defined in Eq. (2.4). For $t < \tau$, the calculation will come back to the clean case [18]. Furthermore, we consider energy scales satisfy $\omega \gg \tau^{-1} \gg \Omega$. The integral is complicated and has several regimes to be discussed in detail. Also we assume that $T_{BG}\tau \ll 1$, with $T_{BG} = 54\sqrt{n/10^{12}\mathrm{c}m^2}$ for the Bloch-Gruneisen temperature of FP. Then, it follows $\tau^{-1} \ll \frac{\tau^{-1}}{T_{BG}\tau} \ll T$. After carefully evaluating the different asymptotics, we arrive the conclusion that

$$\begin{aligned} F &= \frac{t}{2}g^2\frac{\nu_p\tau^{-1}T^2}{2\rho^2\alpha^2}2\int_{\tau^{-1}}^{T}\frac{(d\omega)}{\omega^2}\frac{\tau\mu}{(2\pi)^2 v_F^2} \\ &\sim t\frac{T^2}{\mu}T_{BG}\tau. \end{aligned} \tag{8.1}$$

Here, μ is the chemical potential of the Graphene and g (in this chapter) denotes the electron phonon coupling constant. Therefore due to the cut off τ^{-1}, τ_ϕ^{-1} is a factor $T_{BG}\tau$ larger than the 'golden rule' rate [80, 18].

8.1.1 Diffuson Contribution

Taking the contribution of the diffuson propagator into account, we will perform the calculation in the following limit: $\omega \gg \tau^{-1} \gg \Omega$, $\Omega^2 \ll 2D\tau^{-1}Q^2 = 4\omega\omega_Q$, and $\mathbf{k} \gg \mathbf{Q}$, $DQ^2\tau \ll 1$ (the limit is set in the similar sense for electron-impurity diffuson calculation). Thus, the self-energy can now be written as

$$\Sigma^k(\Omega, Q) = -\frac{\pi\nu_p}{4\rho^2\alpha^2}\int (d\omega)\left(\frac{2T}{\omega}\right)^2 \Re\frac{1}{DQ^2 + i\Omega}.$$

In the Eq. (8.1), we performed energy integral first, while here, we first integrate out the momentum, which is similar to the way done in field theoretical approach to solve the electron transport problem [197]. Here, we define

$$\omega_D(\omega) \equiv 4Dk_F^2 = \omega(\omega_{2k_F}\tau),$$

which is the energy of diffuson of momentum $2k_F$. After introducing the bending energy scale $\kappa \sim 1eV$, one gets for $\omega \gg \tau^{-1} \gg \Omega \gg \omega_D$,

$$
\begin{aligned}
F(t) &= \frac{Ntg^2T^2}{(128\pi\kappa)^2} T_{BG}\tau \frac{T_{BG}t}{\mu} \int_{\tau^{-1}}^{T} \frac{d\omega}{\omega} \int_{\omega_D t}^{t/\tau} ds \frac{1}{s^2} \left(1 - \frac{\sin(s)}{s}\right) \\
&= \left(\frac{g}{128\pi\kappa}\right)^2 N T_{BG}\tau \frac{T_{BG}}{\mu} t^2 T^2 \int_{\tau^{-1}}^{T} \frac{d\omega}{\omega} \begin{cases} \frac{1}{\omega_D t} & \text{for } \omega_D t \gg 1 \\ \pi/4 & \text{for } \omega_D t \ll 1 \ \& \ t/\tau \gg 1 \\ \frac{t/\tau}{6} & \text{for } t/\tau \ll 1 \end{cases} \\
&= \left(\frac{g}{128\pi\kappa}\right)^2 N T_{BG}\tau \frac{T_{BG}}{\mu} t^2 T^2 \begin{cases} \frac{t^{-1}}{T_{BG}\tau}\tau & \text{for } t \gg T_{BG}^{-1} \\ 1 - \pi/4 \log T_{BG} t & \text{for } T^{-1}(T_{BG}\tau)^{-1} \ll t \ll T_{BG}^{-1} \\ \pi/4 \log T\tau & \text{for } \tau \ll t \ll T^{-1}(T_{BG}\tau)^{-1} \\ \frac{t/\tau}{6} \log T\tau & \text{for } T^{-1} \ll t \ll \tau \end{cases}.
\end{aligned}
\tag{8.2}
$$

Here $N \sim 1.05$ is a numerical factor.

8.1.2 Crossover to Ballistic Regime

One can use the factor S (defined in Eq. (2.5)) to substitute the diffusion pole, and get

$$
\Sigma^k(\Omega, Q) = \frac{\pi\nu_p}{4\rho^2\alpha^2} \int (d\omega) \left(\frac{2T}{\omega}\right)^2 \Re\left[\frac{\tau^2}{\tau - S^{-1}}\right].
$$

Introduce $\hat{\omega} = \omega\tau$, $\hat{\Omega} = \Omega\tau$ and $\hat{Q} = Q/2k_F$, then

$$
\hat{S} \equiv S\tau = \sqrt{1 + 4T_{BG}\tau\hat{\omega}\hat{Q}^2 - \hat{\Omega}^2 + 2i\hat{\Omega}}.
$$

In principle, one can perform some numerical calculation based on this more general form and gain some insights about the ballistic regime, which is again beyond our scope in my

dissertation work.

9. SUMMARY AND DISCUSSION

9.1 Summary of the Results

In the dissertation work we studied an effective model for flexural phonon localization. In our discretization of Eq. (3.3), one pinned site represents an attached area of the size of the order of 10nm. We have neglected the effects of anharmonicity and ripples. According to the analysis of Ref. [81], at any temperature only a small fraction of the phase space of FPs is modified by anharmonicity. Concerning the ripples, according to Ref. [82] at the interested temperatures range $(\sim 1\mathrm{K})$ ripples are expected to be too large and too smooth to influence motion of the FPs. Our analysis is thus built on the following three assumptions: (I) flexural phonons were decoupled from other modes, (II) scattering from the attached areas is similar to the scattering from a rigid obstacle, and (III) we are talking only about low energies/low temperatures, and physics on large scales about 10nm and more. We summarize the findings of the dissertation work here:

1. Anderson Localization of FPs at low energy seems confirmed. The Randomly Pinned Flexural Phonon model (RPFP) reveals the physics of Anderson localization for flexural phonons in 2D material.

2. Dimensionless conductance extracted using various quantities are highly consistent. Here, we list in the Table 9.1 the estimated g_{ph} from various properties of our system ranging from level statistics to IPR distributions. Except for some minor difference, one sees an excellent match between different ways of calculating g_{ph}.

3. Physics in the diffusive (to the ergodic) regime reveals quite universal features that are consistent with the Non-linear σ-model in Gaussian Orthogonal Ensemble systems.

A general question which we raised in the beginning has been answered in the numerical study discussed in this dissertation: If we compare with the electrons propagating in a disordered lattice, will the statistical properties of the randomly pinned FPs be the same or different? We have calculated numerically a number of quantities characterizing statistical properties of FPs. Using the values for g_{ph} extracted from the data via various quantities, we found a very good agreement with the theoretical predictions existing for the disordered Anderson model in the case of the Orthogonal Class of Universality. This, of course, is not surprising because there is no reason to expect anything different from the 2d Anderson model. (The squared Laplacian should not be so different from a simple Laplacian since the shortest scale is the mean-free path. Also pinning instead of other random potential do not change symmetry properties.) Furthermore, the theoretical expressions for the number of variance $\Sigma^2(\omega, \Omega)$ and the wave function intensity distribution $\mathcal{P}(y)$, both are intimately connected with the effects of the WL originating from the Cooperons [61, 108]. The excellent agreement demonstrated in Figs. 4.7, 4.8 and 5.5 justifies that in the discussed model, the regime of WL is the same as in the Anderson model in $2d$. We believe that the reason for the observed universal behavior is that the FPs in the lattice with pinned sites are eventually described with the same Non-Linear σ-model as disordered electrons in the orthogonal class of universality. Thus, from the results of the numerical study we assert that the answer to the question is positive: the pinned FPs share the same statistical properties with those electrons in the orthogonal class of universality. Moreover, the numerical results shows that our model is very suitable for studying other universal features in 2D disordered system. I have mentioned the potential future study object in various places of the dissertation. In one sentence, we could say that the randomly pinned FP model will open a new avenue for localization physics in 2D phononic system, in particular, the transport properties that are associated with FPs need to be carefully reconsidered.

Let us finally come back to physical situations in Graphene and have an estimation of

Methods of Calculation	Estimated g_{ph}
Level number variance Eq. (4.9) with 80×80 lattice	1.6
Level number variance Eq. (4.9) with 200×200 lattice	1.4
Wave function intensity (not too large) Eq. (5.23) with 80×80 lattice	1.6
Fal'ko-Efetov exact solution Eq. (6.5) with 80×80 lattice	1.6
IPR tail distribution Eq. (7.7) with 40×40 lattice	3.5
Fractal dimension D_q from Eq. (7.4)	1.9
Variance of $\log$ IPR distribution from Eq. (7.5)	1.5

Table 9.1: Comparison of different methods of estimating g_{ph} for lattice with 20% of pinned sites at $E \sim 3.5$.

at what conditions one can achieve the physics discussed above. To be more specific, let us estimate energy of FPs at which a crossover from strong to weak localization occurs. Strong localization, where $\omega \lesssim 1/\tau$, holds for momenta $k^2 \lesssim 8n_i$ that for our choice of a_i yields $k < 0.14nm^{-1}$. The corresponding energy is about $0.1K$. So far, we didn't consider the effect of strain. The strain $\bar{u}$, ignoring anisotropy, is known to add the term $\rho\bar{u}v_L^2k^2$ into the equation of motion, Eq. (3.1), where v_L is the velocity of the longitudinal phonons. In the isotropic approximation this yields $\omega(k) = \sqrt{(\alpha k^2)^2 + \bar{u}(v_L k)^2}$. One has to keep in mind that the scattering of an FP from a high enough barrier doesn't depend on details, and the cross-section remains $4/k$, if $k < a^{-1}$. Then, for the linear spectrum the condition for strong localization is $k^2 \lesssim 4n_i$, which is similar to what we have got above. Typically, $\bar{u}$ is $\backsim 10^{-4}$, and the effects of bending and strain are of comparable strength for the discussed scales. Note that our estimate for the scale of strong localization is conservative. In reality, the size of the attached areas can be comparable with the distances between them. Then, owing to the factor $f \approx ka > 1$, the energy of the localized FPs can be few times larger, which is very prominent for the experimental realization. Furthermore, effects of the weak localization noticeably expand localization of the FPs. One may easily show that, as compared to the strong localization, the weak localization increases

momenta of the FPs which undergo localization by a factor of $\ln(L/l)$. (In this estimate, it is necessary to take into consideration the factor f in the scattering cross-section.) Correspondingly, weak localization boosts the energy of the localized FPs by a factor $\ln^2(L/l)$. For a standard micron size sample, $\ln \frac{L}{10\text{nm}} \simeq 5$. As a result, the energy of localized FPs increases up to few K.

9.2 Potential Impact of Research

In the community of localization physics, there exists a "power-law random banded matrix ensemble" (PRBM) which describes a kind of one-dimensional system with a long-range hopping whose amplitude decreases as $r^{-\alpha}$ with distance [137, 198]. In various contexts such as quantum chaos [199, 200] and disordered systems [201, 202], PRBM appears as a natural model. Again, the model can be mapped onto a SUSY σ-model. Statistics of levels and eigenfunctions in the PRBM model are then studied, which gives great insight on the problem of Anderson localization. Part of reasons why PRBM is popular for studying localization physics is due to its ease for numerical computation. In the rest of the dissertation, we have seen that our model of randomly pinned FP (RPFP) is also a great tool for reproducing various established results in the disordered system. Moreover, from my experience with working on the RPFP model, one will expect that potentially the community could also embrace the model due to its simplicity. In conclusion, we demonstrate that elastic system with randomly pinned centers is an excellent polygon for numerical study of the physics of random systems. Localization of the FPs is much more similar to the localization of electrons in well studied models rather than to the problematic localization of chiral electrons in disordered graphene.

For systems in the strongly localized phase, until recently, it still only exists very limited theoretical methods to study the statistical properties of the system. One of them is the generalized Dorokhov-Mello-Pereyra-Kuma (DMPK) equation, which has been

used in numerical simulation of electron transport problems [185, 203, 186, 204, 205]. Another way to study the localized regime is through the finite size scaling properties [206, 207, 208, 209] of the conductance which is also connected to the multifractal properties of the wave function [210, 211]. Our model of pinned flexural phonons to some extent also serves as an ideal model to mimic the Anderson model. Recently, localization to ergodic phase transition in become a hot research topic.[212, 213] The many-body localization (MBL) concept emerged as an extension to the idea of Anderson localization. It would not be a wild conjecture that our model could be a good testing ground for MBL physics. [214, 215] Furthermore, apart from its theoretical and numerical convenience which we have shown in the dissertation, one can even think of experimental realization, which will shed light on the Anderson localization and related problems 60 years after its birth.

REFERENCES

[1] S. Das Sarma, S. Adam, E. H. Hwang, and E. Rossi, "Electronic transport in two-dimensional graphene," *Reviews of Modern Physics*, vol. 83, no. 2, pp. 407–470, 2011.

[2] A. H. Castro Neto, N. M. R. Peres, K. S. Novoselov, and A. K. Geim, "The electronic properties of graphene," *Reviews of Modern Physics*, vol. 81, no. 1, pp. 109–162, 2009.

[3] E. Mariani and F. von Oppen, "Flexural phonons in free-standing graphene," *Phys. Rev. Lett.*, vol. 100, no. 7, p. 076801, 2008.

[4] H. Ochoa, E. V. Castro, M. I. Katsnelson, and F. Guinea, "Temperature-dependent resistivity in bilayer graphene due to flexural phonons," *Phys. Rev. B*, vol. 83, no. 23, p. 235416, 2011.

[5] I. V. Gornyi, V. Y. Kachorovskii, and A. D. Mirlin, "Conductivity of suspended graphene at the dirac point," *Phys. Rev. B*, vol. 86, no. 16, p. 165413, 2012.

[6] A. A. Balandin, S. Ghosh, W. Bao, I. Calizo, D. Teweldebrhan, F. Miao, and C. N. Lau, "Superior thermal conductivity of single-layer graphene," *Nano Letters*, vol. 8, no. 3, pp. 902–907, 2008.

[7] J. H. Seol, I. Jo, A. L. Moore, L. Lindsay, Z. H. Aitken, M. T. Pettes, X. Li, Z. Yao, R. Huang, D. Broido, N. Mingo, R. S. Ruoff, and L. Shi, "Two-dimensional phonon transport in supported graphene," *Science*, vol. 328, no. 5975, pp. 213–6, 2010.

[8] K. I. Bolotin, K. J. Sikes, J. Hone, H. L. Stormer, and P. Kim, "Temperature-dependent transport in suspended graphene," *Phys. Rev. Lett.*, vol. 101, no. 9, p. 096802, 2008.

[9] E. V. Castro, H. Ochoa, M. I. Katsnelson, R. V. Gorbachev, D. C. Elias, K. S. Novoselov, A. K. Geim, and F. Guinea, "Limits on charge carrier mobility in suspended graphene due to flexural phonons," *Phys. Rev. Lett.*, vol. 105, no. 26, p. 266601, 2010.

[10] E. H. Hwang and S. Das Sarma, "Acoustic phonon scattering limited carrier mobility in two-dimensional extrinsic graphene," *Phys. Rev. B*, vol. 77, no. 11, p. 115449, 2008. Note that the phonon's contribution to resistivity is about 100 Ohm on the background of few kOhms.

[11] B. L. Altshuler, A. G. Aronov, and D. E. Khmelnitsky, "Effects of electron-electron collisions with small energy transfers on quantum localization," *Journal of Physics C-Solid State Physics*, vol. 15, no. 36, pp. 7367–7386, 1982.

[12] X. Wu, X. Li, Z. Song, C. Berger, and W. A. de Heer, "Weak antilocalization in epitaxial graphene: Evidence for chiral electrons," *Phys. Rev. Lett.*, vol. 98, no. 13, p. 136801, 2007.

[13] F. V. Tikhonenko, D. W. Horsell, R. V. Gorbachev, and A. K. Savchenko, "Weak localization in graphene flakes," *Phys. Rev. Lett.*, vol. 100, no. 5, p. 056802, 2008.

[14] F. V. Tikhonenko, A. A. Kozikov, A. K. Savchenko, and R. V. Gorbachev, "Transition between electron localization and antilocalization in graphene," *Physical Review Letters*, vol. 103, no. 22, p. 226801, 2009.

[15] M. B. Lundeberg and J. A. Folk, "Rippled graphene in an in-plane magnetic field: Effects of a random vector potential," *Phys. Rev. Lett.*, vol. 105, no. 14, p. 146804, 2010.

[16] J. Jobst, D. Waldmann, I. V. Gornyi, A. D. Mirlin, and H. B. Weber, "Electron-electron interaction in the magnetoresistance of graphene," *Phys. Rev. Lett.*,

vol. 108, p. 106601, Mar 2012.

[17] E. Mariani and F. von Oppen, "Flexural phonons in free-standing graphene," *Phys. Rev. Lett.*, vol. 100, no. 7, p. 076801, 2008.

[18] K. S. Tikhonov, W. L. Z. Zhao, and A. M. Finkel'stein, "Dephasing time in graphene due to interaction with flexural phonons," *Physical Review Letters*, vol. 113, no. 7, p. 076601, 2014.

[19] C. R. Dean, A. F. Young, I. Meric, C. Lee, L. Wang, S. Sorgenfrei, K. Watanabe, T. Taniguchi, P. Kim, K. L. Shepard, *et al.*, "Boron nitride substrates for high-quality graphene electronics," *Nature nanotechnology*, vol. 5, no. 10, pp. 722–726, 2010.

[20] M. Ishigami, J. Chen, W. Cullen, M. Fuhrer, and E. Williams, "Atomic structure of graphene on sio2," *Nano Letters*, vol. 7, no. 6, pp. 1643–1648, 2007.

[21] A. N. Norris and C. Vemula, "Scattering of flexural waves on thin plates," *Journal of Sound and Vibration*, vol. 181, no. 1, pp. 115–125, 1995.

[22] C. Vemula and A. N. Norris, "Flexural wave propagation and scattering on thin plates using mindlin theory," *Wave Motion*, vol. 26, no. 1, pp. 1–12, 1997.

[23] P. W. Anderson, "Absence of diffusion in certain random lattices," *Phys. Rev.*, vol. 109, pp. 1492–1505, Mar 1958.

[24] D. J. Thouless, "Electrons in disordered systems and the theory of localization," *Physics Reports*, vol. 13, no. 3, pp. 93–142, 1974.

[25] P. Markos, "Numerical analysis of the anderson localization," *Acta Physica Slovaca. Reviews and Tutorials*, vol. 56, no. 5, 2006.

[26] B. Kramer and A. MacKinnon, "Localization: theory and experiment," *Reports on Progress in Physics*, vol. 56, no. 12, pp. 1469–1564, 1993.

[27] F. Evers and A. Mirlin, "Anderson transitions," *Reviews of Modern Physics*, vol. 80, no. 4, pp. 1355–1417, 2008.

[28] S. John, H. Sompolinsky, and M. J. Stephen, "Localization in a disordered elastic medium near two dimensions," *Physical Review B*, vol. 27, no. 9, p. 5592, 1983.

[29] T. R. Kirkpatrick, "Localization of acoustic waves," *Physical Review B*, vol. 31, no. 9, pp. 5746–5755, 1985.

[30] E. Akkermans and R. Maynard, "Weak localization and anharmonicity of phonons," *Physical Review B*, vol. 32, no. 12, pp. 7850–7862, 1985.

[31] S. M. Cohen and J. Machta, "Localization of third sound by a disordered substrate," *Phys Rev Lett*, vol. 54, no. 20, pp. 2242–2245, 1985.

[32] C. A. Condat and T. R. Kirkpatrick, "Resonant scattering and anderson localization of acoustic waves," *Physical Review B*, vol. 36, no. 13, pp. 6782–6793, 1987.

[33] M. L. Williams and H. J. Maris, "Numerical study of phonon localization in disordered systems," *Physical Review B*, vol. 31, no. 7, pp. 4508–4515, 1985.

[34] H. Bottger and M. Theuerkauf, "Phonon localization in disordered systems application of a probabilistically-based self-consistent theory," *physica status solidi (b)*, vol. 156, no. 2, pp. 431–439, 1989.

[35] J. E. Graebner, B. Golding, and L. C. Allen, "Phonon localization in glasses," *Physical Review B*, vol. 34, no. 8, pp. 5696–5701, 1986.

[36] D. R. Luhman, J. C. Herrmann, and R. B. Hallock, "Observation of two-dimensional classical wave localization: third sound on superfluid 4he films on a disordered substrate," *Phys Rev Lett*, vol. 94, no. 17, p. 176401, 2005.

[37] N. Perrin, "Phonon localization in two-dimensional self-supported films," *Physical Review B*, vol. 48, no. 16, pp. 12151–12154, 1993.

[38] M. P. Blencowe, "Phonon localization in mesoscopic free-standing films," *Journal of Physics: Condensed Matter*, vol. 7, no. 27, pp. 5177–5193, 1995.

[39] C. W. Chang, A. M. Fennimore, A. Afanasiev, D. Okawa, T. Ikuno, H. Garcia, D. Li, A. Majumdar, and A. Zettl, "Isotope effect on the thermal conductivity of boron nitride nanotubes," *Phys. Rev. Lett.*, vol. 97, p. 085901, Aug 2006.

[40] I. Savic, N. Mingo, and D. A. Stewart, "Phonon transport in isotope-disordered carbon and boron-nitride nanotubes: is localization observable?," *Phys Rev Lett*, vol. 101, no. 16, p. 165502, 2008.

[41] C. Monthus and T. Garel, "Anderson localization of phonons in dimension d= 1, 2, 3: Finite-size properties of the inverse participation ratios of eigenstates," *Physical Review B*, vol. 81, no. 22, p. 224208, 2010.

[42] J. Mendoza and G. Chen, "Anderson localization of thermal phonons leads to a thermal conductivity maximum," *Nano Lett*, vol. 16, no. 12, pp. 7616–7620, 2016.

[43] S. John, "Localization of light," *Physics Today*, vol. 44, no. 5, pp. 32–40, 1991.

[44] S. John, C. Soukoulis, M. H. Cohen, and E. N. Economou, "Theory of electron band tails and the urbach optical-absorption edge," *Phys. Rev. Lett.*, vol. 57, pp. 1777–1780, Oct 1986.

[45] E. P. Wigner, "On a class of analytic functions from the quantum theory of collisions," *Annals of mathematics*, pp. 36–67, 1951.

[46] F. J. Dyson, "Statistical theory of the energy levels of complex systems. i," *Journal of Mathematical Physics*, vol. 3, no. 1, pp. 140–156, 1962.

[47] F. J. Dyson, "Statistical theory of the energy levels of complex systems. ii," *Journal of Mathematical Physics*, vol. 3, no. 1, pp. 157–165, 1962.

[48] F. J. Dyson, "Statistical theory of the energy levels of complex systems. iii," *Journal of Mathematical Physics*, vol. 3, no. 1, pp. 166–175, 1962.

[49] M. L. Mehta, *Random matrices*, vol. 142. Academic press, 2004.

[50] J. Wishart, "The generalised product moment distribution in samples from a normal multivariate population," *Biometrika*, vol. 20A, no. 1-2, pp. 32–52, 1928.

[51] C. Sarkar and S. Jalan, "Social patterns revealed through random matrix theory," *EPL (Europhysics Letters)*, vol. 108, no. 4, p. 48003, 2014.

[52] V. Plerou, P. Gopikrishnan, B. Rosenow, L. A. N. Amaral, T. Guhr, and H. E. Stanley, "Random matrix approach to cross correlations in financial data," *Phys. Rev. E*, vol. 65, p. 066126, Jun 2002.

[53] J. Bun, J.-P. Bouchaud, and M. Potters, "Cleaning large correlation matrices: Tools from random matrix theory," *Physics Reports*, vol. 666, no. Supplement C, pp. 1 – 109, 2017. Cleaning large correlation matrices: tools from random matrix theory.

[54] O. Bohigas, M. J. Giannoni, and C. Schmit, "Characterization of chaotic quantum spectra and universality of level fluctuation laws," *Physical Review Letters*, vol. 52, no. 1, pp. 1–4, 1984.

[55] L. Gor'kov and G. Éliashberg, "Minute metallic particles in an electromagnetic field," *Soviet Journal of Experimental and Theoretical Physics*, vol. 21, p. 940, 1965.

[56] K. Efetov, "Supersymmetry and theory of disordered metals," *Advances in Physics*, vol. 32, no. 1, pp. 53–127, 1983.

[57] K. Efetov, *Supersymmetry in disorder and chaos*. Cambridge University Press, 1999.

[58] A. Ishimaru, *Wave propagation and scattering in random media*, vol. 2. Academic press New York, 1978.

[59] B. Shapiro, "Large intensity fluctuations for wave propagation in random media," *Phys. Rev. Lett.*, vol. 57, pp. 2168–2171, Oct 1986.

[60] A. D. Mirlin, R. Pnini, and B. Shapiro, "Intensity distribution for waves in disordered media: Deviations from rayleigh statistics," *Phys. Rev. E*, vol. 57, pp. R6285–R6288, Jun 1998.

[61] A. Mirlin, "Statistics of energy levels and eigenfunctions in disordered systems," *Physics Reports*, vol. 326, no. 5-6, pp. 259–382, 2000.

[62] A. Pandey and M. L. Mehta, "Gaussian ensembles of random hermitian matrices intermediate between orthogonal and unitary ones," *Comm. Math. Phys.*, vol. 87, no. 4, pp. 449–468, 1982.

[63] A. Altland, S. Iida, and K. B. Efetov, "The crossover between orthogonal and unitary symmetry in small disordered systems: a supersymmetry approach," *Journal of Physics A: Mathematical and General*, vol. 26, no. 14, p. 3545, 1993.

[64] P. M. Chaikin and T. C. Lubensky, *Principles of condensed matter physics*, vol. 1. Cambridge Univ Press, 2000.

[65] H. Conley, N. V. Lavrik, D. Prasai, and K. I. Bolotin, "Graphene bimetallic-like cantilevers: probing graphene/substrate interactions," *Nano letters*, vol. 11, no. 11, pp. 4748–4752, 2011.

[66] J. Sabio, C. Seoanez, S. Fratini, F. Guinea, A. C. Neto, and F. Sols, "Electrostatic interactions between graphene layers and their environment," *Physical Review B*, vol. 77, no. 19, p. 195409, 2008.

[67] S. V. Kusminskiy, D. Campbell, A. C. Neto, and F. Guinea, "Pinning of a two-dimensional membrane on top of a patterned substrate: The case of graphene," *Physical Review B*, vol. 83, no. 16, p. 165405, 2011.

[68] Y. Zhang, V. W. Brar, C. Girit, A. Zettl, and M. F. Crommie, "Origin of spatial charge inhomogeneity in graphene," *Nature Physics*, vol. 5, no. 10, pp. 722–726, 2009.

[69] A. Deshpande, W. Bao, F. Miao, C. N. Lau, and B. J. LeRoy, "Spatially resolved spectroscopy of monolayer graphene on sio 2," *Physical Review B*, vol. 79, no. 20, p. 205411, 2009.

[70] A. Deshpande, W. Bao, Z. Zhao, C. N. Lau, and B. J. LeRoy, "Imaging charge density fluctuations in graphene using coulomb blockade spectroscopy," *Physical Review B*, vol. 83, no. 15, p. 155409, 2011.

[71] F. Schedin, A. Geim, S. Morozov, E. Hill, P. Blake, M. Katsnelson, and K. Novoselov, "Detection of individual gas molecules adsorbed on graphene," *Nature Materials*, vol. 6, no. 9, pp. 652–655, 2007.

[72] J. Moser, A. Verdaguer, D. Jiménez, A. Barreiro, and A. Bachtold, "The environment of graphene probed by electrostatic force microscopy," *Applied Physics Letters*, vol. 92, no. 12, p. 123507, 2008.

[73] V. Geringer, M. Liebmann, T. Echtermeyer, S. Runte, M. Schmidt, R. Rückamp, M. C. Lemme, and M. Morgenstern, "Intrinsic and extrinsic corrugation of monolayer graphene deposited on sio 2," *Physical Review Letters*, vol. 102, no. 7, p. 076102, 2009.

[74] J. C. Meyer, A. K. Geim, M. I. Katsnelson, K. S. Novoselov, T. J. Booth, and S. Roth, "The structure of suspended graphene sheets," *Nature*, vol. 446, no. 7131,

pp. 60–63, 2007.

[75] A. Laitinen, M. Oksanen, A. Fay, D. Cox, M. Tomi, P. Virtanen, and P. J. Hakonen, "Electron–phonon coupling in suspended graphene: Supercollisions by ripples," *Nano Letters*, vol. 14, no. 6, pp. 3009–3013, 2014.

[76] J. Rammer, *Quantum Field Theory of Non-equilibrium States*. Cambridge University Press, 2007.

[77] G. Zala, B. N. Narozhny, and I. L. Aleiner, "Interaction corrections at intermediate temperatures: Longitudinal conductivity and kinetic equation," *Phys. Rev. B*, vol. 64, p. 214204, Nov 2001.

[78] P. Le Doussal and L. Radzihovsky, "Self-consistent theory of polymerized membranes," *Phys. Rev. Lett.*, vol. 69, no. 8, pp. 1209–1212, 1992.

[79] D. Nelson, T. Piran, and S. Weinberg, *Statistical Mechanics of Membranes and Surfaces*. World Scientific Pub., 2004.

[80] I. V. Gornyi, V. Y. Kachorovskii, and A. D. Mirlin, "Conductivity of suspended graphene at the dirac point," *Phys. Rev. B*, vol. 86, no. 16, p. 165413, 2012.

[81] H. Ochoa, E. V. Castro, M. I. Katsnelson, and F. Guinea, "Temperature-dependent resistivity in bilayer graphene due to flexural phonons," *Phys. Rev. B*, vol. 83, no. 23, p. 235416, 2011.

[82] A. Fasolino, J. H. Los, and M. I. Katsnelson, "Intrinsic ripples in graphene," *Nature Materials*, vol. 6, no. 11, pp. 858–861, 2007.

[83] F. L. Braghin and N. Hasselmann, "Thermal fluctuations of free-standing graphene," *Physical Review B*, vol. 82, no. 3, p. 035407, 2010.

[84] P. Morse and H. Feshbach, "Methods of theoretical physics, vol. 2," *NewYork: MeGraw-Hill*, 1986.

[85] J. W. S. B. Rayleigh, *The theory of sound*, vol. 2. Macmillan, London, 1896.

[86] E. Stolyarova, K. T. Rim, S. Ryu, J. Maultzsch, P. Kim, L. E. Brus, T. F. Heinz, M. S. Hybertsen, and G. W. Flynn, "High-resolution scanning tunneling microscopy imaging of mesoscopic graphene sheets on an insulating surface," *Proceedings of the National Academy of Sciences*, vol. 104, no. 22, pp. 9209–9212, 2007.

[87] J. Jackle, "On phonon localization in nearly one-dimensional solids," *Solid State Communications*, vol. 39, no. 11, pp. 1261–1263, 1981.

[88] S. John and M. J. Stephen, "Wave propagation and localization in a long-range correlated random potential," *Phys. Rev. B*, vol. 28, pp. 6358–6368, Dec 1983.

[89] R. Sepehrinia, M. R. R. Tabar, and M. Sahimi, "Numerical simulation of the localization of elastic waves in two-and three-dimensional heterogeneous media," *Physical Review B*, vol. 78, no. 2, p. 024207, 2008.

[90] Y. He, W. Chen, W. Yu, G. Ouyang, and G. Yang, "Anomalous interface adhesion of graphene membranes," *Scientific reports*, vol. 3, 2013.

[91] R. Podgornik and P. L. Hansen, "Membrane pinning on a disordered substrate," *EPL (Europhysics Letters)*, vol. 62, no. 1, p. 124, 2003.

[92] M. V. Medvedyeva and Y. M. Blanter, "Eigenfrequencies of the randomly pinned drum and conductivity of graphene," *Physical Review B*, vol. 88, no. 12, 2013.

[93] G. D. Smith, *Numerical solution of partial differential equations: finite difference methods*. Oxford university press, 1985.

[94] M. Abramowitz and I. A. Stegun, *Handbook of mathematical functions: with formulas, graphs, and mathematical tables*, vol. 55. Courier Corporation, 1964.

[95] U. Elsner, V. Mehrmann, F. Milde, R. A. RÃűmer, and M. Schreiber, "The anderson model of localization: A challenge for modern eigenvalue methods," *SIAM Journal on Scientific Computing*, vol. 20, no. 6, pp. 2089–2102, 1999.

[96] V. I. Yudson, "Field theory for the global density of states distribution function of disordered conductors," *Phys. Rev. Lett.*, vol. 94, p. 156601, Apr 2005.

[97] A. Eilmes, R. Römer, and M. Schreiber, "The two-dimensional anderson model of localization with random hopping," *The European Physical Journal B - Condensed Matter and Complex Systems*, vol. 1, no. 1, pp. 29–38, 1998.

[98] D. J. Thouless, "A relation between the density of states and range of localization for one dimensional random systems," *Journal of Physics C: Solid State Physics*, vol. 5, no. 1, pp. 77–81, 1972.

[99] A. D. Mirlin, "Statistics of energy levels and eigenfunctions in disordered systems," *Physics Reports*, vol. 326, no. 5, pp. 259–382, 2000.

[100] O. Bohigas and M.-J. Giannoni, *Chaotic motion and random matrix theories*, pp. 1–99. Springer Berlin Heidelberg, 1984.

[101] V. E. Kravtsov and I. I. Lerner, "Level correlations driven by weak localization in 2d systems," *Phys Rev Lett*, vol. 74, no. 13, pp. 2563–2566, 1995.

[102] N. Argaman, Y. Imry, and U. Smilansky, "Semiclassical analysis of spectral correlations in mesoscopic systems," *Phys. Rev. B*, vol. 47, pp. 4440–4457, Feb 1993.

[103] E. Bogomolny and O. Giraud, "Eigenfunction entropy and spectral compressibility for critical random matrix ensembles," *Phys Rev Lett*, vol. 106, no. 4, p. 044101, 2011.

[104] M. L. Ndawana, R. A. Romer, and M. Schreiber, "Finite-size scaling of the level compressibility at the anderson transition," *The European Physical Journal B - Condensed Matter*, vol. 27, no. 3, pp. 399–407, 2002.

[105] M. L. Ndawana, R. A. Römer, and M. Schreiber, "Scaling of the level compressibility at the anderson metal-insulator transition," *Journal of the Physical Society of Japan*, vol. 72, 2003.

[106] E. Akkermans and G. Montambaux, "Conductance and statistical properties of metallic spectra," *Phys. Rev. Lett.*, vol. 68, pp. 642–645, Feb 1992.

[107] E. Kanzieper and V. E. Kravtsov, "Topological universality of level dynamics in quasi-one-dimensional disordered conductors," *Phys. Rev. B*, vol. 60, pp. 16774–16787, Dec 1999.

[108] E. Akkermans and G. Montambaux, *Mesoscopic Physics of Electrons and Photons*. Cambridge University Press, 2007.

[109] B. I. Shklovskii, B. Shapiro, B. R. Sears, P. Lambrianides, and H. B. Shore, "Statistics of spectra of disordered systems near the metal-insulator transition," *Phys. Rev. B*, vol. 47, pp. 11487–11490, May 1993.

[110] E. Hofstetter and M. Schreiber, "Statistical properties of the eigenvalue spectrum of the three-dimensional anderson hamiltonian," *Physical Review B*, vol. 48, no. 23, pp. 16979–16985, 1993.

[111] S. N. Evangelou and D. E. Katsanos, "Energy level statistics in disordered metals with an anderson transition," *Journal of Statistical Physics*, vol. 85, no. 5-6, pp. 525–550, 1996.

[112] I. K. Zharekeshev, M. Batsch, and B. Kramer, "Crossover of level statistics between strong and weak localization in two dimensions," *Europhysics Letters*, vol. 34, no. 8,

pp. 587–592, 1996.

[113] A. M. Garcia-Garcia and E. Cuevas, "Dimensional dependence of the metal-insulator transition," *Physical Review B*, vol. 75, no. 17, 2007.

[114] E. Louis, E. Cuevas, J. A. Vergés, and M. Otuño, "Mean free path and energy fluctuations in quantum chaotic billiards," *Phys. Rev. B*, vol. 56, pp. 2120–2126, Jul 1997.

[115] A. Altland and Y. Gefen, "Spectral statistics in nondiffusive regimes," *Phys Rev Lett*, vol. 71, no. 20, pp. 3339–3342, 1993.

[116] A. Altland and Y. Gefen, "Spectral statistics of nondiffusive disordered electron systems: A comprehensive approach," *Physical Review B*, vol. 51, no. 16, pp. 10671–10690, 1995.

[117] A. Altland and R. Loosen, "Disorder in ballistic systems: A numerical analysis," *Annalen Der Physik*, vol. 5, no. 2, pp. 203–212, 1996.

[118] N. Dupuis and G. Montambaux, "Aharonov-bohm flux and statistics of energy levels in metals," *Physical Review B*, vol. 43, no. 18, pp. 14390–14395, 1991.

[119] D. Braun and G. Montambaux, "Spectral correlations from the metal to the mobility edge," *Physical Review B*, vol. 52, no. 19, p. 13903, 1995.

[120] D. Braun, G. Montambaux, and M. Pascaud, "Boundary conditions at the mobility edge," *Physical Review Letters*, vol. 81, no. 5, pp. 1062–1065, 1998.

[121] E. Cuevas, "Two-level correlation function of critical random-matrix ensembles," *Physical Review B*, vol. 71, no. 2, 2005.

[122] A. Ossipov, I. Rushkin, and E. Cuevas, "Level-number variance and spectral compressibility in a critical two-dimensional random-matrix model," *Phys. Rev. E*, vol. 85, p. 021127, Feb 2012.

[123] G. Lemarie, J. Chabe, P. Szriftgiser, J. C. Garreau, B. Gremaud, and D. Delande, "Observation of the anderson metal-insulator transition with atomic matter waves: Theory and experiment," *Physical Review A*, vol. 80, no. 4, 2009.

[124] B. Altshuler and B. Shklovskii, "Repulsion of energy levels and conductivity of small metal samples," *Sov. Phys. JETP*, vol. 64, no. 1, pp. 127–135, 1986.

[125] V. E. Kravtsov and A. D. Mirlin, "Level statistics in a metallic sample: corrections to the wigner-dyson distribution," *JETP Letters*, vol. 60, no. 9, pp. 656–660, 1994.

[126] A. V. Andreev and B. L. Altshuler, "Spectral statistics beyond random matrix theory," *Phys Rev Lett*, vol. 75, no. 5, pp. 902–905, 1995.

[127] B. Al'tshuler, I. K. Zharekeshev, S. Kotochigova, and B. Shklovskii, "Repulsion between energy levels and the metal-insulator transition," *JETP*, vol. 67, no. 3, p. 625, 1988.

[128] E. Abrahams, P. Anderson, D. Licciardello, and T. Ramakrishnan, "Scaling theory of localization: Absence of quantum diffusion in two dimensions," *Physical Review Letters*, vol. 42, no. 10, p. 673, 1979.

[129] S. Hikami, "Anderson localization in a nonlinear-sigma-model representation," *Physical Review B*, vol. 24, no. 5, pp. 2671–2679, 1981.

[130] C. Porter and R. Thomas, "Fluctuations of nuclear reaction widths," *Physical Review*, vol. 104, no. 2, p. 483, 1956.

[131] C. E. Porter, *Statistical Theories of Spectra: Fluctuations*. Academic Press, New York, 1965.

[132] R. A. Jalabert, A. D. Stone, and Y. Alhassid, "Statistical theory of coulomb blockade oscillations: Quantum chaos in quantum dots," *Phys. Rev. Lett.*, vol. 68, pp. 3468–3471, Jun 1992.

[133] J. Stein and H.-J. Stöckmann, "Experimental determination of billiard wave functions," *Phys. Rev. Lett.*, vol. 68, pp. 2867–2870, May 1992.

[134] A. Kudrolli, V. V. Kidambi, and S. Sridhar, "Experimental studies of chaos and localization in quantum wave functions," *Phys Rev Lett*, vol. 75, no. 5, pp. 822–825, 1995.

[135] H. Alt, H. D. Gräf, H. L. Harney, R. Hofferbert, H. Lengeler, A. Richter, P. Schardt, and H. A. Weidenmüller, "Gaussian orthogonal ensemble statistics in a microwave stadium billiard with chaotic dynamics: Porter-thomas distribution and algebraic decay of time correlations," *Phys. Rev. Lett.*, vol. 74, pp. 62–65, Jan 1995.

[136] Y. C. Lin, P. H. Tuan, Y. T. Yu, H. C. Liang, K. W. Su, K. F. Huang, and Y. F. Chen, "Observation of disordered wave functions with conical second-harmonic generation and verification of transition from extended to prelocalized states in weak localization," *Physical Review B*, vol. 87, no. 4, p. 045117, 2013.

[137] A. D. Mirlin and Y. V. Fyodorov, "The statistics of eigenvector components of random band matrices - analytical results," *Journal of Physics A-Mathematical and General*, vol. 26, no. 12, pp. L551–L558, 1993.

[138] Y. V. Fyodorov and A. D. Mirlin, "Level-to-level fluctuations of the inverse participation ratio in finite quasi 1d disordered systems," *Phys Rev Lett*, vol. 71, no. 3, pp. 412–415, 1993.

[139] Y. V. Fyodorov and A. D. Mirlin, "Analytical derivation of the scaling law for the inverse participation ratio in quasi-one-dimensional disordered systems," *Phys. Rev. Lett.*, vol. 69, pp. 1093–1096, Aug 1992.

[140] Y. V. FYODOROV and A. D. MIRLIN, "Statistical properties of eigenfunctions of random quasi 1d one-particle hamiltonians," *International Journal of Modern*

Physics B, vol. 08, no. 27, pp. 3795–3842, 1994.

[141] Y. V. Fyodorov and A. D. Mirlin, "Mesoscopic fluctuations of eigenfunctions and level-velocity distribution in disordered metals," *Physical Review B*, vol. 51, no. 19, p. 13403, 1995.

[142] B. K. Nikolic, "Statistical properties of eigenstates in three-dimensional mesoscopic systems with off-diagonal or diagonal disorder," *Physical Review B*, vol. 64, no. 1, p. 014203, 2001.

[143] A. M. Chang, H. U. Baranger, L. N. Pfeiffer, K. W. West, and T. Y. Chang, "Non-gaussian distribution of coulomb blockade peak heights in quantum dots," *Phys. Rev. Lett.*, vol. 76, pp. 1695–1698, Mar 1996.

[144] A. D. Mirlin and Y. V. Fyodorov, "Distribution of local densities of states, order parameter function, and critical behavior near the anderson transition," *Phys. Rev. Lett.*, vol. 72, pp. 526–529, Jan 1994.

[145] K. Muller, B. Mehlig, F. Milde, and M. Schreiber, "Statistics of wave functions in disordered and in classically chaotic systems," *Physical Review Letters*, vol. 78, no. 2, pp. 215–218, 1997.

[146] V. Uski, B. Mehlig, and R. Romer, "A numerical study of wave-function and matrix-element statistics in the anderson model of localization," *Annalen der Physik*, vol. 7, no. 5-6, pp. 437–441, 1998.

[147] V. I. Falko and K. B. Efetov, "Multifractality: Generic property of eigenstates of 2d disordered metals.," *Europhysics Letters*, vol. 32, no. 8, pp. 627–632, 1995.

[148] V. I. Falko and K. B. Efetov, "Statistics of wave functions in mesoscopic systems," *Journal of Mathematical Physics*, vol. 37, no. 10, pp. 4935–4967, 1996.

[149] B. A. Muzykantskii and D. E. Khmelnitskii, "Nearly localized states in weakly disordered conductors," *Physical Review B*, vol. 51, no. 8, pp. 5480–5483, 1995.

[150] T. Kottos, A. Ossipov, and T. Geisel, "Signatures of classical diffusion in quantum fluctuations of two-dimensional chaotic systems," *Phys. Rev. E*, vol. 68, p. 066215, Dec 2003.

[151] V. Uski, B. Mehlig, R. A. Romer, and M. Schreiber, "Exact diagonalization study of rare events in disordered conductors," *Physical Review B*, vol. 62, no. 12, pp. R7699–R7702, 2000.

[152] V. Uski, B. Mehlig, and M. Schreiber, "Signature of ballistic effects in disordered conductors," *Physical Review B*, vol. 63, no. 24, p. 241101, 2001.

[153] V. Uski, R. A. Romer, and M. Schreiber, "Numerical study of eigenvector statistics for random banded matrices," *Physical Review E*, vol. 65, no. 5, p. 056204, 2002.

[154] B. Altshuler, V. Kravtsov, and I. Lerner, "Spectrum of relaxation times in disordered conductors," *JETP Lett*, vol. 45, no. 3, 1987.

[155] B. L. Altshuler, V. E. Kravtsov, and I. V. Lerner in *Mesoscopic phenomena in solids* (B. L. Altshuler, P. A. Lee, and W. R. Webb, eds.), vol. 30, Elsevier, 2012.

[156] B. Muzykantskii and D. Khmelnitskii, "Nearly localised states in weakly disordered conductors. ii. beyond diffusion approximation," *arXiv preprint cond-mat/9601045*, 1996.

[157] A. D. Mirlin, "Distribution of local density of states in disordered metallic samples: Logarithmically normal asymptotics," *Phys. Rev. B*, vol. 53, pp. 1186–1192, Jan 1996.

[158] A. D. Mirlin, "Spatial structure of anomalously localized states in disordered conductors," *Journal of Mathematical Physics*, vol. 38, no. 4, pp. 1888–1917, 1997.

[159] V. E. Kravtsov and I. V. Yurkevich, "Quasilocalized states in disordered metals and nonanalyticity of the level curvature distribution function," *Physical Review Letters*, vol. 78, no. 17, pp. 3354–3357, 1997.

[160] A. Abrikosov, "The paradox with the static conductivity of a one-dimensional metal," *Solid State Communications*, vol. 37, no. 12, pp. 997 – 1000, 1981.

[161] A. Mirlin, "Long–time relaxation of current in a 2d weakly disordered conductor," *JETP-Lett*, vol. 62, p. 603, 1995.

[162] I. E. Smolyarenko and B. L. Altshuler, "Statistics of rare events in disordered conductors," *Physical Review B*, vol. 55, no. 16, pp. 10451–10466, 1997.

[163] V. M. Apalkov, M. E. Raikh, and B. Shapiro, "Crossover between universality classes in the statistics of rare events in disordered conductors," *Phys. Rev. Lett.*, vol. 89, p. 126601, Aug 2002.

[164] V. M. Apalkov, M. E. Raikh, and B. Shapiro, "Anomalously localized states in the anderson model," *Phys Rev Lett*, vol. 92, no. 6, p. 066601, 2004.

[165] F. Wegner, "Inverse participation ratio in $2 + \epsilon$ dimensions," *Zeitschrift fr Physik B Condensed Matter and Quanta*, vol. 36, no. 3, pp. 209–214, 1980.

[166] C. Castellani, C. D. Castro, and L. Peliti, "On the upper critical dimension in anderson localisation," *Journal of Physics A: Mathematical and General*, vol. 19, no. 17, p. L1099, 1986.

[167] M. Schreiber and H. Grussbach, "Multifractal wave functions at the anderson transition," *Phys. Rev. Lett.*, vol. 67, pp. 607–610, Jul 1991.

[168] M. JANSSEN, "Multifractal analysis of broadly-distributed observables at criticality," *International Journal of Modern Physics B*, vol. 08, no. 08, pp. 943–984, 1994.

[169] B. Huckestein, "Scaling theory of the integer quantum hall effect," *Rev. Mod. Phys.*, vol. 67, pp. 357–396, Apr 1995.

[170] Y. M. Blanter and A. D. Mirlin, "Gor'kov and eliashberg linear-response theory: Rigorous derivation and limits of applicability," *Phys. Rev. B*, vol. 53, pp. 12601–12604, May 1996.

[171] Y. M. Blanter and A. D. Mirlin, "Correlations of eigenfunctions in disordered systems," *Phys. Rev. E*, vol. 55, pp. 6514–6518, Jun 1997.

[172] S. Hikami, "Localization length and inverse participation ratio of two dimensional electron in the quantized hall effect," *Progress of Theoretical Physics*, vol. 76, no. 6, pp. 1210–1221, 1986.

[173] J. H. Pixley, P. Goswami, and S. Das Sarma, "Anderson localization and the quantum phase diagram of three dimensional disordered dirac semimetals," *Phys. Rev. Lett.*, vol. 115, p. 076601, Aug 2015.

[174] B. B. Mandelbrot, "Intermittent turbulence in self-similar cascades: divergence of high moments and dimension of the carrier," *Journal of Fluid Mechanics*, vol. 62, no. 2, pp. 331–358, 1974.

[175] R. Benzi, G. Paladin, G. Parisi, and A. Vulpiani, "On the multifractal nature of fully developed turbulence and chaotic systems," *Journal of Physics A: Mathematical and General*, vol. 17, no. 18, p. 3521, 1984.

[176] U. Frisch, *Turbulence: The Legacy of A. N. Kolmogorov*. Cambridge University Press, 1995.

[177] P. Grassberger, "Generalized dimensions of strange attractors," *Physics Letters A*, vol. 97, no. 6, pp. 227 – 230, 1983.

[178] H. Hentschel and I. Procaccia, "The infinite number of generalized dimensions of fractals and strange attractors," *Physica D: Nonlinear Phenomena*, vol. 8, no. 3, pp. 435 – 444, 1983.

[179] T. C. Halsey, P. Meakin, and I. Procaccia, "Scaling structure of the surface layer of diffusion-limited aggregates," *Phys. Rev. Lett.*, vol. 56, pp. 854–857, Feb 1986.

[180] J. Lee and H. E. Stanley, "Phase transition in the multifractal spectrum of diffusion-limited aggregation," *Phys. Rev. Lett.*, vol. 61, pp. 2945–2948, Dec 1988.

[181] G. Paladin and A. Vulpiani, "Anomalous scaling laws in multifractal objects," *Physics Reports*, vol. 156, no. 4, pp. 147 – 225, 1987.

[182] M. Schreiber, "Fractal character of eigenstates in weakly disordered three-dimensional systems," *Physical Review B*, vol. 31, no. 9, pp. 6146–6149, 1985.

[183] A. Mildenberger, A. R. Subramaniam, R. Narayanan, F. Evers, I. A. Gruzberg, and A. D. Mirlin, "Boundary multifractality in critical one-dimensional systems with long-range hopping," *Physical Review B*, vol. 75, no. 9, 2007.

[184] V. N. Prigodin and B. L. Altshuler, "Long-range spatial correlations of eigenfunctions in quantum disordered systems," *Physical Review Letters*, vol. 80, no. 9, pp. 1944–1947, 1998.

[185] K. A. Muttalib and J. R. Klauder, "Generalized fokker-planck equation for multichannel disordered quantum conductors," *Physical Review Letters*, vol. 82, no. 21, pp. 4272–4275, 1999.

[186] K. A. Muttalib, P. Markos, and P. Wolfle, "Conductance distribution in strongly disordered mesoscopic systems in three dimensions," *Physical Review B*, vol. 72, no. 12, 2005.

[187] P. Markos, K. A. Muttalib, P. Wolfle, and J. R. Klauder, "Conductance distribution in 3d anderson insulators: Deviation from log-normal form," *Europhysics Letters (EPL)*, vol. 68, no. 6, pp. 867–873, 2004.

[188] A. M. Somoza, J. Prior, and M. Ortuño, "Conductance fluctuations in the localized regime: Numerical study in disordered noninteracting systems," *Physical Review B*, vol. 73, no. 18, 2006.

[189] B. Kramer, A. Kawabata, and M. Schreiber, "Quantum fluctuations of the conductance in the hopping regime," *Philosophical Magazine Part B*, vol. 65, no. 4, pp. 595–605, 2006.

[190] J. Prior, A. M. Somoza, and M. Ortuño, "Conductance distribution in two-dimensional localized systems with and without magnetic fields," *The European Physical Journal B*, vol. 70, no. 4, pp. 513–521, 2009.

[191] A. D. Mirlin and F. Evers, "Multifractality and critical fluctuations at the anderson transition," *Physical Review B*, vol. 62, no. 12, pp. 7920–7933, 2000.

[192] D. A. Parshin and H. R. Schober, "Distribution of fractal dimensions at the anderson transition," *Physical Review Letters*, vol. 83, no. 22, pp. 4590–4593, 1999.

[193] A. Mildenberger, F. Evers, and A. D. Mirlin, "Dimensionality dependence of the wave-function statistics at the anderson transition," *Phys. Rev. B*, vol. 66, p. 033109, Jul 2002.

[194] E. Cuevas, M. Ortuño, V. Gasparian, and A. Pérez-Garrido, "Fluctuations of the correlation dimension at metal-insulator transitions," *Phys. Rev. Lett.*, vol. 88, p. 016401, Dec 2001.

[195] F. Evers and A. D. Mirlin, "Fluctuations of the inverse participation ratio at the anderson transition," *Physical Review Letters*, vol. 84, no. 16, pp. 3690–3693, 2000.

[196] I. S. Burmistrov, S. Bera, F. Evers, I. V. Gornyi, and A. D. Mirlin, "Wave function multifractality and dephasing at metalâĂŞinsulator and quantum hall transitions," *Annals of Physics*, vol. 326, no. 6, pp. 1457–1478, 2011.

[197] A. Altland and B. Simons, *Condensed Matter Field Theory*. Cambridge books online, Cambridge University Press, 2010.

[198] A. D. Mirlin, Y. V. Fyodorov, F.-M. Dittes, J. Quezada, and T. H. Seligman, "Transition from localized to extended eigenstates in the ensemble of power-law random banded matrices," *Phys. Rev. E*, vol. 54, pp. 3221–3230, Oct 1996.

[199] J. V. José and R. Cordery, "Study of a quantum fermi-acceleration model," *Phys. Rev. Lett.*, vol. 56, pp. 290–293, Jan 1986.

[200] B. Altshuler and L. Levitov, "Weak chaos in a quantum kepler problem," *Physics Reports*, vol. 288, no. 1, pp. 487 – 512, 1997. I.M. Lifshitz and Condensed Matter Theory.

[201] A. V. Balatsky and M. I. Salkola, "Impurity states and the absence of quasiparticle localization in disordered d-wave superconductors," *Phys. Rev. Lett.*, vol. 76, pp. 2386–2389, Mar 1996.

[202] M. A. Skvortsov, M. V. Feigel'man, and V. E. Kravtsov, "Level statistics inside the core of a superconductive vortex," *Journal of Experimental and Theoretical Physics Letters*, vol. 68, pp. 84–90, Jul 1998.

[203] K. A. Muttalib and V. A. Gopar, "Generalization of the dmpk equation beyond quasi one dimension," *Physical Review B*, vol. 66, no. 11, 2002.

[204] J. Brndiar, R. Derian, and P. Markoš, "Generalized dorokhov-mello-pereyra-kumar equation for strongly localized regime: Numerical solution," *Physical Review B*, vol. 76, no. 15, 2007.

[205] P. Markos, "Electron transport in strongly disordered structures," *Physica B: Condensed Matter*, vol. 405, no. 14, pp. 3029–3032, 2010.

[206] A. Mackinnon, "The conductivity of the one-dimensional disordered anderson model - a new numerical-method," *Journal of Physics C-Solid State Physics*, vol. 13, no. 35, pp. 1031–1034, 1980.

[207] A. MacKinnon and B. Kramer, "One-parameter scaling of localization length and conductance in disordered systems," *Physical Review Letters*, vol. 47, no. 21, pp. 1546–1549, 1981.

[208] A. MacKinnon and B. Kramer, "The scaling theory of electrons in disordered solids: Additional numerical results," *Zeitschrift fur Physik B Condensed Matter*, vol. 53, no. 1, pp. 1–13, 1983.

[209] I. M. Suslov, "Finite-size scaling from the self-consistent theory of localization," *Journal of Experimental and Theoretical Physics*, vol. 114, no. 1, pp. 107–117, 2012.

[210] H. Grussbach and M. Schreiber, "Determination of the mobility edge in the anderson model of localization in three dimensions by multifractal analysis," *Physical Review B*, vol. 51, no. 1, pp. 663–666, 1995.

[211] A. Rodriguez, L. J. Vasquez, K. Slevin, and R. A. Romer, "Multifractal finite-size scaling and universality at the anderson transition," *Physical Review B*, vol. 84, no. 13, 2011.

[212] B. L. Altshuler, E. Cuevas, L. B. Ioffe, and V. E. Kravtsov, "Nonergodic phases in strongly disordered random regular graphs," *Phys Rev Lett*, vol. 117, no. 15, p. 156601, 2016.

[213] P. Shukla, "Localization to ergodic transitions: is rosenzweig - porter ensemble the hidden skeleton?," *New Journal of Physics*, vol. 18, no. 2, p. 021004, 2016.

[214] V. E. Kravtsov, I. M. Khaymovich, E. Cuevas, and M. Amini, "A random matrix model with localization and ergodic transitions," *New Journal of Physics*, vol. 17, no. 12, p. 122002, 2015.

[215] D. Facoetti, P. Vivo, and G. Biroli, "From non-ergodic eigenvectors to local resolvent statistics and back: A random matrix perspective," *EPL (Europhysics Letters)*, vol. 115, no. 4, p. 47003, 2016.

APPENDIX A

PYTHON CODE USED IN THE NUMERICAL STUDY

Here we attach our program coded in Python for calculating the eigenvalue and eigenfunctions of randomly pinned flexural phonons, see Chapter 3 for details.

```
from mpi4py import MPI
import sys
import random
import numpy as np
from scipy import sparse
from scipy.sparse.linalg import eigs, eigsh
from datetime import datetime
import time


comm = MPI.COMM_WORLD
size = comm.Get_size()
rank = comm.Get_rank()


random.seed(rank + time.time())


def CreateFreeMatrixPBC(N):


    # our matrix will be banded, with the following offsets
        of the diagonals
    upoff   = np.array([1, 2, N-2, N-1, N, N+1, 2*N-1, 2*N,
```

```
                        N*(N-2), N*(N-2)+1, N*(N-1)-1, N*(N
                            -1), N*(N-1)+1, N**2-1])
dnoff   = -upoff
offsets = np.append(0, np.append(upoff, dnoff))

# we solve for the (N)^2 interior points

# diagonal
di = 20 * np.ones(N ** 2)

# upper part
u1 = np.tile(np.append(2,     -8*np.ones(N-1)),  N)
u2 = np.tile(np.append([0,0],    np.ones(N-2)),  N)
u3 = np.tile(np.append(0 * np.ones(N-2), [1,1]),N)
u4 = np.tile(np.append(2 * np.ones(N-1), -8),    N)
u5 = -8 * np.ones(N ** 2)
u6 = np.tile(np.append(0,      2*np.ones(N-1)),  N)
u7 = np.tile(np.append(0*np.ones(N-1), 2),       N)
u8 =  1 * np.ones(N ** 2)
u9 =  1 * np.ones(N ** 2)
u10= np.tile(np.append(2, 0 * np.ones(N-1)),  N)
u11= np.tile(np.append(2*np.ones(N-1), 0),    N)
u12= -8 * np.ones(N ** 2)
u13= 2  * np.ones(N**2)
u14= 2  * np.ones(N**2)
```

```
# lower part
l1 = np.tile(np.append(-8*np.ones(N-1),2),    N)
l2 = np.tile(np.append(np.ones(N-2), [0,0]), N)
l3 = np.tile(np.append([1,1], 0 * np.ones(N-2)),N)
l4 = np.tile(np.append(-8, 2 * np.ones(N-1)),    N)
l5 = -8 * np.ones(N ** 2)
l6 = np.tile(np.append(2*np.ones(N-1), 0),   N)
l7 = np.tile(np.append(2, 0*np.ones(N-1)),       N)
l8 =  1 * np.ones(N ** 2)
l9 =  1 * np.ones(N ** 2)
l10= np.tile(np.append(0 * np.ones(N-1), 2),   N)
l11= np.tile(np.append(0, 2*np.ones(N-1)),     N)
l12= -8 * np.ones(N ** 2)
l13= 2  * np.ones(N**2)
l14= 2  * np.ones(N**2)

# datafilling
data = np.array([di, u1, u2, u3, u4, u5, u6, u7, u8, u9
    , u10, u11, u12, u13, u14,
                        l1, l2, l3, l4, l5, l6, l7, l8, l9
                            , l10, l11, l12, l13, l14])
A = sparse.dia_matrix((data, offsets), shape = (N**2, N
    **2))
```

```
    return A


def CreateRandMat(N, NumImp):
    FreeMatPBC = CreateFreeMatrixPBC(N)
    removelist = random.sample(range(N**2), NumImp)
    removelist.sort()
    colrow_list = np.delete(np.arange(0,N**2), removelist)
    RandmatPBC = sparse.lil_matrix(FreeMatPBC)[colrow_list
        ,:][:,colrow_list]
    return RandmatPBC, removelist


def calculateRandEig(N, NumImp):
    matPBC, removelist = CreateRandMat(N, NumImp)
    k = matPBC.shape[0]-1
    eig2PBC, eigvPBC = eigsh(matPBC, k, which = 'SM')
    addlist = np.array(removelist) - np.arange(len(
        removelist))
    wavefuncPBC = np.insert(eigvPBC.T, addlist, 0, axis =
        1)
    return np.sqrt(eig2PBC), wavefuncPBC


N = int(sys.argv[1])
#N = 20


# impurity concentration
```

```
ImpCon = float(sys.argv[2])
#ImpCon = .2
imp     = np.int((N**2 * ImpCon))


MPIeigenPBCs  = np.array([])
MPIwavr1s     = np.array([])
MPIwavr2s     = np.array([])
MPIipr2PBCs   = np.array([])
MPIipr3PBCs   = np.array([])
MPIipr4PBCs   = np.array([])


eigPBC = []
wavPBC = []
wavr1  = []
wavr2  = []
ipr2PBC = []
ipr3PBC = []
ipr4PBC = []


#Avg over different realization of imp
loopnum = int(sys.argv[3])
#loopnum = 3
r1 = int(N/4)   *(N+1)
r2 = int(3*N/4)*(N+1)
```

```
for i in range(0, loopnum):
    eigPBC0, wavPBC0 = calculateRandEig(N, imp)
    eigPBC.append(eigPBC0)
    #wavPBC.append(wavPBC0)
    wavr1.append(wavPBC0[:, r1])
    wavr2.append(wavPBC0[:, r2])
    ipr2PBC.append(np.sum(np.power(wavPBC0, 4), axis=1))
    ipr3PBC.append(np.sum(np.power(wavPBC0, 6), axis=1))
    ipr4PBC.append(np.sum(np.power(wavPBC0, 8), axis=1))


eigPBC  = np.array(eigPBC)
#wavPBC = np.array(wavPBC)
wavr1   = np.array(wavr1)
wavr2   = np.array(wavr2)
ipr2PBC = np.array(ipr2PBC)
ipr3PBC = np.array(ipr3PBC)
ipr4PBC = np.array(ipr4PBC)

len = eigPBC.shape[1]

if rank == 0:
        MPIeigenPBCs  = np.empty([size, loopnum, len],
           dtype=np.float64)
        MPIwavr1s     = np.empty([size, loopnum, len],
           dtype=np.float64)
```

```
        MPIwavr2s      = np.empty([size, loopnum, len],
            dtype=np.float64)
        MPIipr2PBCs    = np.empty([size, loopnum, len],
            dtype=np.float64)
        MPIipr3PBCs    = np.empty([size, loopnum, len],
            dtype=np.float64)
        MPIipr4PBCs    = np.empty([size, loopnum, len],
            dtype=np.float64)

comm.Gather(eigPBC,  MPIeigenPBCs, root = 0)
comm.Gather(wavr1,   MPIwavr1s   , root = 0)
comm.Gather(wavr2,   MPIwavr2s   , root = 0)
comm.Gather(ipr2PBC, MPIipr2PBCs , root = 0)
comm.Gather(ipr3PBC, MPIipr3PBCs , root = 0)
comm.Gather(ipr4PBC, MPIipr4PBCs , root = 0)

if rank == 0:
    filename = './data/wave_imp'+ str(int(ImpCon*100)) + '
        _lat'+ str(N) + '_avg' + sys.argv[4] + '.npy'
    np.save(filename, (MPIeigenPBCs, MPIipr2PBCs,
        MPIipr3PBCs, MPIipr4PBCs, MPIwavr1s, MPIwavr2s))
```